Chemical and structural investigation of the paroxetine-human serotonin transporter complex

Jonathan A. Coleman[‡a], Vikas Navratna[‡a], Daniele Antermite[b], Dongxue Yang[a], James A. Bull[b] and Eric Gouaux[a,c]

‡ These authors contributed equally.

a. Vollum Institute, Oregon Health & Science University, Portland, Oregon 97239, USA.

b. Department of Chemistry, Imperial College London, Molecular Sciences Research Hub, White City Campus, Wood Lane, London W12 0BZ, UK.

c. Howard Hughes Medical Institute, Oregon Health & Science University, Portland, Oregon 97239, USA.

Correspondence to Eric Gouaux: gouauxe@ohsu.edu

ABSTRACT

Antidepressants target the serotonin transporter (SERT) by inhibiting serotonin reuptake. Structural and biochemical studies aiming to understand binding of small-molecules to conformationally dynamic transporters like SERT often require thermostabilizing mutations and antibodies to stabilize a specific conformation, leading to questions about relationships of these structures to the bonafide conformation and inhibitor binding poses of wild-type transporter. To address these concerns, we determined the structures of ΔN72/ΔC13 and ts2-inactive SERT bound to paroxetine analogues using single-particle cryo-EM and x-ray crystallography, respectively. We synthesized enantiopure analogues of paroxetine containing either bromine or iodine instead of fluorine. We exploited the anomalous scattering of bromine and iodine to define the pose of these inhibitors and investigated inhibitor binding to Asn177 mutants of ts2-active SERT. These studies provide mutually consistent insights into how paroxetine and its analogues bind to the central substrate-binding site of SERT, stabilize the outward-open conformation, and inhibit serotonin transport.

INTRODUCTION

Serotonin or 5-hydroxytryptamine (5-HT) is a chemical messenger which acts on cells throughout the human body, beginning in early development and throughout adulthood[1]. 5-HT acts as both a neurotransmitter and a hormone that regulates blood vessel constriction and intestinal motility[1]. In the central nervous system, 5-HT is released from presynaptic neurons where it diffuses across the synaptic space and binds to 5-HT receptors, promoting downstream signaling and activating postsynaptic neurons[2,3]. Thus, 5-HT is a master regulator of circuits, physiology and behavioral functions including the sleep/wake cycle, sexual interest, locomotion, thermoregulation, hunger, mood, and pain[1]. 5-HT is cleared from synapses and taken into presynaptic neurons by the serotonin transporter (SERT), thus terminating serotonergic signaling[2-4]. SERT resides in the plasma membrane of neurons and belongs to a family of neurotransmitter sodium symporters (NSSs) which also includes the dopamine (DAT) and norepinephrine transporters (NET)[2-4]. NSSs are twelve transmembrane spanning secondary active transporters which utilize sodium and chloride gradients to energize the transport of neurotransmitter across the membrane[4-6] (Figure 1a).

The function of NSSs is modulated by a spectrum of small-molecule drugs, thus in turn controlling the availability of neurotransmitter at synapses. Selective serotonin reuptake inhibitors (SSRIs) are a class of drugs which inhibit SERT and are used to treat major depression and anxiety disorders[7]. Using x-ray crystallography and cryo-EM, we have determined structures of thermostabilized variants of human SERT complexed with SSRIs, which together explain many of the common features and differences associated with SERT-SSRI interactions[8,9]. SSRIs are competitive inhibitors that bind with high-affinity and specificity to a central substrate-binding site in SERT, preventing 5-HT binding and arresting SERT in an outward-open conformation[2,3,9].

The central site in NSSs is composed of three subsites: A, B, and C[10] (Figure 1b). In all NSS-ligand structures, the amine group of ligands resides in subsite A and interacts with a

63 conserved Asp residue (Asp98 in SERT). The heterocyclic electronegative group of the ligand is
64 positioned in subsite B[5]. For example, the alkoxyphenoxy groups of reboxetine and nisoxetine[11]
65 in *Drosophila* DAT (dDAT) structures, the halophenyl groups of cocaine analogs in dDAT and *S*-
66 citalopram in SERT, and the catechol derivatives in DCP-dDAT and sertraline-SERT all occupy
67 subsite B[8,9,12]. In addition to the central binding site, the activity of SERT and NSSs can also be
68 modulated by small-molecules which bind to an allosteric site located in an extracellular
69 vestibule, typically resulting in non-competitive inhibition of transport[9,13-15].
70 Paroxetine is an SSRI which exhibits the highest known binding affinity for the central
71 site of SERT (70.2 $\pm$ 0.6 pM) compared to any other currently prescribed antidepressants[16].
72 Despite its high affinity, paroxetine is frequently associated with serious side effects including
73 infertility, birth defects, cognitive impairment, sexual dysfunction, weight gain, suicidality, and
74 cardiovascular issues[17]. As a result, the mechanism of paroxetine binding to SERT has been
75 studied extensively in order to design drugs with higher-specificity and less adverse side-effects.
76 Despite these efforts, however, the binding pose of paroxetine remains a subject of debate[8,9,18-
77 20].
78 Paroxetine is composed of a secondary amine which resides in a piperidine ring, which
79 in turn is connected to benzodioxol and fluorophenyl groups (Figure 1b). X-ray structures of the
80 SERT-paroxetine complex revealed that the piperidine ring binds to subsite A while the
81 benzodioxol and fluorophenyl groups occupy subsite B and C in the central site, respectively[8,9]
82 (ABC pose, Figure 1b). However, recent mutagenesis, molecular dynamics, and binding studies
83 with paroxetine analogues suggest that paroxetine might either occupy ABC pose as observed
84 in the crystal structure, or an ACB pose where the benzodioxol and fluorophenyl groups occupy
85 subsite C and B of the central site respectively[18,20] (Figure 1c). Paroxetine is also thought to
86 interact with the allosteric site of SERT, albeit with low-affinity[15]. We have, however, been
87 unable to visualize paroxetine binding at the allosteric site using structural methods. Our x-ray

maps, by contrast, resolve a density feature at the allosteric site which instead resembles a molecule of detergent[9].

To resolve the ambiguity of paroxetine binding poses at the central binding site, we turned to paroxetine derivatives whereby the 4-fluoro group is substituted with either a bromine or an iodine group. Using transport and binding assays, anomalous x-ray diffraction, and cryo-EM, we have examined the binding poses of these paroxetine analogs and their interactions at the central site. Our studies provide key insights into the recognition of high-affinity inhibitors by SERT and the rational design of new small-molecule therapeutics.

RESULTS

To provide a robust molecular basis for the interaction of paroxetine (**1**) with SERT, we devised synthetic routes for two derivatives of paroxetine where the 4-fluoro moiety is substituted with either bromo (Br-paroxetine, **2**) or iodo (I-paroxetine, **3**) groups (Figure 2a,b). We envisaged the use of a C–H functionalization strategy to access enantiopure hydroxymethyl intermediates **I**, from readily available *N*-Boc (*R*)-nipecotic acid **4** (Figure 2b, Appendix 1). Transition metal-catalyzed C–H functionalization can promote the reaction of unactivated C(sp^3)–H bonds with the aid of a directing group[21-26]. Here, C–H functionalization enabled installation of the appropriate aryl group on the pre-existing piperidine ring[27], providing an attractive and short route to vary this functionality with inherent control of enantiomeric excess. In contrast, common methods for (–)-paroxetine synthesis can require the aromatic substituent to be introduced before stereoselective steps or ring construction, reducing flexibility of the process[20,28-34]. Nevertheless, during the preparation of this work, the synthesis of Br-paroxetine was reported using an asymmetric conjugate addition and its binding to SERT has been extensively studied[20,30].

Our synthesis commenced with the C–H arylation of piperidine **(–)-5** bearing Daugulis' aminoquinoline amide directing group[35] at C(3). Adapting our reported method[27], Pd-catalyzed C–H functionalization was achieved in moderate yields using 4-bromoiodobenzene or 1,4-

diiodobenzene in excess to prevent bis-functionalization, with palladium acetate, K_2CO_3 and pivalic acid (Figure 2c). The *cis*-arylated derivatives **(+)-6a** and **(+)-6b** were obtained with >98% *ee* and complete C(4) selectivity. Minor enantiopure *trans*-functionalized products, formed via a *trans*-palladacycle[27], were also isolated (Appendix 1). Subsequent treatment with 1,8-diazabicyclo(5.4.0)undec-7-ene (DBU) gave complete C(3)-epimerization affording **(+)-7a** and **(+)-7b** with the desired *trans*-stereochemistry in 94% and 91% yields. The aminoquinoline group was removed through telescoped amide activation and reduction with $LiAlH_4$ at 20 °C to give enantiopure hydroxymethyl intermediates **(–)-8a** and **(–)-8b** in 77% and 75% yield. Mesylation and nucleophilic substitution with sesamol formed ether derivatives **(–)-9a** and **(–)-9b**, which were deprotected to give Br- and I-paroxetine **2** and **3**. An overall yield of 12% over 8 steps from commercial material was obtained in both cases. At each stage the identity of the products and purity was established by acquiring ^{1}H and ^{13}C nuclear magnetic resonance spectra, IR spectra, and by high resolution mass spectrometry. Enantiopurity was assessed by high-performance liquid chromatography (HPLC) with reference to racemic or scalemic samples (Appendix 1).

We also employed several SERT variants and the 8B6 Fab in the biochemical and structural studies described here. The wild-type SERT construct used in transport experiments contains the full-length SERT sequence fused to a C-terminal GFP tag (Table 1). The ts2-active variant contains two thermostabilizing mutations (Ile291Ala, Thr439Ser) which allows for purification of the apo transporter for binding studies and has kinetics of 5-HT transport (K_m: 4.5 ± 0.6 μM, V_{max}: 21 ± 5 pmol min^{-1}) that are in a similar range as wild-type SERT (K_m: 1.9 ± 0.3 μM, V_{max}: 23 ± 1 pmol min^{-1})[9,36]. The ts2-inactive variant (Tyr110Ala, Ile291Ala)[8], by contrast, is unable to transport 5-HT but can be crystallized due to the stabilizing Tyr110Ala mutation[36] and binds SSRIs with high-affinity. The ΔN72/ΔC13 SERT variant used for cryo-EM is otherwise wild-type SERT which has been truncated at the N- and C-termini (Table 1) and yet retains

transport and ligand binding activities[37]. Finally, the recombinant 8B6 Fab[9,38] was used to produce SERT-Fab complexes which were studied by x-ray crystallography and cryo-EM.

We began by assessing the functional effects of paroxetine, Br-paroxetine, and I-paroxetine on SERT activity by measuring their inhibition of 5-HT transport and *S*-citalopram competition binding. We assayed the ability of the Br- and I-paroxetine derivatives to inhibit 5-HT transport in HEK293 cells expressing wild-type SERT, observing that upon substituting the 4-fluoro group with 4-bromo or 4-iodo groups, the potency of inhibition of 5-HT transport in wild-type SERT decreased significantly from 4 $\pm$ 1 for paroxetine to 40 $\pm$ 20 for Br-paroxetine and 180 $\pm$ 70 nM for I-paroxetine (Figure 3a, Table 2). Next, we measured the binding of paroxetine, Br-paroxetine, and I-paroxetine to ts2-active and ts2-inactive SERT using *S*-citalopram competition binding assays, finding that the SERT variants employed in this study exhibited high-affinity for paroxetine and its derivatives (Table 3). A decrease in the binding affinity upon substituting the 4-fluoro group of paroxetine with 4-bromo or 4-iodo groups was observed in the competition binding assays. However, the difference in the binding affinities between paroxetine variants measured by the competition binding assay was not as pronounced as the difference in the inhibition potencies observed in the 5-HT transport assays (Table 2 and 3). For example, the ts2-inactive (Tyr110Ala, Ile291Ala) variant employed in the previous[8] and present x-ray studies exhibited a K_i of 0.17 $\pm$ 0.02 nM for paroxetine, 0.94 $\pm$ 0.01 nM for Br-paroxetine, and a further decrease in affinity to I-paroxetine (2.3 $\pm$ 0.1 nM). The ts2-active SERT variant binds with similar affinity to paroxetine and Br-paroxetine, and shows a 4-5 fold decrease in affinity to I-paroxetine (Figure 3b, Table 3).

In the x-ray structures of SERT, paroxetine was modeled in the ABC pose such that the benzodioxol group is in subsite B[8,9]. A recent study suggested that binding affinity and potency to inhibit the transport of Br-paroxetine was only moderately affected upon mutating a non-conserved residue Ala169 to Asp in subsite B of SERT[20] (Figure 1b). We recently also identified

a conserved residue, Asn177 in the subsite B, which upon mutation exhibited differential effects on the inhibitory potency of ibogaine and noribogaine[37]. To further probe the role of Asn177 in subsite B, we studied the binding of paroxetine and its derivatives to selected Asn177 mutants designed in the ts2-active background (Figure 1b). We observed that the affinity of paroxetine to ts2-active SERT decreased by 3-fold when Asn177 is substituted with small non-polar or polar residues such as valine and threonine, while only a 2-fold change in K_i was observed for glutamine (Asn177Gln) (Figure 3c). In the case of Br-paroxetine, the Asn177 variants (K_i between 4-5 nM) display up to a 10-13 fold decrease in K_i when compared with ts2-active SERT (0.4 ± 0.2 nM) (Figure 3d, Table 3). The Asn177 variants show 2-4 fold decrease in affinity to I-paroxetine, with ts2-active SERT exhibiting a K_i of 1.7 ± 0.3 nM and the mutants a K_i of 4-7 nM. In the case of all three paroxetine variants, the reduction in affinity was the lowest for glutamine substitution. Irrespective of the SERT variant used, substitution of fluoro group with bromo or iodo group invariably decreased the affinity of paroxetine (Figure 3e, Table 3).

To define the binding poses of paroxetine and its analogues to SERT, we solved the structures of the ΔN72/ΔC13 and the ts2-inactive SERT variants complexed with Br- and I-paroxetine using single particle cryo-EM and x-ray crystallography (Figure 4 - figure supplements 1,2). We began by collecting cryo-EM data sets for ΔN72/ΔC13 SERT-8B6 Fab complexes with each ligand. The TM densities in all three reconstructions were well-defined and contiguous allowing for clear positioning of the main chain in an outward-open conformation (Figure 4 – figure supplements 3,4). Large aromatic side-chains were well-resolved for all three complexes, also suggesting that the aromatic moieties of paroxetine and its analogues could be identified and positioned in our cryo-EM maps. In addition, the particle distribution and orientations of SERT-Fab complexes in presence of Br- and I-paroxetine were similar to paroxetine, allowing for uniform comparison between the maps.

The ~3.3 Å resolution map of the ΔN72/ΔC13 SERT-8B6 paroxetine complex allowed us to locate a density feature for the inhibitor at the central site (Figure 4a). The resolution of the Br- and I-paroxetine complexes was comparatively lower at ~4.1 Å and ~3.8 Å, respectively (Table 4, Figure 4 - figure supplement 4). Nevertheless, these ligands could also be modeled into the density at the central site with a correlation coefficient (CC) of 0.75 and 0.77, respectively (Figure 4b-e). To compare paroxetine in the ABC *vs.* the ACB pose, we flexibly modeled paroxetine in both poses at the central site followed by real space refinement. We observed that in the ACB pose, paroxetine could be positioned with a CC of 0.70 compared with 0.84 for the ABC pose suggesting that while ABC pose is clearly preferred under the conditions we tested, the possibility of an ACB pose cannot be excluded (Figure 4 - figure supplement 5a,b). Based on the higher CC value, and the binding pose information from the ts2-inactive and ts3 SERT x-ray structures, the density in cryo-EM maps for paroxetine at the central site was interpreted to best accommodate ABC pose[8,9]. We also compared the reconstructed complexes by calculating difference maps, attempting to identify features associated with the scattering of bromine and iodine at the central and allosteric sites. However, the resulting difference maps did not contain any interpretable difference densities and thus did not further assist in ligand modeling. In the cryo-EM maps, the maltose headgroup of a DDM molecule could also be visualized in the allosteric site with the detergent tail inserted between TMs 10, 11, and 12. In contrast, in the x-ray maps only the head group of the octyl-maltoside detergent could be modeled due to the weak density of the hydrocarbon chain.

We then explored the binding pose of paroxetine by growing crystals and collecting x-ray data of the ts2-inactive SERT-8B6 Fab complex with Br- and I-paroxetine (Table 5). Anomalous difference maps calculated from the previously determined ts2-inactive paroxetine structure (PDB ID: 6AWN) after refinement, showed clear densities for Br- and I- atoms of the paroxetine derivatives in subsite C (Figure 4f,g). No detectable anomalous peaks were observed in either subsite B or in the allosteric site and there were no other peaks in any other location above

2.5σ, suggesting that under these conditions, Br-paroxetine and I-paroxetine do not bind substantially in the ACB orientation or to the allosteric site. Next, we calculated isomorphous difference maps (F_o-F_o) using the ts2-inactive paroxetine dataset (PDB: 6AWN) and either the Br-paroxetine or I-paroxetine datasets. The F_o(paroxetine)-F_o(Br-paroxetine) map also revealed a difference peak in subsite C near the halogenated groups while no significant peaks were detected in subsite B (Figure 4 – figure supplement 6a). Similarly, the F_o(paroxetine)-F_o(I-paroxetine) map also contained a difference peak which overlapped with the position of the halogen (Figure 4 – figure supplement 6b) while the F_o(Br-paroxetine)-F_o(I-paroxetine) difference map did not contain any interpretable features, likely due to the low resolution of both datasets (Figure 4 - figure supplement 6c).

We next compared the cryo-EM structure of the SERT-paroxetine complex to the x-ray structure of the ts3 SERT paroxetine complex. Overall comparison of the transporter revealed only minor variation between structures solved by each method, with a Cα root-mean-square-deviation (RMSD) of 0.68 Å. The most significant differences between the cryo-EM and the x-ray structures were found at the extracellular and intracellular sites of TM12 and also in EL2, while the core of the transporter (TM1-10) was largely unchanged (Figure 5a). These changes can largely be explained on the basis of a crystal packing interface formed by TM12 and a highly flexible EL2 that is bound to the 8B6 Fab. We also compared central site residues involved in paroxetine binding, finding that the best fit to the cryo-EM density revealed only minor differences in the side-chains of Asp98, Tyr176, and Phe335 when compared to the x-ray structure (all atom RMSD: 0.91 Å) (Figure 5b). Finally, we compared the cryo-EM structures of the SERT 15B8 Fab/8B6 scFv paroxetine complex (PDB: 6DZW) to the SERT 8B6 Fab paroxetine complex to understand if these antibodies induce changes in transporter structure. Here we found that the most significant differences occurred in the extracellular domain and involved localized regions of EL2 and EL4 that interact with the antibody (Figure 5c). The

transporter core was largely unchanged, with the only other significant differences being found in EL6, TM12, and IL4.

DISCUSSION

The binding of paroxetine to SERT has been extensively debated[8,9,18-20]. The first x-ray structure of the ts3-SERT variant demonstrated that the binding pose is such that the piperidine, benzodioxol, and fluorophenyl groups occupy subsites A, B, and C respectively, in the ABC pose[9] (Figure 1b). Competition binding experiments using a variant of SERT containing a central binding site that has been genetically engineered to possess photo-cross-linking amino acids corroborated that paroxetine binds in a fashion which is similar to that observed in crystal structure[8,9], where the fluorophenyl group is in proximity to Val501[39]. However, computational docking experiments using wild type SERT predicted that the position of benzodioxol and fluorophenyl groups of paroxetine are 'flipped', with paroxetine occupying an ACB pose[19] (Figure 1c). Subsequent studies involving wild-type and mutant SERT variants, that include modelling, mutagenesis, and Br-paroxetine docking experiments suggested that paroxetine could bind in both ABC and ACB poses. These studies also suggested that bromination of paroxetine and certain mutations near the central site, such as Ala169Asp, favored ABC pose[18,20]. Hence, the authors in these studies hypothesized that the ABC pose observed in the crystal structure could be because of the crystallization conditions and thermostabilizing mutations.

One of the thermostabilizing mutations in ts3-SERT, Thr439Ser, is near the central binding site and Thr439 participates in a hydrogen bonding network in subsite B that, in turn, includes the dioxol group of paroxetine. To probe the role of the Thr439Ser mutation in modulating the binding pose of paroxetine, we solved the x-ray structure of ts2-inactive (Tyr110Ala, Ile291Ala) SERT, wherein the residue at position 439 was the wild-type threonine. Paroxetine could be modeled in the ABC pose in the x-ray structure of ts2-inactive SERT[8]. MD simulations of ts2-inactive SERT suggested that the Thr439Ser mutation weakens the Na2 site.

Furthermore, MD simulations and binding and uptake kinetics experiments using wild-type SERT in presence of paroxetine and a variant of paroxetine where in the 4-fluoro group is substituted with 4-bromo group suggested that the paroxetine binding pose in SERT could be ambiguous because of the pseudo symmetry of the paroxetine molecule. It was noted that paroxetine could occupy both ABC and ACB poses with almost equivalent preference. Upon substituting the 4-fluoro with a bulkier 4-bromo group, the ABC pose was favored[18,20].

Structural studies of SERT in complex with paroxetine and its analogues were thus required to resolve the uncertainty in paroxetine binding pose at the central site. Previously, we had demonstrated that cryo-EM can be used to define the position of ligands at the central site of SERT[37]. Here, we employed a similar methodology using the ΔN72/ΔC13 SERT variant complexed with 8B6 Fab to study binding of paroxetine at the central site. The density feature of paroxetine in the cryo-EM map at ~3.3 Å clearly resolved the larger benzodioxol and smaller fluorophenyl groups in subsite B and C respectively (Figure 4b). Though this reconstruction suggests that paroxetine binds in the ABC pose, we also considered the possibility that the inhibitor density feature may represent an average of the ABC and ACB poses. We expected that if Br- and I-paroxetine were suitable surrogates for paroxetine, their binding pose would be unaffected by their reduced electronegativity and the size of the halogenated groups and therefore that they would also be associated with a comparable density feature at this site, as demonstrated by our cryo-EM maps. To further explore if there was a fraction of Br- or I-paroxetine in the ACB pose, we examined the position of the Br- or I- atoms at the central site by x-ray crystallography. If Br- and I-paroxetine were to bind in both the ABC or ACB poses, we expected to observe two anomalous peaks in our x-ray maps in subsites B and C; for both ligands, however, only a single detectable peak was observed in subsite C (Figure 4f,g). Thus, our direct biophysical observations reveal that under the conditions that we tested the ABC pose of paroxetine is preferred over the the ACB pose.

289 Paroxetine is stabilized at the central binding site by aromatic, ionic, non-ionic, hydrogen
290 bonding, and cation-π interactions[8]. In the ABC pose, the amine of the piperidine ring of
291 paroxetine binds with Asp98 (3.5 Å) and also makes a cation-π interaction with Tyr95 of subsite
292 A (Figure 4a). The benzodioxol group of paroxetine, a catechol-like entity, occupies a position in
293 subsite B which is similar to the binding of catechol derivative groups of sertraline and 3,4-
294 dichlorophenethylamine in SERT[8] and dDAT[12] structures, respectively. In subsite B, the ring of
295 Tyr176 makes an aromatic interaction with the benzodioxol while the hydrogen-bonding network
296 in subsite B formed by Asn177, Thr439, backbone carbonyl oxygens, and amides are likely
297 responsible for stabilization of the dioxol. The side-chain of Ile172 inserts between the
298 benzodioxol and fluorophenyl, while the rings of Phe341 and Phe335 stack on either side of the
299 fluorophenyl, 'sandwiching' it within subsite C. The halogen group of paroxetine and its
300 analogues reside adjacent to the side-chain of Thr497 (4.0 Å), which may act to stabilize these
301 groups through hydrogen bonding (Figure 4a). The larger atomic radius, the longer length of the
302 carbon-halogen bond, and the difference in electronegativity of bromine (radius: 1.85 Å, bond-
303 length: 1.92 Å, electronegativity: 2.96) and iodine (radius: 1.98 Å, bond-length: 2.14 Å,
304 electronegativity: 2.66) relative to fluorine (radius: 1.47 Å, bond-length: 1.35 Å, electronegativity:
305 3.98) would explain why the fluorine analogue binds with greater affinity than Br-paroxetine and
306 I-paroxetine.

307 We also explored the effect of conservative and non-conservative mutations in subsite B
308 of SERT at Asn177 (Figure 3). Asn177 participates in a hydrogen-bond network with the
309 hydroxyl group of noribogaine and with the dioxol of paroxetine. However, this network of
310 interactions is also important for binding halogenated inhibitors in subsite B, as in the case for
311 *S*-citalopram, fluvoxamine, and sertraline. All of the mutants that we tested at Asn177 resulted
312 in a loss of binding affinity to paroxetine and its analogues. Furthermore, the Ala169Asp
313 mutation in subsite B[20] (Figure 1b,c) also reduced paroxetine inhibition and binding, likely also

disrupting these interactions. Although the effects were less severe when compared to paroxetine, Br-paroxetine binding and inhibition was also reduced for Ala169Asp[20]. Thus, these mutations highlight the importance of subsite B interactions in paroxetine binding but they cannot be used to demonstrate the inhibitor pose because, in the ABC or ACB poses, either the dioxol or fluorine of paroxetine could act as a hydrogen-bond acceptor in subsite B.

Using a combination of chemical biology, cryo-EM, and x-ray crystallography we observed that under the conditions that we studied, the SSRI paroxetine preferably occupies the ABC pose at the central site, where it is involved in numerous interactions. However, the data presented in the manuscript does not completely exclude the possibility of an ACB pose at the central site. Our studies of the mechanism of paroxetine binding to SERT provide a robust framework for the design of experiments to identify new highly specific small-molecule SERT inhibitors.

MATERIALS AND METHODS

SERT expression and purification

The human SERT constructs used in this study were the wild-type, the N- and C-terminally truncated wild-type (ΔN72/ΔC13), ts2-inactive (Tyr110Ala, Ile291Ala), and ts2-active (Ile291Ala, Thr439Ser)[8,9,36-38] proteins (Table 1). The Asn177 mutants were generated in the ts2-active background. The expression and purification of SERT was carried out as previously described with minor modifications[8,9,37,38], as described below. All SERT constructs were cloned into BacMam vector system to be expressed as C-terminal GFP fusion using baculovirus-mediated transduction of HEK293S GnTI$^-$ cells. Cells were solubilized in 20 mM Tris pH 8 with 150 mM NaCl, containing 20 mM n-dodecyl-β-D-maltoside (DDM) and 2.5 mM cholesteryl hemisuccinate (CHS), followed by purification using Strep-Tactin affinity chromatography in 20 mM Tris pH 8 with 100 mM NaCl (TBS), 1 mM DDM, and 0.2 mM CHS.

For cryo-EM of the ΔN72/ΔC13 SERT, 1 mM 5-HT was added during solubilization and affinity purification to stabilize SERT. GFP was cleaved from SERT by digestion with thrombin

and the SERT-8B6 complex was made as described in the previous paragraph. The complex was separated from free Fab and GFP by SEC in TBS containing 1 mM DDM and 0.2 mM CHS, and the peak fractions were concentrated to 4 mg/ml followed by addition of either 200 μM paroxetine, Br-paroxetine or I-paroxetine.

For crystallization, no ligands were added during purification of ts2-inactive SERT, and 5% glycerol and 25 μM lipid (1-palmitoyl-2-oleoyl-sn-glycero-3-phosphocholine, 1-palmitoyl-2-oleoyl-sn-glycero-3-phosphoethanolamine, and 1-palmitoyl-2-oleoyl-sn-glycero-3-phosphoglycerol at a molar ratio of 1:1:1) were included in all the purification buffers. Following affinity purification, the fusion protein was digested by thrombin and EndoH and combined with recombinant 8B6 Fab at a molar ratio of 1:1.2. The SERT-8B6 complex was isolated by size-exclusion chromatography (SEC) on a Superdex 200 column in TBS containing 40 mM n-octyl β-D-maltoside, 0.5 mM CHS. The SERT-8B6 Fab complex was concentrated to 2 mg/ml and 1 μM 8B6 Fab and 50 μM Br-paroxetine or I-paroxetine was added prior to crystallization.

Synthesis of Br- and I-paroxetine

All reactions were carried out under an inert atmosphere (argon) with flame-dried glassware using standard techniques, unless otherwise specified. Anhydrous solvents were obtained by filtration through drying columns (THF, MeCN, CH_2Cl_2 and DMF) or used as supplied (α,α,α-trifluorotoluene). Reactions in sealed tubes were run using Biotage microwave vials (2–5 ml or 10–20 ml recommended volumes). Aluminum caps equipped with molded butyl/PTFE septa were used for reactions in α,α,α-trifluorotoluene and toluene. Simple butyl septa were used for reactions in other solvents. Chromatographic purification was performed using 230–400 mesh silica with the indicated solvent system according to standard techniques. Analytical thin-layer chromatography (TLC) was performed on precoated, glass-backed silica gel plates. Visualization of the developed chromatogram was performed by UV absorbance (254 nm) and/or stained with a ninhydrin solution in ethanol. HPLC analyses were carried out on an

Agilent 1260 Infinity Series system, employing Daicel Chiracel columns, under the indicated conditions. The high-resolution mass spectrometry (HRMS) analyses were performed using electrospray ion source (ESI). ESI was performed using a Waters LCT Premier equipped with an ESI source operated either in positive or negative ion mode. The software used was MassLynx 4.1; this software does not account for the electron and all the calibrations/references are calculated accordingly, *i.e.* $[M+H]^+$ is detected and the mass is calibrated to output [M+H]. Melting points are uncorrected. Infrared spectra (FTIR) were recorded in reciprocal centimeters (cm^{-1}).

Nuclear magnetic resonance spectra were recorded on 400 or 500 MHz spectrometers. The frequency used to record the NMR spectra is given in each assignment and spectrum (^1H NMR at 400 or 500 MHz; ^{13}C NMR at 101 MHz or 126 MHz). Chemical shifts for ^1H NMR spectra were recorded in parts per million from tetramethylsilane with the residual protonated solvent resonance as the internal standard ($CHCl_3$: δ 7.27 ppm, $(CD_2H)_2SO$: δ 2.50 ppm, CD_2HOD: δ 3.31 ppm). Data was reported as follows: chemical shift (multiplicity [s = singlet, d = doublet, t = triplet, m = multiplet and br = broad], coupling constant, integration and assignment). *J* values are reported in Hz. All multiplet signals were quoted over a chemical shift range. ^{13}C NMR spectra were recorded with complete proton decoupling. Chemical shifts were reported in parts per million from tetramethylsilane with the solvent resonance as the internal standard ($^{13}CDCl_3$: δ 77.0 ppm, $(^{13}CD_3)_2SO$: δ 39.5 ppm, $^{13}CD_3OD$: δ 49.0 ppm). Assignments of ^1H and ^{13}C spectra, as well as *cis*- or *trans*-configuration, were based upon the analysis of δ and *J* values, analogy with previously reported compounds[27], as well as DEPT, COSY and HSQC experiments, where appropriate. All Boc containing compounds appeared as a mixture of rotamers in the NMR spectra at room temperature. In some cases, NMR experiments for these compounds were carried out at 373 K to coalesce the signals, which is indicated in parentheses where appropriate. For NMR analysis performed at room temperature, 2D NMR experiments

(COSY and HSQC) are also presented when useful for the assignments. Observed optical rotation (α') was measured at the indicated temperature (T °C) and values were converted to the corresponding specific rotations $[\alpha]_D^T$ in deg cm^2 g^{-1}, concentration (*c*) in g per 100 mL. Full details of the synthetic route, using enantiopure and racemic substrates, and NMR spectra of all reaction intermediates, **2** and **3**, and HPLC analysis are cataloged in Appendix 1.

Crystallization

Crystals of ts2-inactive SERT-8B6 Fab complex were grown by hanging-drop vapor diffusion at 4 °C at a ratio of 2:1 (v/v) protein:reservoir. Br-paroxetine crystals were grown using reservoir solution containing 50 mM Tris pH 8.5, 20 mM $Na_2(SO4)$, 20 mM $LiCl_2$, 36% PEG 400, and 0.5% 6-aminohexanoic acid. I-paroxetine crystals were grown using a reservoir solution containing 100 mM HEPES pH 7.5, 40 mM $MgCl_2$, and 32% PEG 400.

X-ray data collection

Crystals were harvested and flash cooled in liquid nitrogen. Data was collected at the Advanced Photon Source (Argonne National Laboratory, beamline 24-ID-C). Data for Br-paroxetine was collected at a wavelength of 0.91840 Å and at 1.37760 Å for I-paroxetine.

Anomalous difference maps

X-ray data sets were processed with XDS[40]; Friedel pairs were allowed to have different intensities. Molecular replacement was performed with coordinates from the previously determined ts2-inactive SERT-paroxetine structure (Protein Data Bank (PDB) code: 6AWN)[8] using PHASER[41]. B-factors were refined using PHENIX[42] followed by generating anomalous difference maps using the phases derived from the higher resolution structures. To maximize the signal-to-noise ratio of the Br-paroxetine anomalous difference density, the high-resolution phases were blurred with a B-factor of 500 with a high-resolution cutoff of 5.5 Å. Using these optimized parameters for the Fourier analysis of the Br-paroxetine diffraction data, we obtained an anomalous map with the largest difference peak being present at 6.0σ and the noise level

estimated at ~2.5σ. To maximize the signal-noise-ratio of the I-paroxetine anomalous difference density, a high-resolution and low-resolution cutoff of 6.3 and 30 Å was applied during the generation of the anomalous maps. Using these optimized parameters for the Fourier analysis of the I-paroxetine diffraction data, we obtained an anomalous map with the largest difference peak being present at 4.5σ and the noise level estimated at ~2.5σ.

F_o-F_o isomorphous difference maps

Isomorphous difference (F_o-F_o) maps were calculated in PHENIX by analyzing isomorphous pairs of crystals. Difference maps were calculated using the previously determined ts2-inactive SERT-paroxetine dataset and PDB (6AWN) for phasing. High- and low-resolution cutoffs of 6.0 and 30.0 Å were applied for the F_o(paroxetine)- F_o(Br-paroxetine) map and cutoffs of 6.3 and 30.0 Å were used for the F_o(paroxetine)- F_o(I-paroxetine) and F_o(Br-paroxetine)- F_o(I-paroxetine) maps.

Cryo-EM grid preparation

To promote the inclusion of particles in thin ice, 100 μM fluorinated octyl-maltoside (final concentration) from a 10 mM stock was added to SERT-8B6 complexes immediately prior to vitrification. Quantifoil holey carbon gold grids, 2.0/2.0 μm, size/hole space, 200 mesh) were glow discharged for 60 s at 15 mA. SERT-8B6 Fab complex (2.5 μl) was applied to the grid followed by blotting for 2 s in the vitrobot and plunging into liquid ethane cooled by liquid N_2.

Cryo-EM data collection and processing

Images were acquired using the automated program SerialEM[43] on a FEI Titan Krios transmission electron microscope, operating at 300 keV and equipped with a Gatan Image Filter with the slit width set to 20 eV. A Gatan K3 direct electron detector was used to record movies in super-resolution counting mode with a binned pixel size of 0.648 Å per pixel. The defocus values ranged from -0.8 to -2.2 μm. Exposures of 1.0-1.5 s were dose fractioned into 40 frames, resulting in a total dose of 54-60 e^- Å^{-2}. Movies were corrected for beam-induced motion using

MotionCor2[44] with 5x5 patching. The contrast transfer function (CTF) parameters for each micrograph was determined using ctffind4[45] and particles were picked either using DoG-Picker[46] or blob-based picking in cryoSPARC[47]. DoG or cryoSPARC picked particles were independently subjected to 3D classification against a low-resolution volume of the SERT-8B6 complex. After sorting, the DoG and cryoSPARC picked particles were combined in RELION[48] and the duplicate picks were removed (particle picks that are less than 100 Å of one another were considered duplicates). Combined particles were further sorted using reference-free 2D classification in cryoSPARC, followed by refinement in RELION and further 3D classification. Particles were then re-extracted (box size 400, 0.648 Å per pixel) and subjected to non-uniform refinement in cryoSPARC. Local refinement was then performed in *cis*TEM[49] with a mask that excludes the micelle and Fab constant domain to remove low-resolution features. The high-resolution refinement limit was incrementally increased while maintaining a correlation of 0.95 or better until no improvement in map quality was observed. The resolution of the reconstructions was accessed using the Fourier shell correlation (FSC) criterion and a threshold of 0.143[50]. Map sharpening was performed using local sharpening in PHENIX.

Cryo-EM model building and refinement

A starting model was generated by fitting the x-ray structure of SERT-8B6 Fab paroxetine complex (PDB code: 6AWN) into the cryo-EM reconstruction in Chimera[51]. Several rounds of manual adjustment and rebuilding were performed in Coot[52], followed by real space refinement in PHENIX. For cross-validation, the FSC curve between the refined model and half maps was calculated and compared to prevent overfitting. Molprobity was used to evaluate the stereochemistry and geometry of the structures[53].

Radioligand binding and uptake assays

Competition binding experiments were performed using scintillation proximity assays (SPA)[36,38]. The assays contained ~10 nM SERT, 0.5 mg/ml Cu-Ysi beads in TBS with 1 mM DDM, 0.2 mM CHS, and 10 nM [^{3}H]citalopram and 0.01 nM–1 mM of the cold competitors.

Experiments were measured in triplicate. The error bars for each data point represent the s.e.m. Ki values were determined with the Cheng–Prusoff equation[54] in GraphPad Prism. Uptake was measured as described previously in 96-well plates with [^{3}H]5-HT diluted 1:100 with unlabeled 5-HT. After 24 hrs, cells were washed into uptake buffer (25 mM HEPES-Tris, pH 7.0, 130 mM NaCl, 5.4 mM KCl, 1.2 mM $CaCl_2$, 1.2 mM $MgSO_4$, 1 mM ascorbic acid and 5 mM glucose) containing 0.001 – 10,000 nM of the inhibitor. [^{3}H]5-HT was added to the cells and uptake was stopped by washing cells rapidly three times with uptake buffer. Cells were solubilized with 1% Triton-X100, followed by the addition of 200 µl of scintillation fluid to each well. The amount of labelled 5-HT was measured using a MicroBeta scintillation counter. Data were fit to a sigmoidal dose-response curve.

ACKOWLEDGEMENTS

We thank L. Vaskalis for assistance with figures and H. Owen for help with manuscript preparation. We acknowledge the staff of the Northeastern Collaborative Access Team at the Advanced Photon Source. A portion of this research was supported by NIH grant U24GM129547 and performed at the PNCC at OHSU and accessed through EMSL (grid.436923.9), a DOE Office of Science User Facility sponsored by the Office of Biological and Environmental Research. We are particularly grateful to Bernard and Jennifer LaCroute for their generous support. This work was funded by the NIH (5R37MH070039). E.G. is an investigator of the Howard Hughes Medical Institute.

We gratefully acknowledge The Royal Society [University Research Fellowship, UF140161 (to J.A.B.), URF Appointed Grant RG150444].

FIGURE LEGENDS

Figure 1. Topology of SERT. a, The substrate is bound at the central site (sand, triangle), near two sodium ions (purple, spheres +) and a chloride ion (green, sphere -). The light orange and light blue triangles depict pseudo two-fold symmetric helical repeats comprised of TM1-5 and 6-10, respectively. The disulfide bond (purple line) and *N*-linked glycosylation (red ‘Y’ shapes) in

492 extracellular loop 2, along with sites of thermostable mutations (Tyr110Ala, TM1a; Ile291Ala,
493 TM5; Thr439Ser, TM8) are also shown (cyan-filled circles). Structural elements involved in
494 binding allosteric ligands are depicted as black-filled circles. Epitopes for the 8B6 and 15B8 Fab
495 binding sites are in squiggly dark-blue and orange lines, respectively. **b,** Schematic of the ABC
496 pose of paroxetine bound to the central binding site, derived from the previously determined x-
497 ray structures[8,9]. The transmembrane helices are shown with circles and mutated residues in
498 subsite B are in sticks. **c,** The ACB pose of paroxetine bound to the central binding site of SERT
499 predicted by molecular dynamics simulations and mutagenesis[18,20].

500 **Figure 2. Synthesis of paroxetine analogues. a,** Structures of (–)-paroxetine **(1)** and the
501 targeted Br- **(2)** and I-analogues **(3)**. **b,** Retrosynthetic analysis of Br- and I-(–)-paroxetine. **c,**
502 Synthesis of Br- and I-(–)-paroxetine **2** and **3**. Q = 8-quinolinyl-. Reaction conditions: *i*) X = Br: **(–**
503 **)-5** (4.0 mmol), 4-bromo iodobenzene (3 equiv), $Pd(OAc)_2$ (5 mol %), K_2CO_3 (1 equiv), PivOH (1
504 equiv), Ph-CF_3 (2 mL, 2 M), 110 °C, 18 h; *ii*) X = I: **(–)-5** (4.0 mmol), 1,4-diiodobenzene (4
505 equiv), $Pd(OAc)_2$ (5 mol %), K_2CO_3 (1 equiv), PivOH (1 equiv), Ph-CF_3 (2 mL, 2 M), 110 °C, 18 h;
506 *iii*) DBU (3 equiv), toluene (1 M), 110 °C, 24 h; *iv*) Boc_2O (4 equiv), DMAP (20 mol %), CH_3CN
507 (0.5 M), 35 °C, 22 h; *v*) $LiAlH_4$ (2 equiv), THF, 20 °C, 0.5 h; *vi*) MsCl (1.3 equiv), Et_3N
508 (1.4 equiv), CH_2Cl_2 , 0 to 25 °C, 2 h; *vii*) X = Br: sesamol (1.6 equiv), NaH (1.7 equiv), THF, 0 to
509 70 °C, 18 h; *viii*) X = I: sesamol (2.0 equiv), NaH (2.2 equiv), DMF, 0 to 90 °C, 20 h; *ix*) 4 N HCl
510 in dioxane (10 equiv), 0 to 25 °C, 18 h.

511 **Figure 3. Inhibition of [^{3}H]5-HT transport and [^{3}H]citalopram binding by paroxetine and**
512 **the Br- and I-derivatives. a,** 5-HT-transport of wild-type SERT and its inhibition by paroxetine,
513 Br-, and I-paroxetine. Data are mean ± s.e.m. (n = 6). **b,** Competition binding of paroxetine and
514 its derivatives to ts2-inactive SERT. In panels a and b, paroxetine, Br-paroxetine, and I-
515 paroxetine curves are shown as black, red, and blue lines, respectively. Data are mean ± s.e.m.
516 (n = 6). **c,** Competition binding of paroxetine to ts2-active (black), Asn177Val (red), Asn177Thr

(green), and Asn177Gln (blue). Data are mean ± s.e.m. (n = 3). **d,** Competition binding of Br-paroxetine. Data are mean ± s.e.m. (n = 3). **e,** Competition binding of I-paroxetine. Data are mean ± s.e.m. (n = 3). The values associated with these experiments are reported in Table 2 and 3.

Figure 4. Structures of SERT-paroxetine complexes. a, Cryo-EM reconstruction of SERT bound to paroxetine where the shape of the SERT-8B6 Fab complex and detergent micelle is shown in transparent light grey. The density of SERT is shown in dark blue with TM1 and TM6 colored in orange and yellow, respectively, and the density for paroxetine in green. The variable domain of the 8B6 Fab is colored in purple. Inset shows the density features at the central site of paroxetine. **b,** Density feature at the central site of paroxetine. **c,** Density feature at the central site of Br-paroxetine. **d,** Density feature at the central site of I-paroxetine. **e,** Comparison of the binding poses of paroxetine (grey), Br-paroxetine (green), and I-paroxetine (orange). **f,** Anomalous difference electron density (blue) derived from Br-paroxetine, contoured at 5.2σ. **g,** Anomalous difference electron density (blue) derived from I-paroxetine, contoured at 4.3σ.

Figure 4 - figure supplement 1. Work-flow of cryo-EM data processing of ΔN72/ΔC13 SERT/8B6 Fab/paroxetine complexes. A representative zoomed, motion-corrected micrograph with individual single particles circled in white. Bar equals 20 nm. Motion-correction and CTF estimation was performed using MotionCor2 and Ctffind4. The number of movies/particles collected for each data set are shown in black (paroxetine), red (Br-paroxetine), and blue (I-paroxetine). After particle picking using either DoG picker or the blob picker in cryoSPARC, particles were sorted using heterogeneous refinement in cryoSPARC followed by 2D classification. For the DoG-picked particles, 3D classes containing SERT-Fab features (boxed) were combined and subjected to 2D classification. For cryoSPARC-picked particles, heterogeneous refinement was also used to initially sort particles in cryoSPARC. Classes with similar features (boxed) were combined, subjected to three independent 2D classifications, and

2D classes containing SERT-Fab features were combined. Particles picked by both methods were combined and duplicate particle-picks were removed in RELION (particle picks that are less than 100 Å of one another were considered duplicates).

Figure 4 - figure supplement 2. 3D refinement of ΔN72/ΔC13 SERT/8B6 Fab/paroxetine complexes. For the paroxetine complex, 3D refinement was performed in RELION followed by 3D classification without alignment and a mask which isolated SERT and Fab. 3D classification was not performed on the Br-paroxetine and I-paroxetine particles. Particles were further refined using non-uniform refinement in cryoSPARC, followed by local refinement in cisTEM with a mask which isolated SERT and the Fab variable domain and removed the Fab constant domain and micelle (mask is shown overlaid in blue on top of the Br-paroxetine reconstruction). The final reconstructed volume was sharpened using Phenix local sharpening.

Figure 4 - figure supplement 3. Cryo-EM reconstruction of ΔN72/ΔC13 SERT/8B6 Fab/paroxetine complexes. a, Reconstruction of SERT-8B6 paroxetine complex. Left panel, FSC curves for cross-validation, the final map (blue), masked SERT-Fv (red), and a mask which isolated SERT (black). The high-resolution limit cutoff for refinement was 4.5 Å. Middle left panel: model vs. half map 1 (working, red), half map 2 (free, black), model vs. final map (blue). Middle right panel: cryo-EM density map colored by local resolution estimation. Right panel: the angular distribution of particles used in the final reconstruction. **b,** Reconstruction of the SERT-8B6 Br-paroxetine complex. The high-resolution limit cutoff for refinement was 6.5 Å. **c,** Reconstruction of the SERT-8B6 I-paroxetine complex. The high-resolution limit cutoff for refinement was 6.5 Å.

Figure 4 - figure supplement 4. Cryo-EM density segments of the transmembrane helices. a, Density of TM1-12 of the paroxetine reconstruction, shown in blue. **b,** Density of TM1-12 of the Br-paroxetine reconstruction, shown in yellow. **c,** Density of TM1-12 of the I-paroxetine reconstruction, shown in purple.

Figure 4 - figure supplement 5. Comparison of the fit of paroxetine in the ABC and ACB poses. a, Shows the fit of paroxetine to the cryo-EM density in the ABC pose. **b,** Shows the fit in the ACB pose.

Figure 4 - figure supplement 6. Isomorphous difference densities at the central site. a, A negative difference density feature (red mesh, 4σ) was observed in subsite C for the F_o(paroxetine)-F_o(Br-paroxetine) map. **b,** A negative difference density feature (red mesh, 3.5σ) was observed in subsite C for the F_o(paroxetine)-F_o(I-paroxetine) map. **c,** No significant difference densities for the F_o(Br-paroxetine)-F_o(I-paroxetine) map was observed at 3.5σ (shown).

Figure 5. Comparison of the x-ray and cryo-EM structures of the SERT-paroxetine complex. a, Superposition of the x-ray ts3-SERT-8B6 paroxetine structure (PDB: 5I6X) with the SERT-8B6 paroxetine complex determined by cryo-EM. The root-mean-square-deviations (RMSD) for Cα positions were plotted onto the cryo-EM SERT-8B6 paroxetine structure. **b,** Comparison of the central binding site of the x-ray (grey) and cryo-EM (green) paroxetine structures. **c,** The structure of the ts2-inactive SERT-8B6 scFv/15B8 Fab paroxetine (cryo-EM, 6DZW), ts2-inactive SERT-8B6 Fab paroxetine (x-ray, 6AWN), and the SERT-8B6 paroxetine (cryo-EM, this work) complexes were superposed onto the ts3 SERT-8B6 paroxetine complex (x-ray, 5I6X) as a reference. The RMSD for Cα positions were calculated for each structure in comparison with the reference. Regions with RMSD > 3.0 Å are shown boxed in red.

Key resources table

Reagent type (species) or resource	Designation	Source or reference	Identifiers	Additional information
Gene *(Homo sapiens)*	Human serotonin transporter	cDNA	NCBI Reference Sequence : NP_001036.1	Dr. Randy D. Blakely (Florida Atlantic university brain institute)
Cell line *(Homo sapiens)*	HEK293S GnTI-	ATCC	Cat # ATCC CRL-3022	Used for expression of SERT (PMID: 27929454)
Cell line *(Spodoptera frugiperda)*	SF9 cells	ATCC	Cat # ATCC CRL-1711	Used in production of baculovirus for transduction, and SERT antibodies (PMID: 27929454)
Antibody	Mouse monoclonal. Isotype IgG2a, kappa	OHSU VGTI, Monoclonal Antibody Core		8B6
Transfected construct (human)	pEG BacMam	Gouaux lab		PMID: 25299155
Affinity chromatography resin	Strep-Tactin Superflow high capacity resin	Iba life sciences	Cat#2-1208-500	
Chemical compound, drug	n-dodecyl-β-D-maltoside	Anatrace	Cat # D310	Detergent
Chemical compound, drug	n-octyl β-D-maltoside	Anatrace	Cat # O310	Detergent
Chemical compound, drug	fluorinated octyl-maltoside	Anatrace	Cat # O310F	Detergent

Chemical compound, drug	Cholesteryl Hemisuccinate	Anatrace	Cat # CH210	Lipid
Chemical compound, drug	1-palmitoyl-2-oleoyl-sn-glycero-3-phosphocholine	Anatrace	Cat # P516	Lipid
Chemical compound, drug	1-palmitoyl-2-oleoyl-sn-glycero-3-phosphoethanolamine	Anatrace	Cat # P416	Lipid
Chemical compound, drug	1-palmitoyl-2-oleoyl-sn-glycero-3-phosphoglycerol	Anatrace	Cat # P616	Lipid
Chemical compound, drug	Paroxetine hydrochloride hemihydrate	Sigma	Cat # P9623	Inhibitor

Chemical compound, drug	[^{3}H]5-HT	PerkinElmer	Cat # NET1167250UC	Radiolabeled substrate
Chemical compound, drug	[^{3}H]citalopram	PerkinElmer	Cat # NET1039250UC	Radiolabeled inhibitor
Software, algorithm	XDS	PMID: 20124692	RRID:SCR_015652	http://xds.mpimf-heidelberg.mpg.de/
Software, algorithm	Phaser	PMID: 24189240	RRID:SCR_014219	https://www.phaser.cimr.cam.ac.uk/index.php/Phaser_Crystallographic_Software
Software, algorithm	Phenix	PMID: 22505256	RRID:SCR_014224	https://www.phenix-online.org/
Software, algorithm	SerialEM	PMID: 16182563	RRID:SCR_017293	http://bio3d.colorado.edu/SerialEM
Software, algorithm	MotionCor2	PMID: 28250466	RRID:SCR_016499	http://msg.ucsf.edu/em/software/motioncor2.html
Software, algorithm	CTFFIND4	PMID: 26278980	RRID:SCR_016732	https://grigoriefflab.umassmed.edu/ctffind4
Software, algorithm	DoG-Picker	PMID: 19374019		http://emg.nysbc.org/redmine/projects/software/wiki/DoGpicker
Software, algorithm	cryoSPARC	PMID: 28165473	RRID:SCR_016501	https://cryosparc.com/
Software, algorithm	RELION	PMID: 23000701	RRID:SCR_016274	http://www2.mrc-lmb.cam.ac.uk/relion
Software, algorithm	cisTEM	PMID: 29513216	RRID:SCR_016502	https://cistem.org/
Software, algorithm	UCSF-Chimera	PMID: 15264254	RRID:SCR_004097	https://www.cgl.ucsf.edu/chimera/
Software, algorithm	Coot	PMID: 15572765	RRID:SCR_014222	https://www2.mrc-lmb.cam.ac.uk/personal/pemsley/coot
Software, algorithm	MolProbity	PMID: 20057044	RRID:SCR_014226	http://molprobity.biochem.duke.edu/
Other	R 2/2 200 mesh Au holey	Electron Microscopy	Cat # Q2100AR2	Cryo-EM grids

	carbon grids	Sciences		
Other	Copper HIS-Tag YSI	PerkinElmer	Cat # RPNQ0096	SPA beads

591

592 **TABLES**

593 **Table 1. Expression constructs used in this study.**

Name	Expression construct	Experiment
Wild-type SERT	Full-length human SERT with a C-terminal thrombin-GFP-StrepII-His_{10} tag.	[^{3}H] 5-HT transport assays
ΔN72/ ΔC13 SERT	Wild-type SERT modified by deletion of 72 residues on N-term and 13 residues on C-term	Cryo-electron microscopy
ts2-inactive	Full-length SERT with thrombin cleavage sites inserted after Gln76 and Thr618 and carrying the Tyr110Ala, Ile291Ala thermostabilizing mutations with additional mutations of surface-exposed cysteines Cys554, Cys580, and Cys622 to alanine	X-ray crystallography and [^{3}H] citalopram binding assays
ts2-active	Full-length SERT with thrombin cleavage sites inserted after Gln76 and Thr618 and carrying the Ile291Ala, Thr439Ser thermostabilizing mutations with additional mutations of surface-exposed cysteines Cys554, Cys580, and Cys622 to alanine	[^{3}H] citalopram binding assays
Asn177 mutants	Asn177 mutated to either Val, Thr, or Gln in ts2-active background	[^{3}H] citalopram binding assays

594

595

596

597 **Table 2. Inhibition of 5-HT transport by paroxetine and its derivatives.**

Ligand	IC_{50}
Paroxetine	4 ± 1 nM
Br-paroxetine	40 ± 20 nM
I-paroxetine	0.18 ± 0.07 μM

598

599

Table 3. Binding of paroxetine and its derivatives to SERT variants used in this study.

SERT variant	K_i (nM)		
	Paroxetine	**Br-paroxetine**	**I-paroxetine**
ts2-inactive	0.17 ± 0.02	0.94 ± 0.01	2.3 ± 0.1
ts2-active	0.31 ± 0.07	0.4 ± 0.2	1.7 ± 0.3
Asn177Val	1.11 ± 0.04	5 ± 1	7.3 ± 0.9
Asn177Thr	1.0 ± 0.1	5 ± 2	4.4 ± 0.4
Asn177Gln	0.58 ± 0.07	4 ± 1	3.6 ± 0.4

618 **Table 4. Cryo-EM data collection, refinement and validation statistics[a].**

	#1 (EMDB-21368) (PDB 6VRH) (EMPIAR-10380)	#2 (EMDB-21369) (PDB 6VRK)	#3 (EMDB-21370) (PDB 6VRL)
Data collection and processing			
Magnification	77,160	77,160	77,160
Voltage (kV)	300	300	300
Electron exposure (e–/Å^2)	54-60	54	54
Defocus range (μm)	-0.8 to -2.2	-0.8 to -2.2	-0.8 to -2.2
Pixel size (Å)	0.648	0.648	0.648
Symmetry imposed	C1	C1	C1
Initial particle images (no.)	4,147,084	4,545,318	4,470,768
Final particle images (no.)	420,373	503,993	414,091
Map resolution (Å)	3.3	4.1	3.8
FSC threshold	0.143	0.143	0.143
Map resolution range (Å)[b]	4.25-3.25	5.75-3.75	5.50-3.50
Refinement			
Initial model used (PDB code)	6AWN	6VRH	6VRH
Initial model CC	0.64	0.70	0.71
Model resolution (Å)[c]	3.7	4.3	4.1
FSC threshold	0.5	0.5	0.5
Model resolution range (Å)	25.9-3.3	33.0-4.1	29.6-4.2
Map sharpening *B* factor (Å^2)	-85	-174	-161
Model composition			
Non-hydrogen atoms	6143	6142	6142
Protein residues	764	764	764
Ligands (atoms)	254	254	254
B factors (Å^2)			
Protein	138	138	122
Ligand	129	113	112
R.m.s. deviations			
Bond lengths (Å)	0.002	0.002	0.002
Bond angles (°)	0.48	0.59	0.54
Validation			
Refined model CC	0.73	0.74	0.75
MolProbity score	1.86	1.96	1.88
Clashscore	9.67	10.26	10.59
Poor rotamers (%)	0	0	0.00
Ramachandran plot			
Favored (%)	94.84	93.54	95.12
Allowed (%)	5.16	6.46	4.88
Disallowed (%)	0	0	0

619 [a]Data set #1 is the paroxetine reconstruction, #2 is Br-paroxetine, #3 I-paroxetine.
620 [b]Local resolution range.
621 [c]Resolution at which FSC between map and model is 0.5.

Table 5. X-ray data collection statistics.

	Br-paroxetine (PDB 6W2B)	I-paroxetine (PDB 6W2C)
Data collection		
Space group	$C222_1$	$C222_1$
Cell dimensions		
a, *b*, *c* (Å)	128.0, 161.9, 139.7	127.7, 161.9, 140.8
α, β, γ (°)	90, 90, 90	90, 90, 90
Resolution (Å)	20.45-4.69 (4.82-4.69)*	25.98-6.12 (6.30-6.12)*
R_{merge}	13.60 (339.3)	7.9 (292.9)
$I / \sigma I$	5.51 (0.49)	5.01 (0.32)
$CC_{1/2}$	99.9 (16.5)	99.8 (20.0)
Completeness (%)	99.2 (100.0)	92.6 (89.7)
Redundancy	6.8 (6.2)	1.8 (1.7)

*Values in parentheses are for highest-resolution shell.

APPENDIX

Appendix 1. Synthesis and characterization of paroxetine analogues. C-H functionalization strategy was used to generate bromo- and iodo-substituted enantiopure analogues of paroxetine. The enantiopurity was analyzed by HPLC, and the integrity of intermediates and the final products of the synthetic route were characterized using NMR, IR, and mass spectrometric methods.

COMPETING INTERESTS

The authors declare no competing interests.

REFERENCES

1 Berger, M., Gray, J. A. & Roth, B. L. The expanded biology of serotonin. *Annu Rev Med* **60**, 355-366, doi:10.1146/annurev.med.60.042307.110802 (2009).

2 Gether, U., Andersen, P. H., Larsson, O. M. & Schousboe, A. Neurotransmitter transporters: molecular function of important drug targets. *Trends Pharmacol Sci* **27**, 375-383, doi:10.1016/j.tips.2006.05.003 (2006).

3 Kristensen, A. S. *et al.* SLC6 neurotransmitter transporters: structure, function, and regulation. *Pharmacol Rev* **63**, 585-640, doi:10.1124/pr.108.000869 (2011).

4 Rudnick, G., Kramer, R., Blakely, R. D., Murphy, D. L. & Verrey, F. The SLC6 transporters: perspectives on structure, functions, regulation, and models for transporter dysfunction. *Pflugers Arch* **466**, 25-42, doi:10.1007/s00424-013-1410-1 (2014).

5 Navratna, V. & Gouaux, E. Insights into the mechanism and pharmacology of neurotransmitter sodium symporters. *Curr Opin Struct Biol* **54**, 161-170, doi:10.1016/j.sbi.2019.03.011 (2019).

6 Yamashita, A., Singh, S. K., Kawate, T., Jin, Y. & Gouaux, E. Crystal structure of a bacterial homologue of Na+/Cl--dependent neurotransmitter transporters. *Nature* **437**, 215-223, doi:10.1038/nature03978 (2005).

7 Cipriani, A. *et al.* Comparative efficacy and acceptability of 21 antidepressant drugs for the acute treatment of adults with major depressive disorder: a systematic review and network meta-analysis. *Lancet* **391**, 1357-1366, doi:10.1016/S0140-6736(17)32802-7 (2018).

8 Coleman, J. A. & Gouaux, E. Structural basis for recognition of diverse antidepressants by the human serotonin transporter. *Nat Struct Mol Biol* **25**, 170-175, doi:10.1038/s41594-018-0026-8 (2018).

9 Coleman, J. A., Green, E. M. & Gouaux, E. X-ray structures and mechanism of the human serotonin transporter. *Nature* **532**, 334-339, doi:10.1038/nature17629 (2016).

10 Wang, H. *et al.* Structural basis for action by diverse antidepressants on biogenic amine transporters. *Nature* **503**, 141-145, doi:10.1038/nature12648 (2013).

11 Penmatsa, A., Wang, K. H. & Gouaux, E. X-ray structures of Drosophila dopamine transporter in complex with nisoxetine and reboxetine. *Nat Struct Mol Biol* **22**, 506-508, doi:10.1038/nsmb.3029 (2015).

12 Wang, K. H., Penmatsa, A. & Gouaux, E. Neurotransmitter and psychostimulant recognition by the dopamine transporter. *Nature* **521**, 322-327, doi:10.1038/nature14431 (2015).

13 Zhong, H. *et al.* An allosteric binding site at the human serotonin transporter mediates the inhibition of escitalopram by R-citalopram: kinetic binding studies with the ALI/VFL-SI/TT mutant. *Neurosci Lett* **462**, 207-212, doi:10.1016/j.neulet.2009.07.030 (2009).

14 Wennogle, L. P. & Meyerson, L. R. Serotonin modulates the dissociation of [3H]imipramine from human platelet recognition sites. *Eur J Pharmacol* **86**, 303-307, doi:10.1016/0014-2999(82)90333-8 (1982).

15 Plenge, P. & Mellerup, E. T. Antidepressive drugs can change the affinity of [3H]imipramine and [3H]paroxetine binding to platelet and neuronal membranes. *Eur J Pharmacol* **119**, 1-8, doi:10.1016/0014-2999(85)90314-0 (1985).

16 Cool, D. R., Leibach, F. H. & Ganapathy, V. High-affinity paroxetine binding to the human placental serotonin transporter. *Am J Physiol* **259**, C196-204, doi:10.1152/ajpcell.1990.259.2.C196 (1990).

17 Nevels, R. M., Gontkovsky, S. T. & Williams, B. E. Paroxetine-The Antidepressant from Hell? Probably Not, But Caution Required. *Psychopharmacol Bull* **46**, 77-104 (2016).

18 Abramyan, A. M. *et al.* Computation-guided analysis of paroxetine binding to hSERT reveals functionally important structural elements and dynamics. *Neuropharmacology* **161**, 107411, doi:10.1016/j.neuropharm.2018.10.040 (2019).

19 Davis, B. A., Nagarajan, A., Forrest, L. R. & Singh, S. K. Mechanism of Paroxetine (Paxil) Inhibition of the Serotonin Transporter. *Sci Rep* **6**, 23789, doi:10.1038/srep23789 (2016).

20 Slack, R. D. *et al.* A Novel Bromine-Containing Paroxetine Analogue Provides Mechanistic Clues for Binding Ambiguity at the Central Primary Binding Site of the Serotonin Transporter. *ACS Chem Neurosci* **10**, 3946-3952, doi:10.1021/acschemneuro.9b00375 (2019).

21 He, J., Wasa, M., Chan, K. S. L., Shao, Q. & Yu, J. Q. Palladium-Catalyzed Transformations of Alkyl C-H Bonds. *Chem Rev* **117**, 8754-8786, doi:10.1021/acs.chemrev.6b00622 (2017).

22 Rej, S., Ano, Y. & Chatani, N. Bidentate Directing Groups: An Efficient Tool in C-H Bond Functionalization Chemistry for the Expedient Construction of C-C Bonds. *Chem Rev*, doi:10.1021/acs.chemrev.9b00495 (2020).

23 Antermite, D. & Bull, J. Transition Metal-Catalyzed Directed C(sp3)–H Functionalization of Saturated Heterocycles. *Synthesis* **51**, doi:10.1055/s-0037-1611822 (2019).

24 DH, O. D. *et al.* C-H Activation Enables a Concise Total Synthesis of Quinine and Analogues with Enhanced Antimalarial Activity. *Angew Chem Int Ed Engl* **57**, 10737-10741, doi:10.1002/anie.201804551 (2018).

25 Maetani, M. *et al.* Synthesis of a Bicyclic Azetidine with In Vivo Antimalarial Activity Enabled by Stereospecific, Directed C(sp(3))-H Arylation. *J Am Chem Soc* **139**, 11300-11306, doi:10.1021/jacs.7b06994 (2017).

26 Chapman, L. M., Beck, J. C., Wu, L. & Reisman, S. E. Enantioselective Total Synthesis of (+)-Psiguadial B. *J Am Chem Soc* **138**, 9803-9806, doi:10.1021/jacs.6b07229 (2016).

27 Antermite, D., Affron, D. P. & Bull, J. A. Regio- and Stereoselective Palladium-Catalyzed C(sp(3))-H Arylation of Pyrrolidines and Piperidines with C(3) Directing Groups. *Org Lett* **20**, 3948-3952, doi:10.1021/acs.orglett.8b01521 (2018).

28 Johnson, T. A., Curtis, M. D. & Beak, P. Highly diastereoselective and enantioselective carbon-carbon bond formations in conjugate additions of lithiated N-Boc allylamines to nitroalkenes: enantioselective synthesis of 3,4- and 3,4,5-substituted piperidines including (-)-paroxetine. *J Am Chem Soc* **123**, 1004-1005, doi:10.1021/ja005748w (2001).

29 Hughes, G., Kimura, M. & Buchwald, S. L. Catalytic enantioselective conjugate reduction of lactones and lactams. *J Am Chem Soc* **125**, 11253-11258, doi:10.1021/ja0351692 (2003).

30 Brandau, S., Landa, A., Franzen, J., Marigo, M. & Jorgensen, K. A. Organocatalytic conjugate addition of malonates to alpha,beta-unsaturated aldehydes: asymmetric formal synthesis of (-)-paroxetine, chiral lactams, and lactones. *Angew Chem Int Ed Engl* **45**, 4305-4309, doi:10.1002/anie.200601025 (2006).

31 Krautwald, S., Schafroth, M. A., Sarlah, D. & Carreira, E. M. Stereodivergent alpha-allylation of linear aldehydes with dual iridium and amine catalysis. *J Am Chem Soc* **136**, 3020-3023, doi:10.1021/ja5003247 (2014).

32 Wang, Y. M., Bruno, N. C., Placeres, A. L., Zhu, S. & Buchwald, S. L. Enantioselective Synthesis of Carbo- and Heterocycles through a CuH-Catalyzed Hydroalkylation Approach. *J Am Chem Soc* **137**, 10524-10527, doi:10.1021/jacs.5b07061 (2015).

33 Kubota, K., Watanabe, Y., Hayama, K. & Ito, H. Enantioselective Synthesis of Chiral Piperidines via the Stepwise Dearomatization/Borylation of Pyridines. *J Am Chem Soc* **138**, 4338-4341, doi:10.1021/jacs.6b01375 (2016).

34 Amat, M. *et al.* Synthesis of enantiopure trans-3,4-disubstituted piperidines. An enantiodivergent synthesis of (+)- and (-)-paroxetine. *J Org Chem* **65**, 3074-3084, doi:10.1021/jo991816p (2000).

35 Zaitsev, V. G., Shabashov, D. & Daugulis, O. Highly regioselective arylation of sp3 C-H bonds catalyzed by palladium acetate. *J Am Chem Soc* **127**, 13154-13155, doi:10.1021/ja054549f (2005).

36 Green, E. M., Coleman, J. A. & Gouaux, E. Thermostabilization of the Human Serotonin Transporter in an Antidepressant-Bound Conformation. *PLoS One* **10**, e0145688, doi:10.1371/journal.pone.0145688 (2015).

37 Coleman, J. A. *et al.* Serotonin transporter-ibogaine complexes illuminate mechanisms of inhibition and transport. *Nature* **569**, 141-145, doi:10.1038/s41586-019-1135-1 (2019).

38 Coleman, J. A., Green, E. M. & Gouaux, E. Thermostabilization, Expression, Purification, and Crystallization of the Human Serotonin Transporter Bound to S-citalopram. *J Vis Exp*, doi:10.3791/54792 (2016).

39 Rannversson, H., Andersen, J., Bang-Andersen, B. & Stromgaard, K. Mapping the Binding Site for Escitalopram and Paroxetine in the Human Serotonin Transporter Using Genetically Encoded Photo-Cross-Linkers. *ACS Chem Biol* **12**, 2558-2562, doi:10.1021/acschembio.7b00338 (2017).

40 Kabsch, W. Xds. *Acta Crystallogr D Biol Crystallogr* **66**, 125-132, doi:10.1107/S0907444909047337 (2010).

41 Bunkoczi, G. *et al.* Phaser.MRage: automated molecular replacement. *Acta Crystallogr D Biol Crystallogr* **69**, 2276-2286, doi:10.1107/S0907444913022750 (2013).

42 Afonine, P. V. *et al.* Towards automated crystallographic structure refinement with phenix.refine. *Acta Crystallogr D Biol Crystallogr* **68**, 352-367, doi:10.1107/S0907444912001308 (2012).

43 Mastronarde, D. N. Automated electron microscope tomography using robust prediction of specimen movements. *J Struct Biol* **152**, 36-51, doi:10.1016/j.jsb.2005.07.007 (2005).

44 Zheng, S. Q. *et al.* MotionCor2: anisotropic correction of beam-induced motion for improved cryo-electron microscopy. *Nat Methods* **14**, 331-332, doi:10.1038/nmeth.4193 (2017).

45 Rohou, A. & Grigorieff, N. CTFFIND4: Fast and accurate defocus estimation from electron micrographs. *J Struct Biol* **192**, 216-221, doi:10.1016/j.jsb.2015.08.008 (2015).

46 Voss, N. R., Yoshioka, C. K., Radermacher, M., Potter, C. S. & Carragher, B. DoG Picker and TiltPicker: software tools to facilitate particle selection in single particle electron microscopy. *J Struct Biol* **166**, 205-213, doi:10.1016/j.jsb.2009.01.004 (2009).

47 Punjani, A., Rubinstein, J. L., Fleet, D. J. & Brubaker, M. A. cryoSPARC: algorithms for rapid unsupervised cryo-EM structure determination. *Nat Methods* **14**, 290-296, doi:10.1038/nmeth.4169 (2017).

48 Scheres, S. H. RELION: implementation of a Bayesian approach to cryo-EM structure determination. *J Struct Biol* **180**, 519-530, doi:10.1016/j.jsb.2012.09.006 (2012).

49 Grant, T., Rohou, A. & Grigorieff, N. cisTEM, user-friendly software for single-particle image processing. *Elife* **7**, doi:10.7554/eLife.35383 (2018).

50 Rosenthal, P. B. & Henderson, R. Optimal determination of particle orientation, absolute hand, and contrast loss in single-particle electron cryomicroscopy. *J Mol Biol* **333**, 721-745, doi:10.1016/j.jmb.2003.07.013 (2003).

51 Pettersen, E. F. *et al.* UCSF Chimera--a visualization system for exploratory research and analysis. *J Comput Chem* **25**, 1605-1612, doi:10.1002/jcc.20084 (2004).

52 Emsley, P. & Cowtan, K. Coot: model-building tools for molecular graphics. *Acta Crystallogr D Biol Crystallogr* **60**, 2126-2132, doi:10.1107/S0907444904019158 (2004).

53 Chen, V. B. *et al.* MolProbity: all-atom structure validation for macromolecular crystallography. *Acta Crystallogr D Biol Crystallogr* **66**, 12-21, doi:10.1107/S0907444909042073 (2010).

54 Cheng, Y. & Prusoff, W. H. Relationship between the inhibition constant (K1) and the concentration of inhibitor which causes 50 per cent inhibition (I50) of an enzymatic reaction. *Biochem Pharmacol* **22**, 3099-3108, doi:10.1016/0006-2952(73)90196-2 (1973).

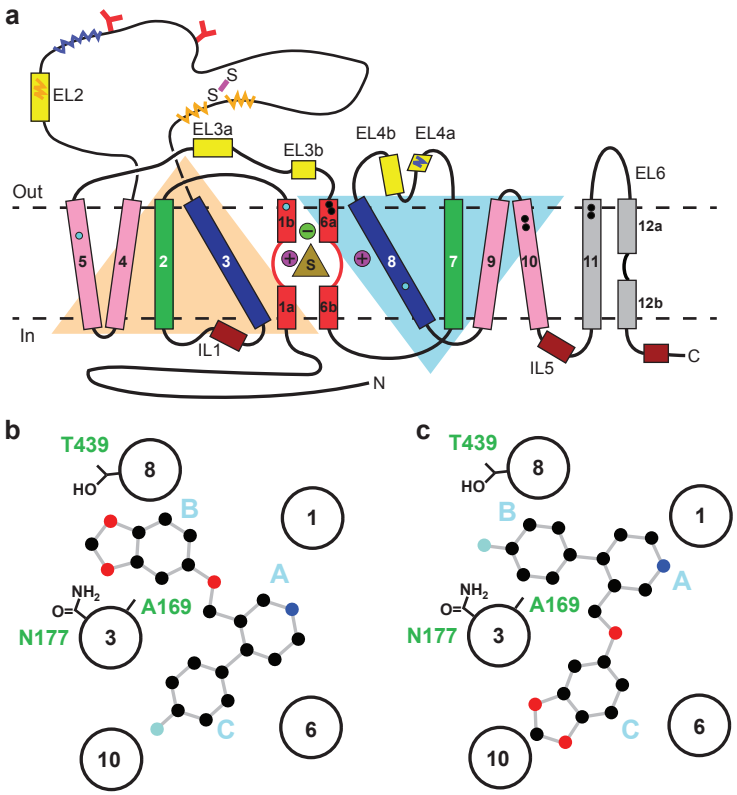
a
EL2
S
S
EL3a
EL3b
EL4b
EL4a
EL6
Out
In
1b
6a
1a
6b
S
5
4
2
3
8
7
9
10
11
12a
12b
IL1
IL5
C
N
b
T439
HO
8
B
1
A
NH2
O=
A169
N177
3
C
6
10
c
T439
HO
8
B
1
A
NH2
O=
A169
N177
3
C
6
10

Figure 1

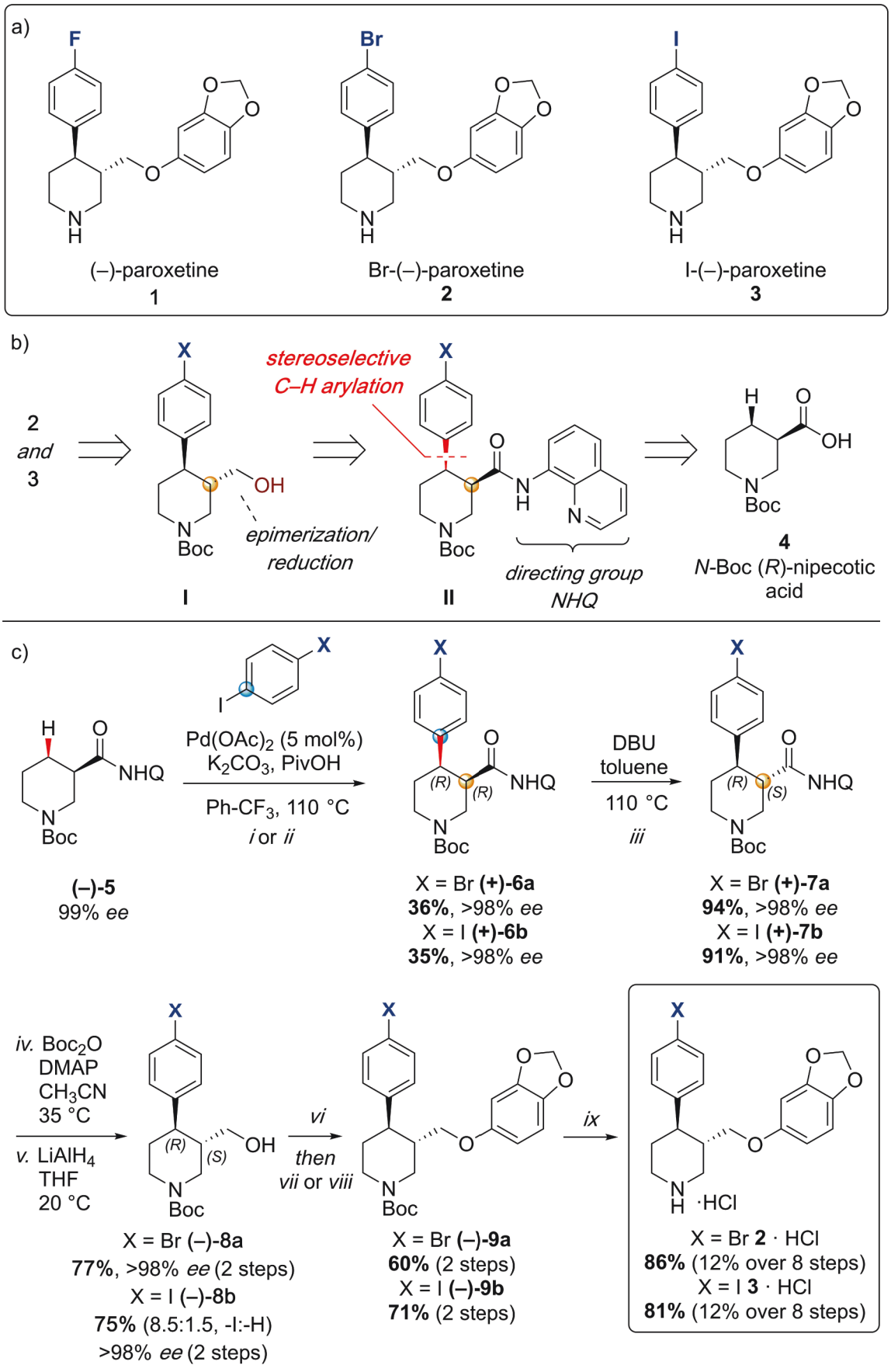
a)
F
Br
I
(–)-paroxetine
1
Br-(–)-paroxetine
2
I-(–)-paroxetine
3
b)
2
and
3
X
OH
epimerization/
reduction
I
stereoselective
C–H arylation
II
directing group
NHQ
H
O
OH
Boc
4
N-Boc (R)-nipecotic
acid
c)
NHQ
Boc
(–)-5
99% ee
Pd(OAc)2 (5 mol%)
K2CO3, PivOH
Ph-CF3, 110 °C
i or ii
(R)
(R)
X = Br (+)-6a
36%, >98% ee
X = I (+)-6b
35%, >98% ee
DBU
toluene
110 °C
iii
(S)
X = Br (+)-7a
94%, >98% ee
X = I (+)-7b
91%, >98% ee
iv. Boc2O
DMAP
CH3CN
35 °C
v. LiAlH4
THF
20 °C
X = Br (–)-8a
77%, >98% ee (2 steps)
X = I (–)-8b
75% (8.5:1.5, -I:-H)
>98% ee (2 steps)
vi
then
vii or viii
X = Br (–)-9a
60% (2 steps)
X = I (–)-9b
71% (2 steps)
ix
·HCl
X = Br 2 · HCl
86% (12% over 8 steps)
X = I 3 · HCl
81% (12% over 8 steps)

Figure 2

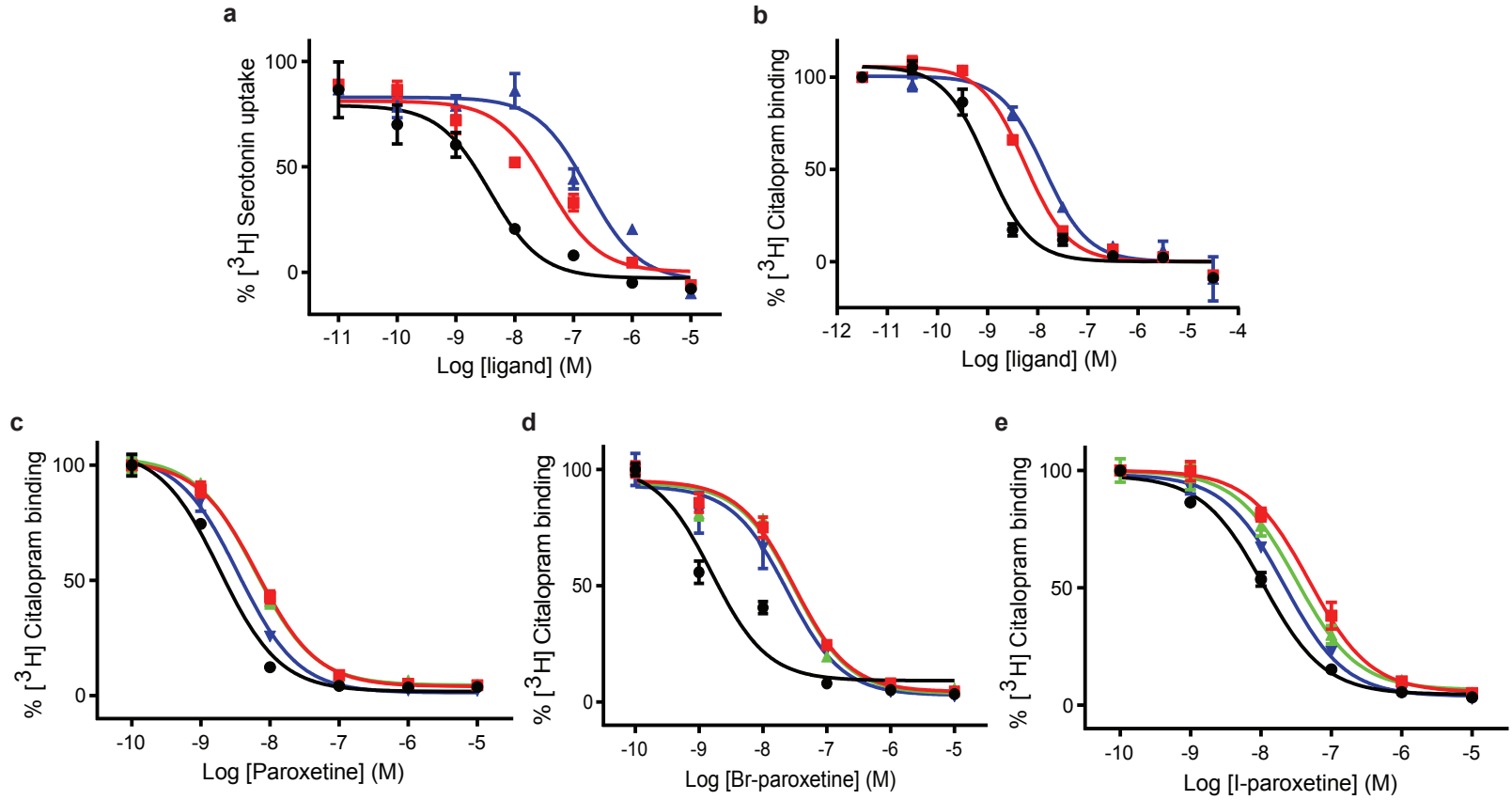
a
% [3H] Serotonin uptake
100
50
0
-11 -10 -9 -8 -7 -6 -5
Log [ligand] (M)
b
% [3H] Citalopram binding
100
50
0
-12 -11 -10 -9 -8 -7 -6 -5 -4
Log [ligand] (M)
c
% [3H] Citalopram binding
100
50
0
-10 -9 -8 -7 -6 -5
Log [Paroxetine] (M)
d
% [3H] Citalopram binding
100
50
0
-10 -9 -8 -7 -6 -5
Log [Br-paroxetine] (M)
e
% [3H] Citalopram binding
100
50
0
-10 -9 -8 -7 -6 -5
Log [I-paroxetine] (M)

Figure 3

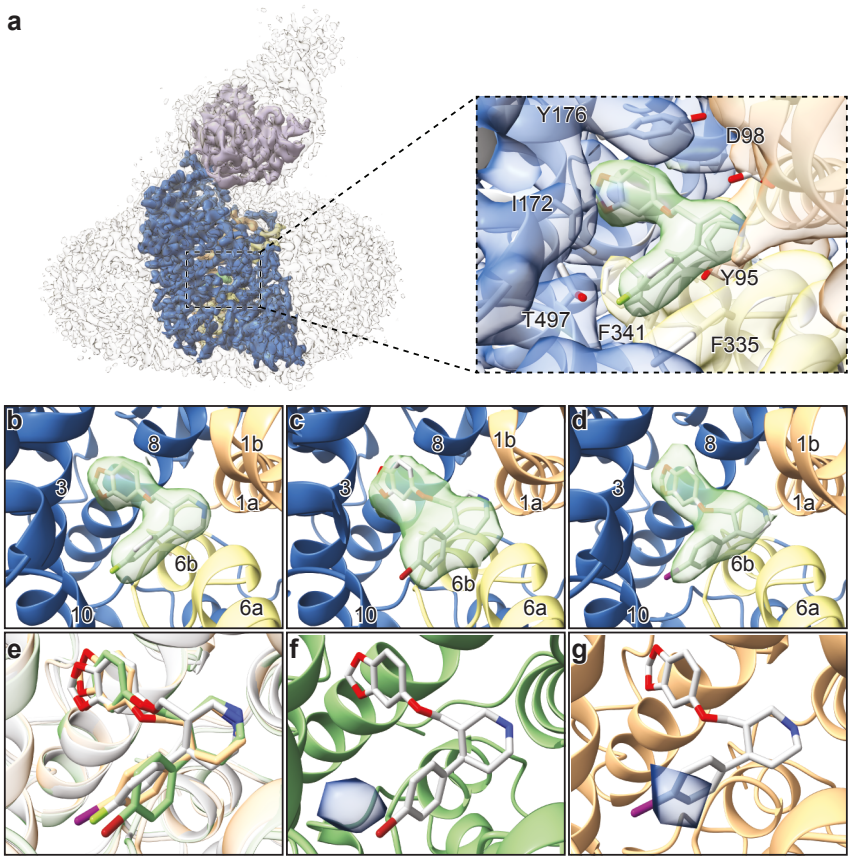
a
Y176
D98
I172
Y95
T497
F341
F335
b
8
1b
3
1a
6b
10
6a
c
8
1b
3
1a
6b
10
6a
d
8
1b
3
1a
6b
10
6a
e
f
g

Figure 4

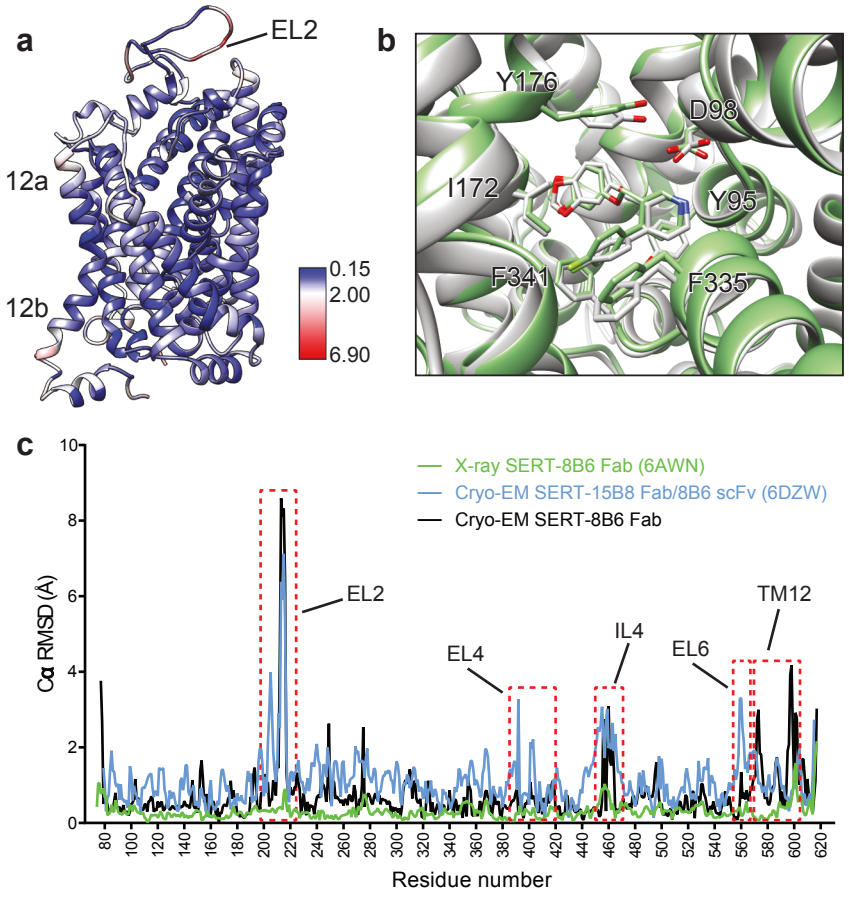
a
EL2
12a
12b
0.15
2.00
6.90
b
Y176
D98
I172
Y95
F341
F335
c
X-ray SERT-8B6 Fab (6AWN)
Cryo-EM SERT-15B8 Fab/8B6 scFv (6DZW)
Cryo-EM SERT-8B6 Fab
Cα RMSD (Å)
EL2
EL4
IL4
EL6
TM12
Residue number

Figure 5

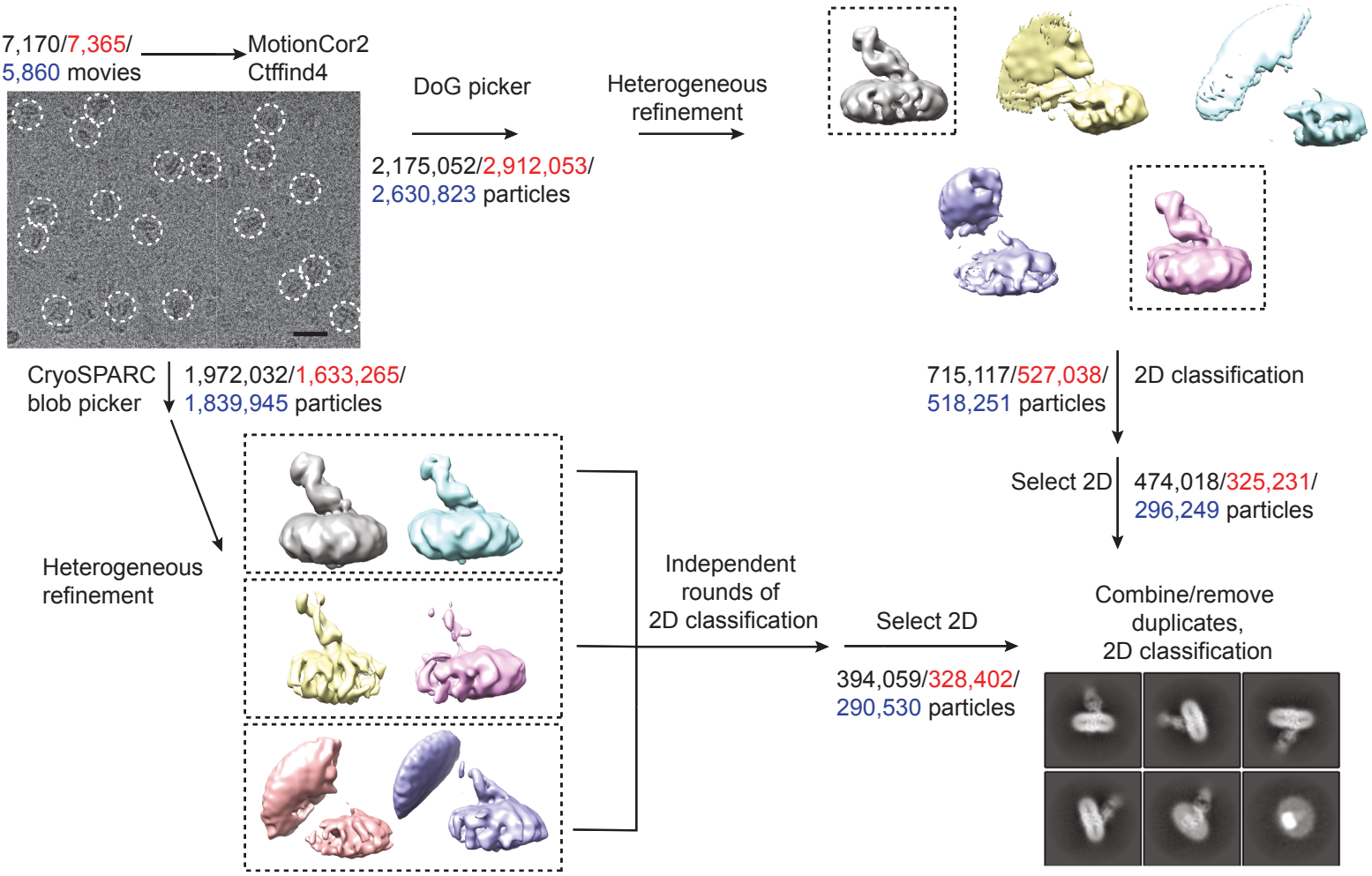

Figure 4 - figure supplement 1

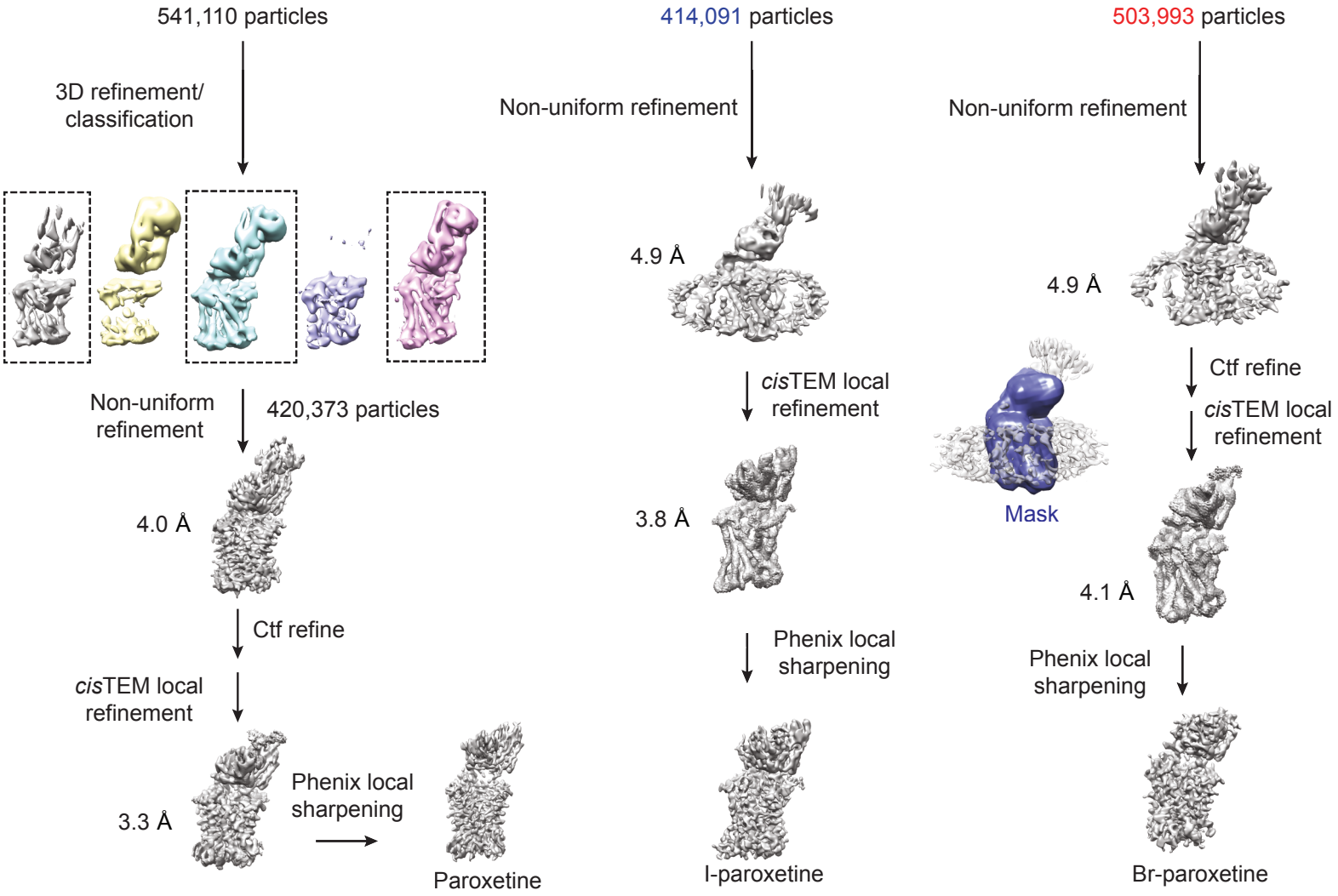

Figure 4 - figure supplement 2

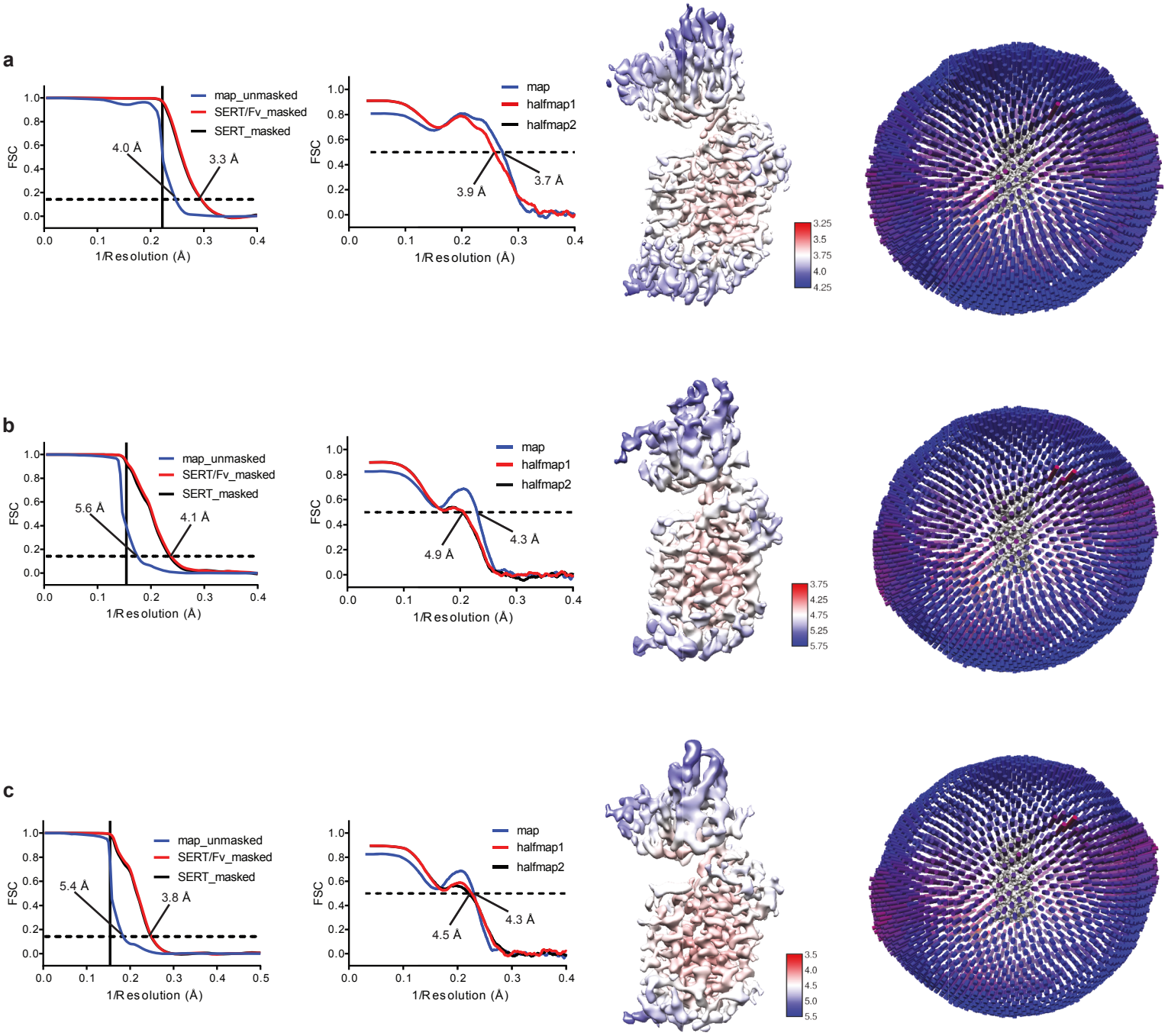

Figure 4 - figure supplement 3

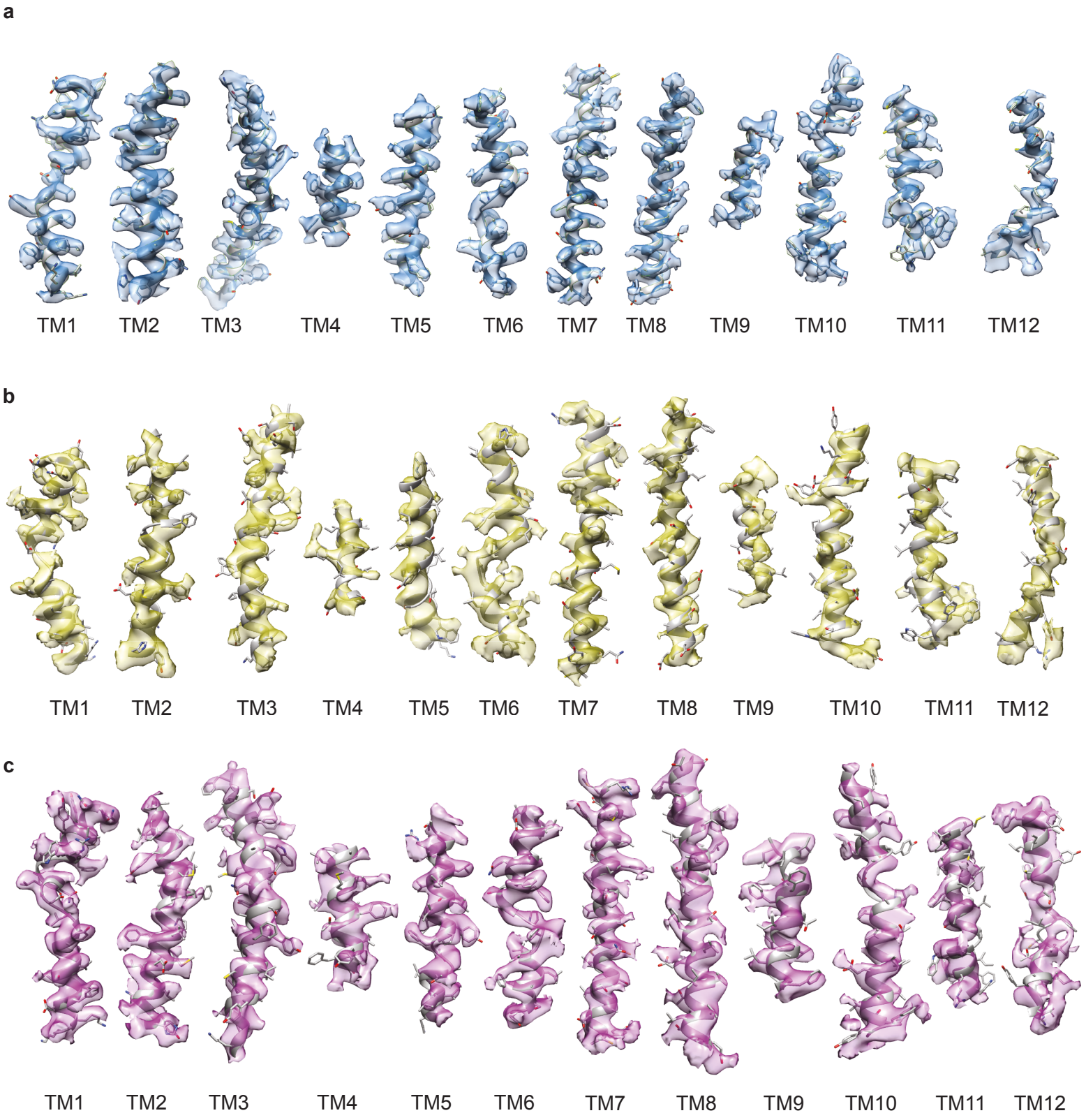

Figure 4 - figure supplement 4

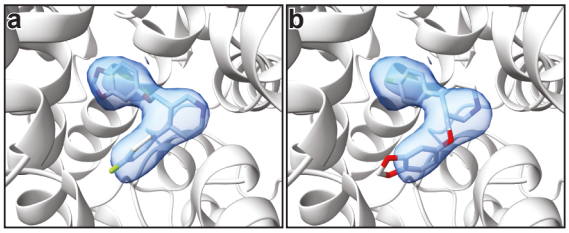

Figure 4 - figure supplement 5

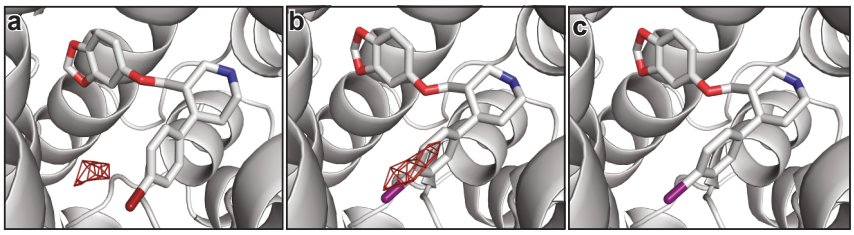

Figure 4 - figure supplement 6

Appendix 1. Synthesis of paroxetine analogues.

Reagents

Commercial reagents were used as supplied or purified by standard techniques where necessary.

$Pd(OAc)_2$, 8-Aminoquinoline, 1-(*tert*-butoxycarbonyl)piperidine-3-carboxylic acid and (*R*)-1-(*tert*-butoxycarbonyl)piperidine-3-carboxylic acid were purchased from Fluorochem Ltd and used as supplied.

PivOH and α,α,α-trifluorotoluene were purchased from Sigma-Aldrich Company Ltd and used as supplied.

K_2CO_3 was purchased from Sigma-Aldrich Company Ltd and flame-dried before use as part of reaction set-up.

Purity: $Pd(OAc)_2$, >98%; PivOH, 99%; K_2CO_3, ≥98% (powder, –325 mesh), α,α,α-trifluorotoluene, anhydrous, ≥99%.

Racemic and enantioenriched substrates *tert*-butyl (±)-3-(quinoline-8-ylcarbamoyl)piperidine-1-carboxylate (**(±)-S1**) and *tert*-butyl (–)-(*R*)-3-(quinolin-8-ylcarbamoyl)piperidine-1-carboxylate (**(–)-5**) were prepared by amide coupling of commercially available 8-aminoquinoline and the corresponding carboxylic acid (1-(*tert*-butoxycarbonyl)piperidine-3-carboxylic acid and (*R*)-1-(*tert*-butoxycarbonyl)piperidine-3-carboxylic acid, respectively) according to our previously reported procedures.[27]

Structures of Additional Compounds in Appendix 1

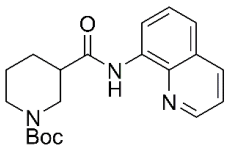

(±)-**S1**

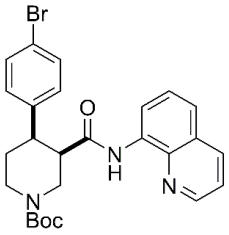

(±)-**S2a**

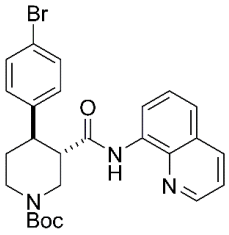

(±)-**S3a**

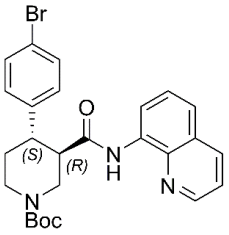

(–)-**S3a**

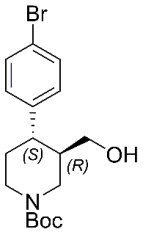

(+)-**S4a**

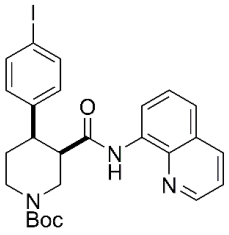

(±)-**S2b**

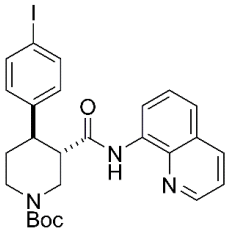

(±)-**S3b**

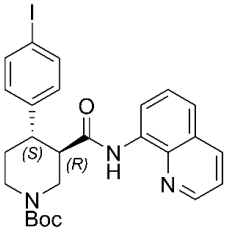

(–)-**S3b**

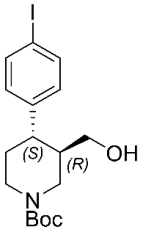

(+)-**S4b**

Full Synthetic Route to Racemic and Enantioenriched Br-Piperidine Derivatives (±)-S2a, (±)-S3a, (+)-6a, (+)-7a, (–)-S3a, (–)-8a, (+)-S4a, (–)-9a and Br-(–)-paroxetine 2

In order to evaluate the enantiomeric excess of key intermediates **(+)-6a** and **(+)-7a** by chiral HPLC, the C–H arylation with 4-bromo iodobenzene was performed on both racemic (**(±)-S1**) and enantioenriched **(–)-5** piperidine amide substrates (Scheme S1).

The racemic synthesis was performed on a 0.5 mmol scale according to our previously reported protocol,[27] and afforded *cis*-arylated derivatives **(±)-S2a** in 34% (Scheme S1a). A minor *trans*-functionalized product **(±)-S3a**, formed via a *trans*-palladacycle,[27] was also isolated in 14%.
C–H Arylation of enantioenriched substrate **(–)-5** proceed smoothly on a 4.0 mmol scale, and *cis*- and *trans*-piperidine products **(+)-6a** and **(–)-S3a** were isolated as single enantiomers in very similar yields (Scheme S1b). Subsequent treatment of enantiopure *cis*-derivative **(+)-6a** with DBU at 100 °C afforded the *trans*-diastereomer as the right-handed enantiomer **(+)-7a** in 94% yield.

Scheme S1. Synthetic sequence, including the Pd-catalyzed C(4)–H arylation step, to access racemic and enantioenriched *cis*- and *trans*-piperidine amide derivatives (±)-S2a, (±)-S3a, (+)-6a, (+)-7a and (–)-S3a

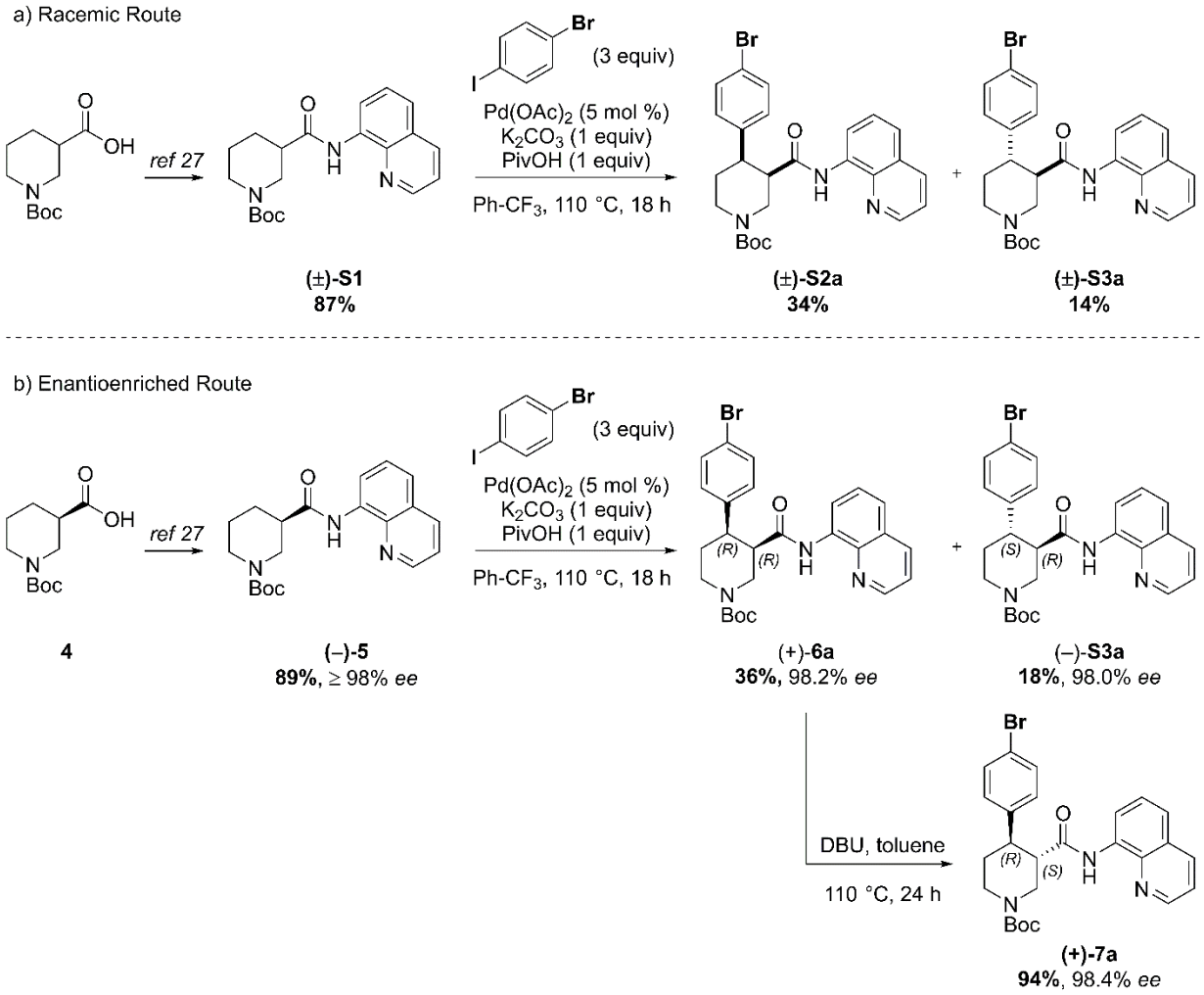

a) C–H Arylation conditions: **(±)-S1** (0.5 mmol, 1 equiv) Ph-CF_3 (500 µL, 1 M). b) C–H Arylation conditions: **(–)-5** (4.0 mmol, 1 equiv), Ph-CF_3 (2.0 mL, 2 M).

The enantiomeric excess of alcohol intermediates **(+)-S4a** and **(–)-8a** was evaluated after aminoquinoline removal on both enantiomeric *trans*-derivatives **(–)-S3a** and **(+)-7a** (Scheme S2).

No undesired debromination was observed for the reductive aminoquinoline removal, and enantiopure alcohols **(+)-S4a** and **(–)-8a** were obtained in 70% and 77% yield, respectively.
No erosion of enantiopurity should be expected after this step, given the literature precedents on the synthesis of (–)-paroxetine[34] and the absence of acidic protons in the substrate. Therefore, the synthesis was continued exclusively on alcohol derivative **(–)-8a**. O-Alkylation and Boc-deprotection with HCl finally afforded enantiopure Br-(–)-paroxetine analogue **2** as the corresponding hydrochloride salt in 12% yield over 8 steps from commercial material.

Scheme S2. Reductive aminoquinoline removal and final steps in the synthesis of Br-(–)-paroxetine 2.

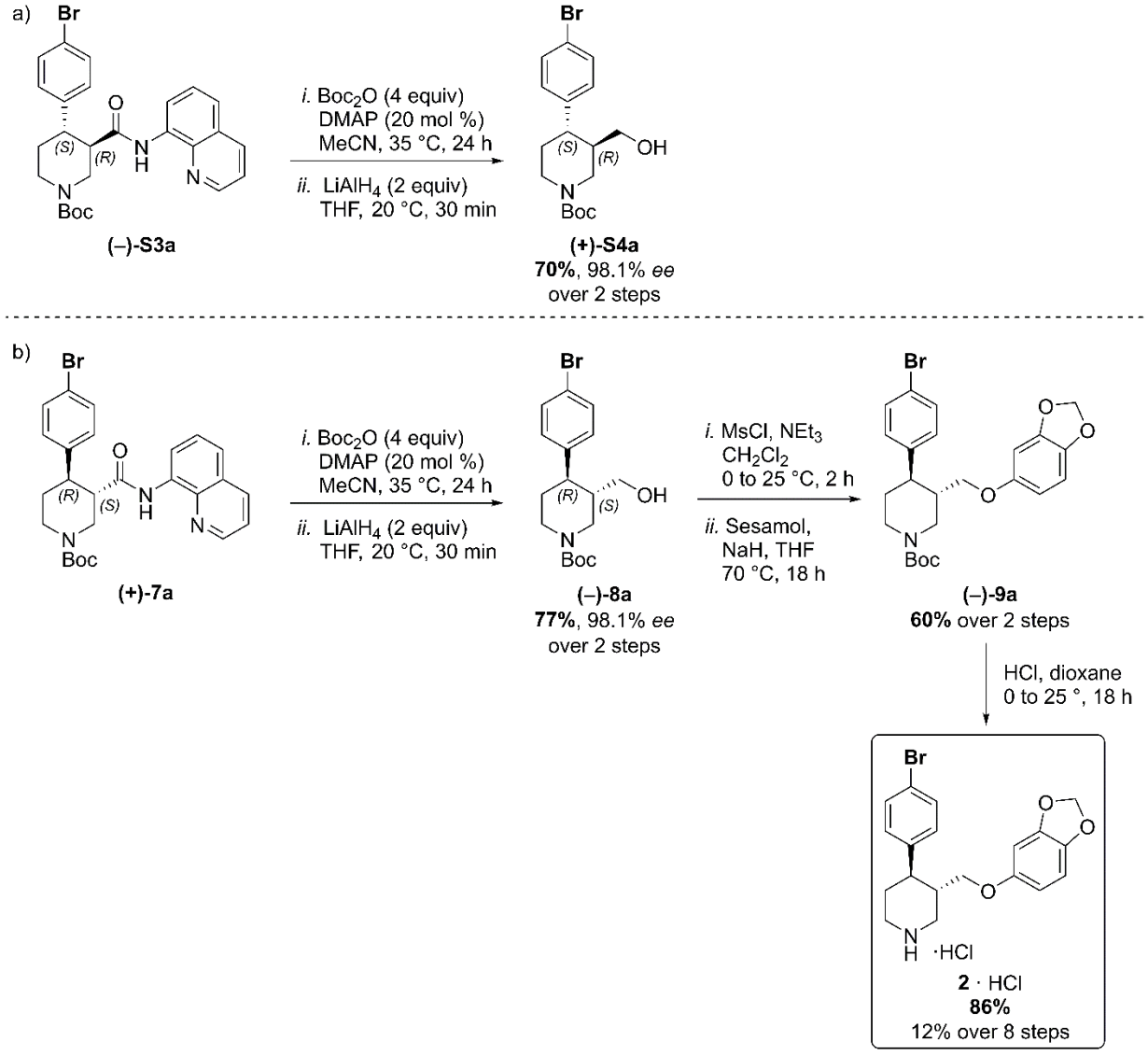

a) AQ removal on enantiomerically pure *trans*-piperidine **(–)-S3a** (0.2 mmol, 1 equiv). b) AQ removal on enantiomerically pure *trans*-piperidine **(+)-7a** (1.1 mmol, 1 equiv) and final steps in the synthesis of Br-(–)-paroxetine **2**.

Full Synthetic Route to Racemic and Enantioenriched I-Piperidine Derivatives (±)-S2b, (±)-S3b, (+)-6b, (+)-7b, (–)-S3b, (–)-8b, (+)-S4b, (–)-9b and I-(–)-paroxetine 3

Similarly to the Br-analogue, C–H arylation with 1,4-diiodobenzene was performed on both racemic (**(±)-S1**) and enantioenriched (**(–)-5**) piperidine amide substrates (Scheme S3).

The reaction proceeded well on both substrates affording racemic *cis*- and *trans*-arylated products **(±)-S2b** and **(±)-S3b** in 35% and 19% yield, and enantioenriched *cis*- and *trans*-derivatives **(+)-6b** and **(–)-S3b** in 35% and 20% yield respectively.

Scheme S3. Synthetic sequence, including the Pd-catalyzed C(4)–H arylation step, to access racemic and enantioenriched *cis*- and *trans*-piperidine amide derivatives (±)-S2b, (±)-S3b, (+)-6b, (+)-7b and (–)-S3b

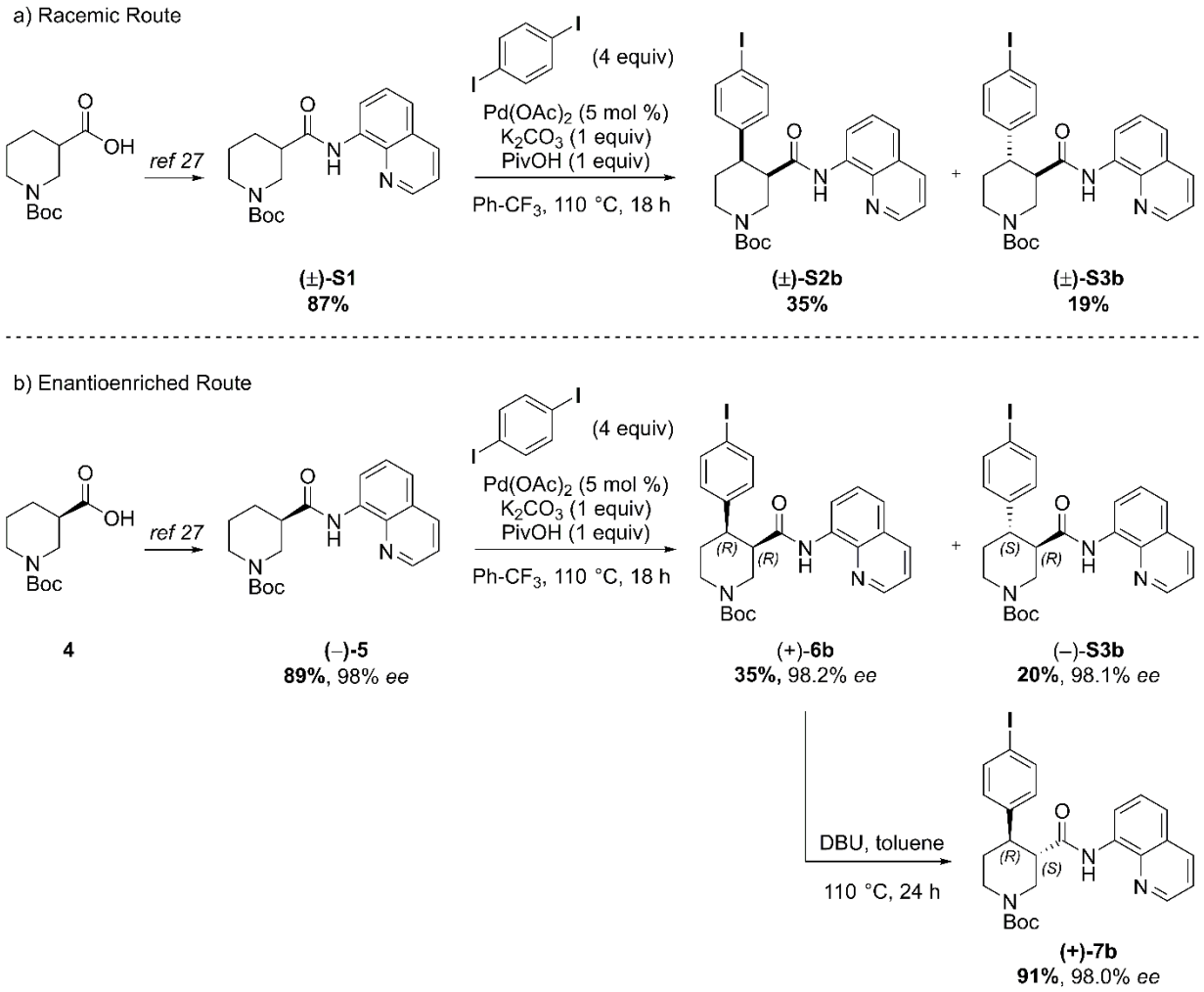

a) C–H Arylation conditions: **(±)-S1** (0.5 mmol, 1 equiv) Ph-CF_3 (500 µL, 1 M). b) C–H Arylation conditions: **(–)-5** (4.0 mmol, 1 equiv), Ph-CF_3 (2.0 mL, 2 M).

Reductive aminoquinoline cleavage was again performed to access enantiomeric *trans*-piperidine alcohols **(+)-S4b** and **(–)-8b** (Scheme S4).

In both cases a small degree of $LiAlH_4$-mediated dehalogenation was observed, and an inseparable mixture of the desired product and 10–15% of deiodinated material was isolated. However, the contaminant could be effectively removed after O-Alkylation, affording the pure aryl ether derivative **(–)-9b** in 71% yield. Final HCl-mediated Boc deprotection formed the desired I-(–)-paroxetine **3** as the corresponding HCl salt in 81% yield (12% yield over 8 steps from commercial material).

Scheme S4. Reductive aminoquinoline removal and final steps in the synthesis of I-(–)-paroxetine 3.

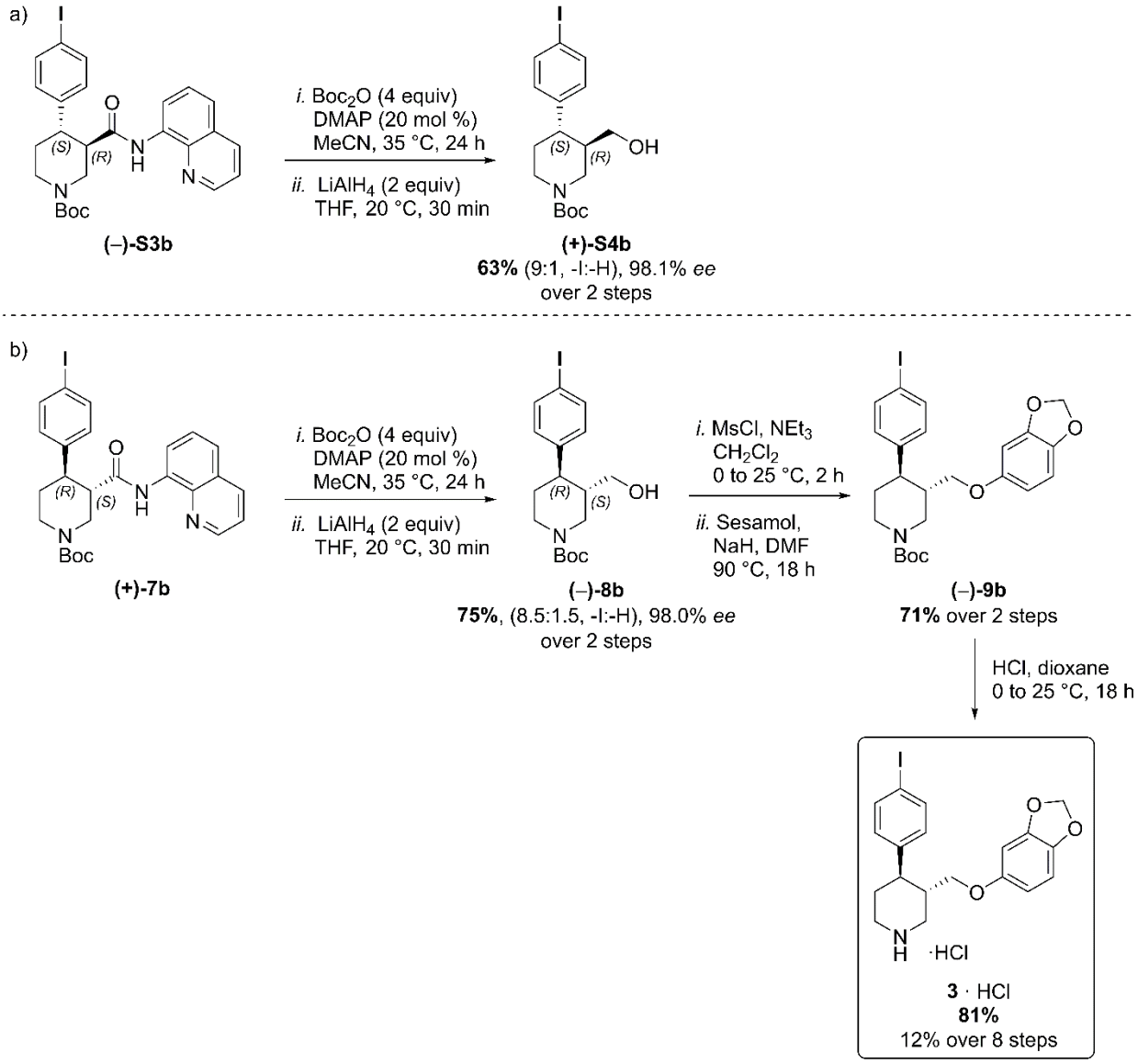

a) AQ removal on enantiomerically pure *trans*-piperidine **(–)-S3b** (0.2 mmol, 1 equiv). b) AQ removal on enantiomerically pure *trans*-piperidine **(+)-7b** (1.0 mmol, 1 equiv) and final steps in the synthesis of I-(–)-paroxetine **3**.

HPLC Traces for Racemic, Scalemic and Enantioenriched Br-Piperidine Derivatives (±)-S2a, (±)-S3a, (+)-6a, (+)-7a, (–)-S3a, (–)-8a and (+)-S4a

***tert*-Butyl *cis*-(±)-4-(4-bromophenyl)-3-(quinolin-8-ylcarbamoyl)piperidine-1-carboxylate ((±)-S2a)**

Conditions: Chiralpak IA 3-column, 85:15 *n*-hexane:*i*-PrOH, flow rate: 1 mL·min^{-1}, 35 ºC, UV detection wavelength: 210.4 nm. Retention times: 11.9 min (3*S*,4*S* enantiomer), 17.3 min (3*R*,4*R* enantiomer).

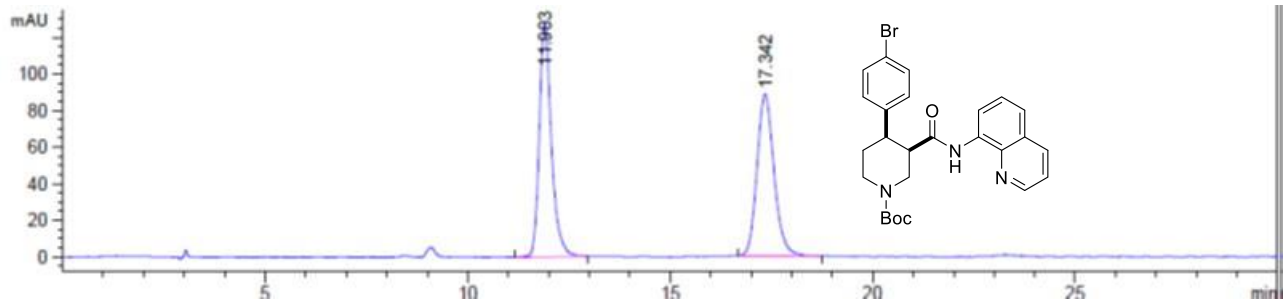

Signal 3: DAD1 C, Sig=210,10 Ref=off

Peak #	RetTime [min]	Type	Width [min]	Area [mAU*s]	Height [mAU]	Area %
1	11.903	BB	0.3134	2649.83203	128.07286	50.6199
2	17.342	BB	0.4515	2584.93091	88.31209	49.3801
Totals :				5234.76294	216.38495	

***tert*-Butyl (+)-(*3R,4R*)-4-(4-bromophenyl)-3-(quinolin-8-ylcarbamoyl)piperidine-1-carboxylate ((+)-6a)**

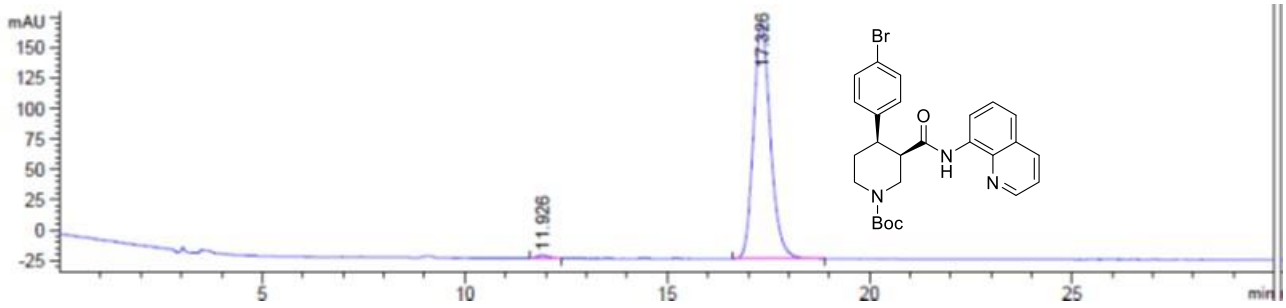

Signal 3: DAD1 C, Sig=210,10 Ref=off

Peak #	RetTime [min]	Type	Width [min]	Area [mAU*s]	Height [mAU]	Area %
1	11.926	BB	0.2556	51.12915	2.64391	0.8973
2	17.326	BB	0.4494	5647.02783	193.00262	99.1027
Totals :				5698.15698	195.64654	

***ee* = 98.2%**

***tert*-Butyl *trans*-(±)-4-(4-bromophenyl)-3-(quinolin-8-ylcarbamoyl)piperidine-1-carboxylate ((±)-S3a)**

Conditions: Chiralpak IA 3-column, 85:15 *n*-hexane:*i*-PrOH, flow rate: 1 mL·min^{-1}, 35 ºC, UV detection wavelength: 254.1 nm. Retention times: 9.1 min (3*R*,4*S* enantiomer), 12.2 min (3*S*,4*R* enantiomer).

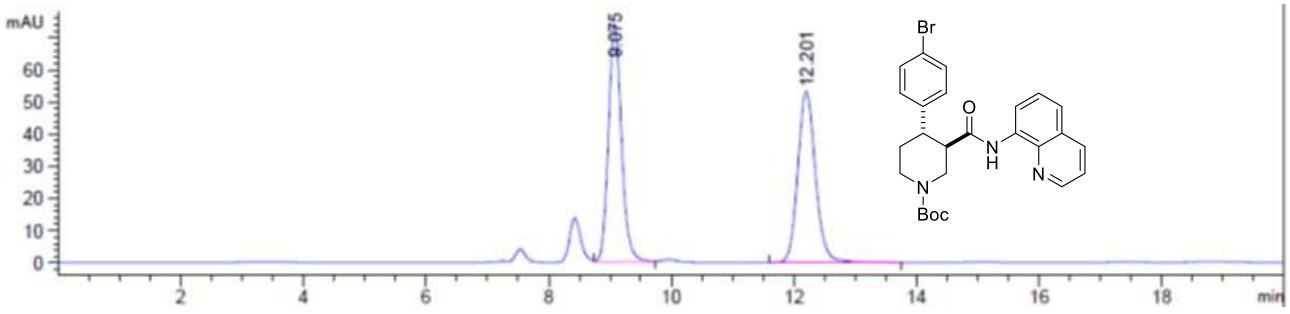

Signal 2: DAD1 B, Sig=254,10 Ref=off

Peak #	RetTime [min]	Type	Width [min]	Area [mAU*s]	Height [mAU]	Area %
1	9.075	VB	0.2266	1093.46033	73.93165	50.5693
2	12.201	BB	0.3080	1068.84167	53.29229	49.4307
Totals :				2162.30200	127.22393	

***tert*-Butyl (–)-(*3R,4S*)-4-(4-bromophenyl)-3-(quinolin-8-ylcarbamoyl)piperidine-1-carboxylate ((–)-S3a)**

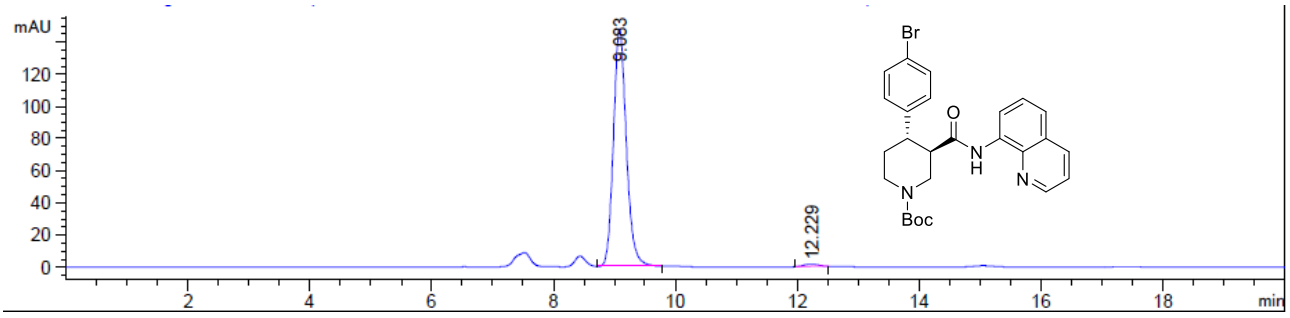

Signal 2: DAD1 B, Sig=254,10 Ref=off

Peak #	RetTime [min]	Type	Width [min]	Area [mAU*s]	Height [mAU]	Area %
1	9.083	MM	0.2445	2163.23486	147.46376	99.0118
2	12.229	MM	0.2733	21.59002	1.31660	0.9882
Totals :				2184.82488	148.78036	

***ee* 98.0%**

***tert*-Butyl (+)-(*3S,4R*)-4-(4-bromophenyl)-3-(quinolin-8-ylcarbamoyl)piperidine-1-carboxylate ((+)-7a)**

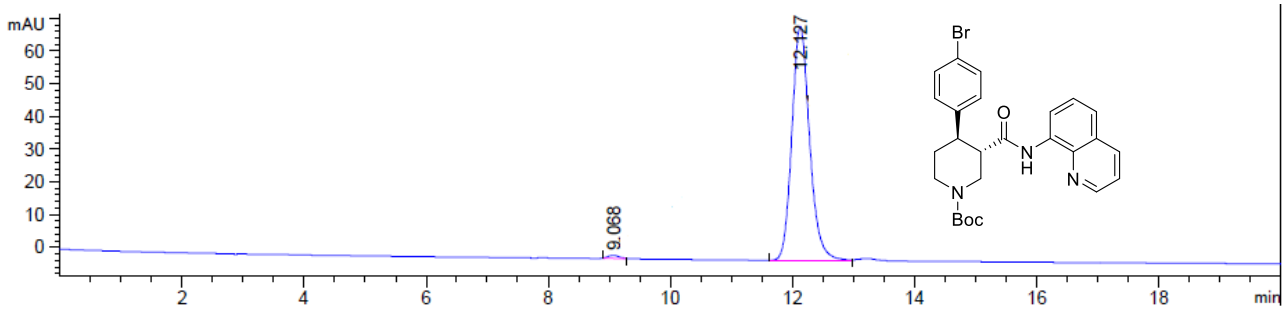

Signal 2: DAD1 B, Sig=254,10 Ref=off

Peak #	RetTime [min]	Type	Width [min]	Area [mAU*s]	Height [mAU]	Area %
1	9.068	MM	0.2108	11.79956	9.32985e-1	0.8026
2	12.127	MM	0.3388	1458.44690	71.75478	99.1974
Totals :				1470.24646	72.68776	

***ee* = 98.4%**

Scalemic Mixture of Enantioenriched Br-Piperidines (+)-S4a and (–)-8a

Conditions: Chiralpak ID 3-column, 90:10 *n*-hexane:*i*-PrOH, flow rate: 1 mL·min^{-1}, 35 ºC, UV detection wavelength: 210.4 nm. Retention times: 8.0 min (3*R*,4*S* enantiomer), 8.6 min (3*S*,4*R* enantiomer).

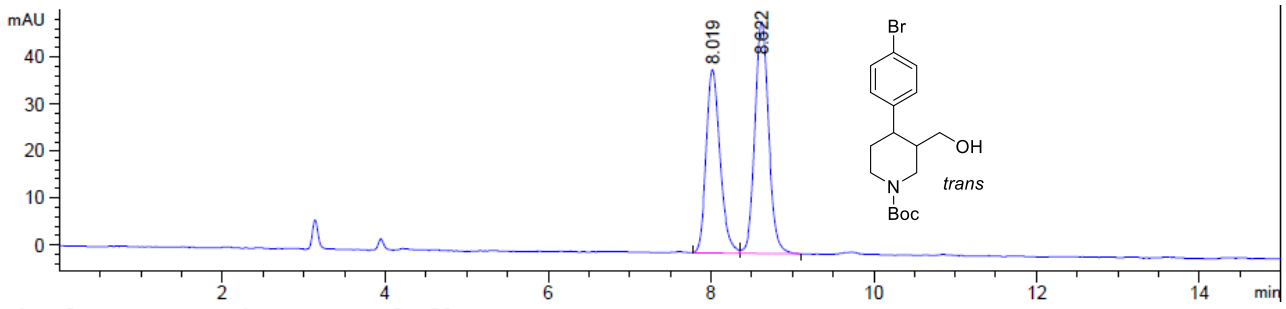

Signal 3: DAD1 C, Sig=210,10 Ref=off

Peak #	RetTime [min]	Type	Width [min]	Area [mAU*s]	Height [mAU]	Area %
1	8.019	BV	0.1793	458.78363	38.98658	44.3601
2	8.622	VB	0.1802	575.44318	49.30547	55.6399
Totals :				1034.22681	88.29205	

tert-Butyl (+)-(*3R,4S*)-4-(4-bromophenyl)-3-(hydroxymethyl)piperidine-1-carboxylate ((+)-S4a)

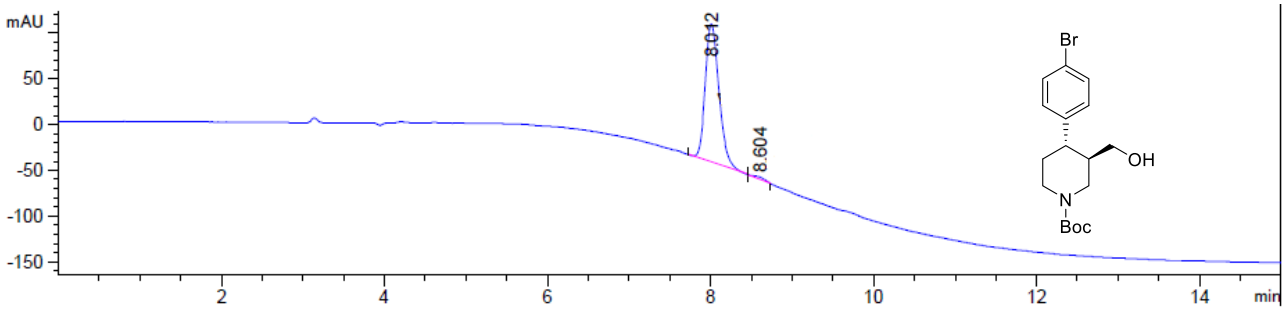

Signal 3: DAD1 C, Sig=210,10 Ref=off

Peak #	RetTime [min]	Type	Width [min]	Area [mAU*s]	Height [mAU]	Area %
1	8.012	MM	0.1924	1740.07422	150.75604	99.0603
2	8.604	MM	0.1355	16.50659	2.03064	0.9397
Totals :				1756.58081	152.78669	

***ee* = 98.1%**

***tert*-Butyl (–)-(*3S,4R*)-4-(4-bromophenyl)-3-(hydroxymethyl)piperidine-1-carboxylate ((–)-8a)**

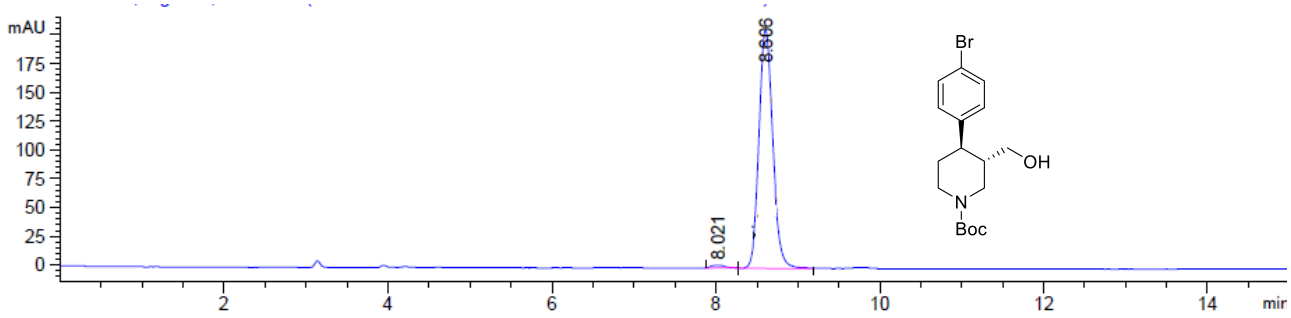

Signal 3: DAD1 C, Sig=210,10 Ref=off

Peak #	RetTime [min]	Type	Width [min]	Area [mAU*s]	Height [mAU]	Area %
1	8.021	MM	0.1640	23.16720	2.35474	0.9470
2	8.606	MM	0.1943	2423.17212	207.84224	99.0530
Totals :				2446.33932	210.19698	

***ee* = 98.1%**

HPLC Traces for Racemic, Scalemic and Enantioenriched I-Piperidine Derivatives (±)-S2b, (±)-S3b, (+)-6b, (+)-7b, (–)-S3b, (–)-8b and (+)-S4b

***tert*-Butyl *cis*-(±)-4-(4-iodophenyl)-3-(quinolin-8-ylcarbamoyl)piperidine-1-carboxylate ((±)-S2b):**

Conditions: Chiralpak IA 3-column, 85:15 *n*-hexane:*i*-PrOH, flow rate: 1 mL·min^{-1}, 35 ºC, UV detection wavelength: 210.4 nm. Retention times: 12.2 min (3*S*,4*S* enantiomer), 17.7 min (3*R*,4*R* enantiomer).

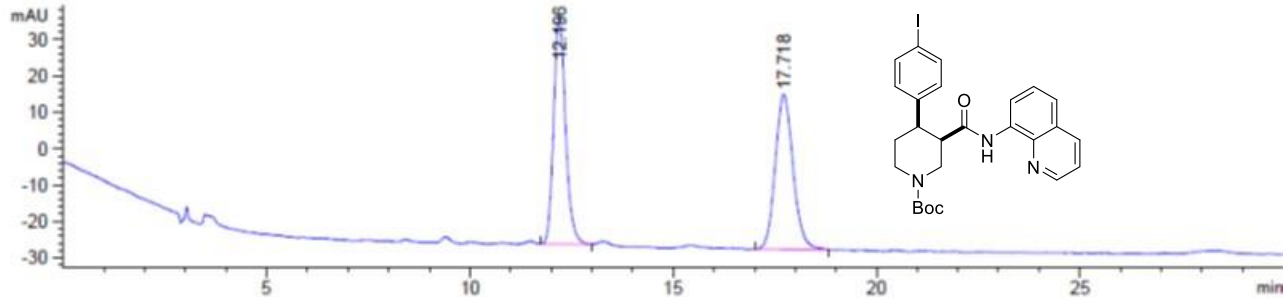

Signal 3: DAD1 C, Sig=210,10 Ref=off

Peak #	RetTime [min]	Type	Width [min]	Area [mAU*s]	Height [mAU]	Area %
1	12.196	BB	0.3093	1270.20874	62.45296	49.4311
2	17.718	BB	0.4698	1299.44507	42.60729	50.5689
Totals :				2569.65381	105.06025	

***tert*-Butyl (+)-(*3R,4R*)-4-(4-iodophenyl)-3-(quinolin-8-ylcarbamoyl)piperidine-1-carboxylate ((+)-6b**

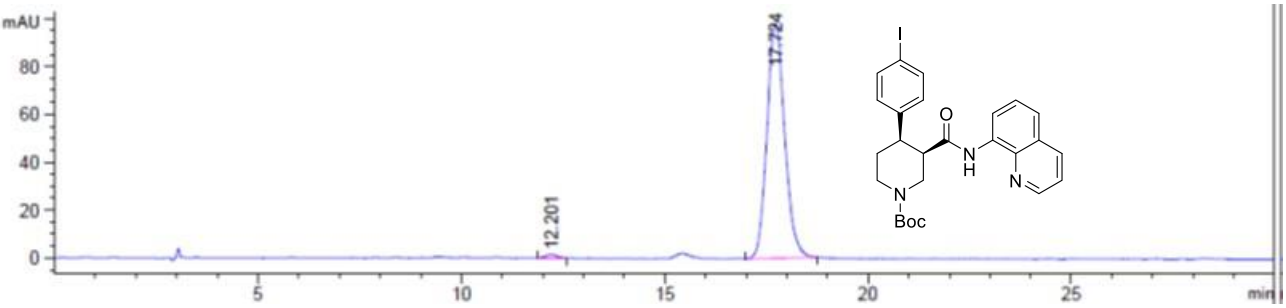

Signal 3: DAD1 C, Sig=210,10 Ref=off

Peak #	RetTime [min]	Type	Width [min]	Area [mAU*s]	Height [mAU]	Area %
1	12.201	BB	0.2287	26.94304	1.45051	0.8982
2	17.724	BB	0.4677	2972.60156	98.05776	99.1018
Totals :				2999.54460	99.50827	

***ee* = 98.2%**

***tert*-Butyl *trans*-(±)-4-(4-iodophenyl)-3-(quinolin-8-ylcarbamoyl)piperidine-1-carboxylate ((±)-S3b)**

Conditions: Chiralpak IA 3-column, 85:15 *n*-hexane:*i*-PrOH, flow rate: 1 mL·min^{-1}, 35 ºC, UV detection wavelength: 254.1 nm. Retention times: 9.4 min (3*R*,4*S* enantiomer), 13.3 min (3*S*,4*R* enantiomer).

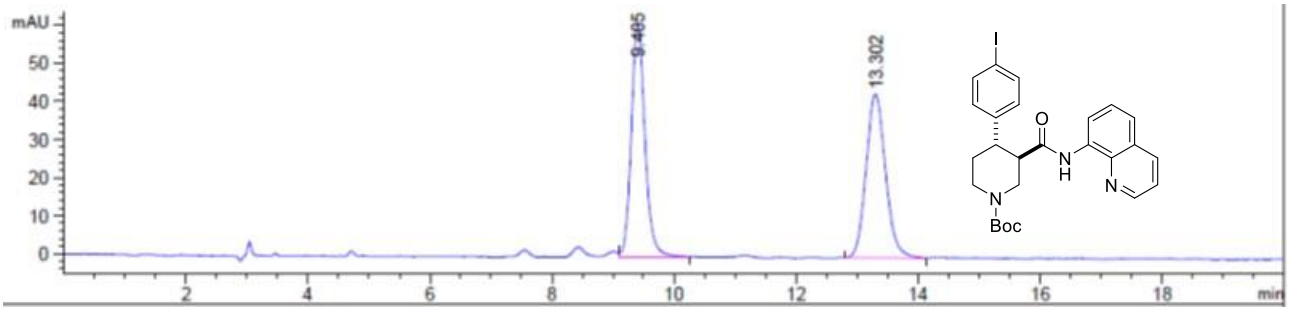

Signal 2: DAD1 B, Sig=254,10 Ref=off

Peak #	RetTime [min]	Type	Width [min]	Area [mAU*s]	Height [mAU]	Area %
1	9.405	VB	0.2368	464.95227	30.00297	49.8782
2	13.301	BB	0.3431	467.22318	21.03599	50.1218
Totals :				932.17545	51.03896	

***tert*-butyl (–)-(*3R,4S*)-4-(4-iodophenyl)-3-(quinolin-8-ylcarbamoyl)piperidine-1-carboxylate ((–)-S3b)**

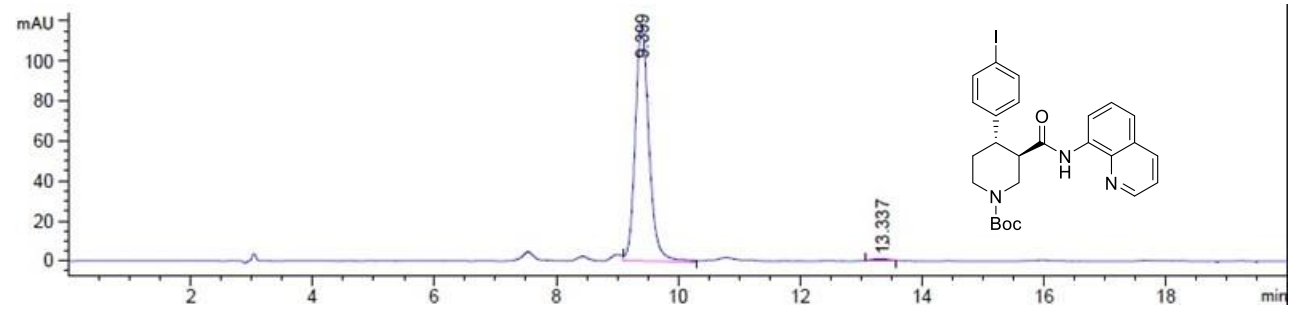

Signal 2: DAD1 B, Sig=254,10 Ref=off

Peak #	RetTime [min]	Type	Width [min]	Area [mAU*s]	Height [mAU]	Area %
1	9.400	MM	0.2584	902.97003	58.23014	99.0491
2	13.314	MM	0.2976	8.66880	4.85432e-1	0.9509
Totals :				911.63883	58.71558	

***ee* = 98.1%**

***tert*-Butyl (+)-(*3S,4R*)-4-(4-iodophenyl)-3-(quinolin-8-ylcarbamoyl)piperidine-1-carboxylate ((+)-7b)**

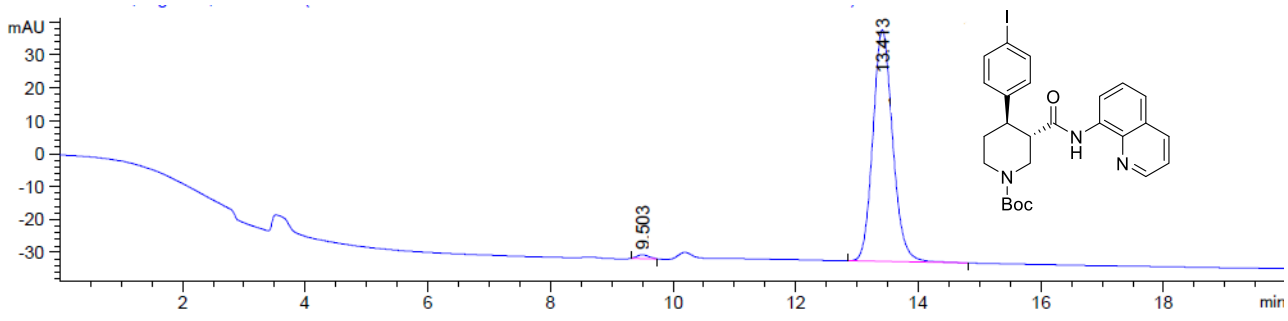

Signal 2: DAD1 B, Sig=254,10 Ref=off

Peak #	RetTime [min]	Type	Width [min]	Area [mAU*s]	Height [mAU]	Area %
1	9.503	MM	0.2272	15.83589	1.16162	0.9922
2	13.413	MP	0.3735	1580.24548	70.51000	99.0078
Totals :				1596.08137	71.67163	

***ee* = 98.0%**

Scalemic Mixture of Enantioenriched I-Piperidines (+)-S4b and (–)-8b

Conditions: Chiralpak ID 3-column, 90:10 *n*-hexane:*i*-PrOH, flow rate: 1 mL·min^{-1}, 35 ºC, UV detection wavelength: 230.1 nm. Retention times: 6.7 min (3*R*,4*S* enantiomer), 7.4 min (3*S*,4*R* enantiomer).

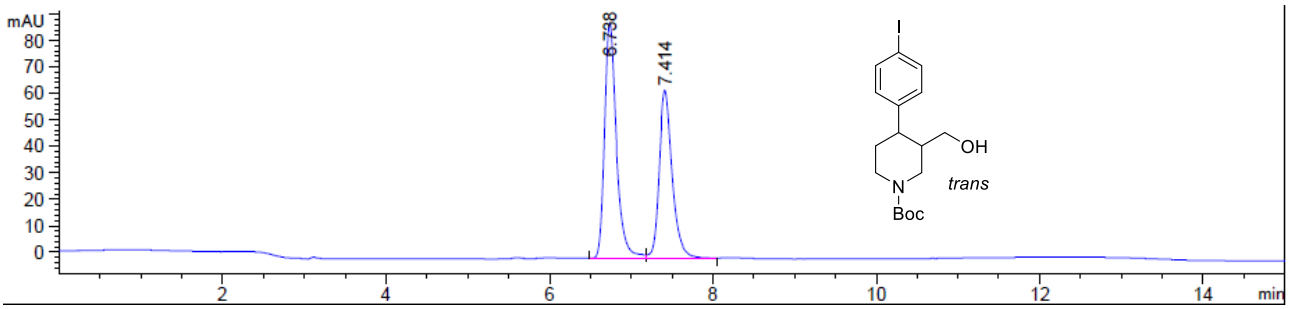

Signal 4: DAD1 D, Sig=230,10 Ref=off

Peak #	RetTime [min]	Type	Width [min]	Area [mAU*s]	Height [mAU]	Area %
1	6.738	BV	0.1527	891.19653	89.06178	56.0128
2	7.414	VB	0.1667	699.86224	63.44310	43.9872
Totals :				1591.05878	152.50488	

tert-Butyl (+)-(*3R,4S*)-4-(4-iodophenyl)-3-(hydroxymethyl)piperidine-1-carboxylate ((+)-S4b)

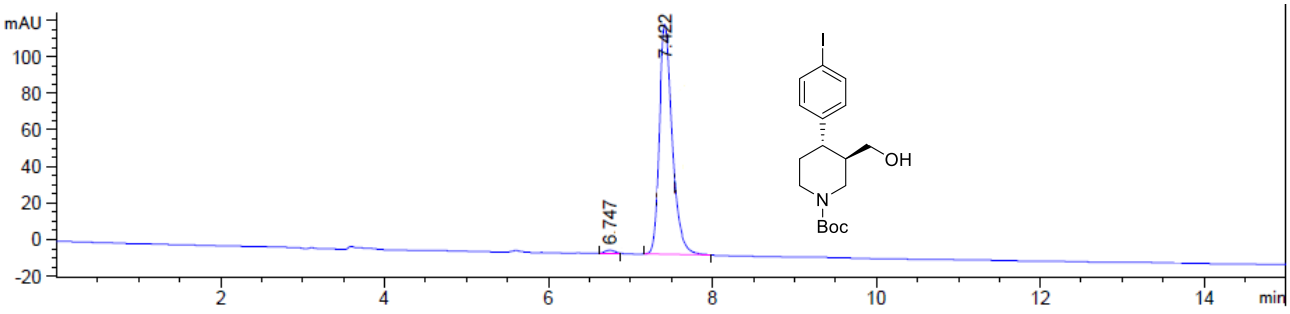

Signal 4: DAD1 D, Sig=230,10 Ref=off

Peak #	RetTime [min]	Type	Width [min]	Area [mAU*s]	Height [mAU]	Area %
1	6.747	PP	0.1304	13.28141	1.69711	0.9559
2	7.422	PP	0.1825	1376.08704	125.65760	99.0441
Totals :				1389.36845	127.35471	

***ee* = 98.1%**

***tert*-Butyl (–)-(*3S,4R*)-4-(4-iodophenyl)-3-(hydroxymethyl)piperidine-1-carboxylate ((–)-8b)**

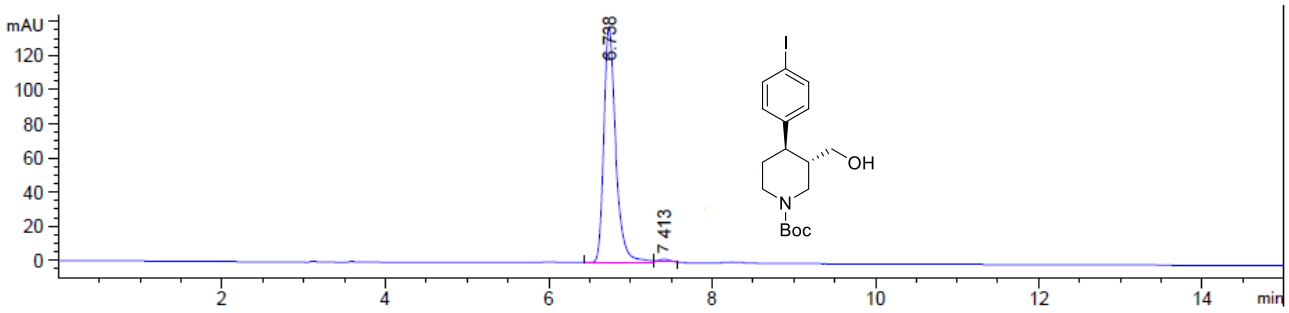

Signal 4: DAD1 D, Sig=230,10 Ref=off

Peak #	RetTime [min]	Type	Width [min]	Area [mAU*s]	Height [mAU]	Area %
1	6.738	MM	0.1672	1386.67920	138.19916	99.0161
2	7.413	MP	0.1557	13.77859	1.47463	0.9839
Totals :				1400.45779	139.67379	

***ee* = 98.0%**

Experimental Details and Characterization Data

Synthesis of Br-analogue of (–)-paroxetine (compounds **(±)-S2a**, **(±)-S3a**, **(+)-6a**, **(+)-7a**, **(–)-S3a**, **(–)-8a**, **(+)-S4a**, **(–)-9a** and **2** · HCl)

***tert*-Butyl *cis*-(±)-4-(4-bromophenyl)-3-(quinolin-8-ylcarbamoyl)piperidine-1-carboxylate ((±)-S2a)** and ***tert*-butyl *trans*-(±)-4-(4-bromophenyl)-3-(quinolin-8-ylcarbamoyl)piperidine-1-carboxylate ((±)-S3a):**

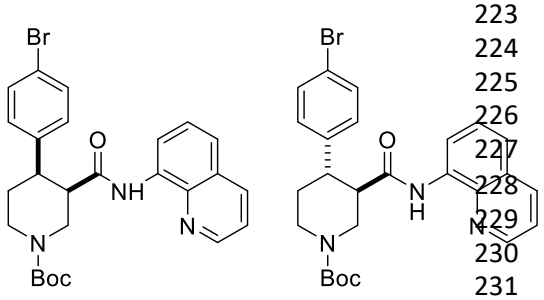

A reaction tube was charged with K_2CO_3 (69.1 mg, 0.50 mmol, 1 equiv), flame-dried, and allowed to cool under argon. *tert*-Butyl (±)-3-(quinoline-8-ylcarbamoyl)piperidine-1-carboxylate (**(±)-S1**) (178 mg, 0.50 mmol, 1 equiv), 4-bromoiodobenzene (424 mg, 1.50 mmol, 3 equiv), $Pd(OAc)_2$ (5.60 mg, 25.0 μmol, 5 mol %) and PivOH (51.2 mg, 0.50 mmol, 1 equiv) were added sequentially. The reaction vessel was sealed with an aluminum cap (with molded butyl/PTFE septa) and purged with argon, then anhydrous $PhCF_3$ (500 μL, 1.0 M) was added by syringe. The reaction tube was then placed in a preheated oil bath and stirred at 110 ºC for 18 h. The reaction mixture was allowed to cool to rt and EtOAc (10 mL) was added. The resulting mixture was filtered through a pad of Celite®, eluting with further EtOAc (2 × 10 mL). The solvent was removed under reduced pressure, and the crude material was purified by flash column chromatography (0% to 5% CH_3CN/CH_2Cl_2). The product containing fractions were combined and the solvent was removed under reduced pressure. Et_2O (5 mL) and pentane (5 mL) were added and the solvent was removed under reduced pressure to afford the minor product *tert*–butyl *trans*-(±)-4-(4-bromophenyl)-3-(quinolin-8-ylcarbamoyl) piperidine-1-carboxylate **(±)-S3a** as a pale yellow solid (34.5 mg, 14%) followed by the major product *tert*-butyl *cis*-(±)-4-(4-bromophenyl)-3-(quinolin-8-ylcarbamoyl)piperidine-1-carboxylate **(±)-S2a** as an off-white solid (87.2 mg, 34%).

Major (**(±)-S2a**):
R_f 0.31 (5% CH_3CN/CH_2Cl_2);
mp = 81–86 °C (from Et_2O/pentane);
ν_{max} (film)/cm^{-1} 3343 (NH), 2859, 1684 (C=O), 1521, 1484, 1423, 1364, 1323, 1245, 1163, 1006, 827, 790, 757;
^{1}H NMR (500 MHz, $(CD_3)_2SO$, 373 K) δ 9.75 (br s, 1 H, NH), 8.83 (dd, *J* = 4.2, 1.7 Hz, 1 H, HC_{Ar}), 8.45 (dd, *J* = 7.7, 1.4 Hz, 1 H, HC_{Ar}), 8.31 (dd, *J* = 8.3, 1.7 Hz, 1 H, HC_{Ar}), 7.60–7.53 (m, 2 H, HC_{Ar}), 7.48 (t, *J* = 7.9 Hz, 1 H, HC_{Ar}), 7.40–7.34 (m, 2 H, HC_{Ar}), 7.33–7.26 (m, 2 H, HC_{Ar}), 4.42 (ddd, *J* = 14.8, 3.6, 1.7 Hz, 1 H, NC*H*HCHCO), 4.25 (ddt, *J* = 13.1, 4.6, 2.3 Hz, 1 H, NC*H*HCH$_2$), 3.36–3.28 (m, 2 H, NCH*H*CHCO, CHCO), 3.16 (dt, *J* = 12.2, 4.0 Hz, 1 H, CHAr), 3.02–2.92 (m, 1 H, NCH*H*CH$_2$), 2.68 (qd, *J* = 12.4, 4.7 Hz, 1 H, NCH$_2$C*H*H), 1.72 (dq, *J* = 12.9, 3.2 Hz, 1 H, NCH$_2$CH*H*), 1.25 (s, 9 H, C(CH$_3$)$_3$);
^{13}C NMR (126 MHz, $(CD_3)_2SO$, 373 K) δ 169.8 (C=O amide), 153.4 (C=O carbamate), 147.9 (C_{Ar}), 142.0 (C_{Ar} quat), 137.6 (C_{Ar} quat), 135.7 (C_{Ar}), 133.9 (C_{Ar} quat), 130.3 (2 × C_{Ar}), 129.1 (2 × C_{Ar}), 127.2 (C_{Ar} quat), 126.1 (C_{Ar}), 121.2 (C_{Ar}), 120.8 (C_{Ar}), 118.7 (BrC_{Ar} quat), 115.7 (C_{Ar}), 77.9 (*C*(CH$_3$)$_3$), 46.2 (N*C*H$_2$CHCO), 45.6 (*C*HCO), 42.9 (N*C*H$_2$CH$_2$), 41.7 (*C*HAr), 27.4 (C(*C*H$_3$)$_3$), 25.0 (NCH$_2$*C*H$_2$);
HRMS (ESI$^+$) *m/z* Calculated for $C_{26}H_{29}N_3O_3{}^{79}Br$ [M+H] 510.1392; Found 510.1386.

SMILES:
O=C([C@H]1CN(C(OC(C)(C)C)=O)CC[C@H]1C2=CC=C(Br)C=C2)NC3=C(N=CC=C4)C4=CC=C3

InChI=1S/C26H28BrN3O3/c1-26(2,3)33-25(32)30-15-13-20(17-9-11-19(27)12-10-17)21(16-30)24(31)29-22-8-4-6-18-7-5-14-28-23(18)22/h4-12,14,20-21H,13,15-16H2,1-3H3,(H,29,31)/t20-,21-/m0/s1

Minor (**(±)-S3a**):
R_f 0.41 (5% CH_3CN/CH_2Cl_2);
mp = 77–83 °C (from Et_2O/pentane);
ν_{max} (film)/cm^{-1} 3340 (NH), 2926, 1677 (C=O), 1521, 1484, 1424, 1323, 1230, 1156, 1126, 999, 824, 757;
^1H NMR (500 MHz, $(CD_3)_2SO$, 373 K) δ 9.73 (br s, 1 H, NH), 8.85 (dd, *J* = 4.2, 1.7 Hz, 1 H, HC_{Ar}), 8.39 (dd, *J* = 7.7, 1.4 Hz, 1 H, HC_{Ar}), 8.31 (dd, *J* = 8.3, 1.7 Hz, 1 H, HC_{Ar}), 7.61–7.54 (m, 2 H, HC_{Ar}), 7.47 (t, *J* = 8.0 Hz, 1 H, HC_{Ar}), 7.39–7.32 (m, 2 H, HC_{Ar}), 7.34–7.28 (m, 2 H, HC_{Ar}), 4.36 (ddd, *J* = 12.9, 3.7, 1.8 Hz, 1 H, NC*H*HCHCO), 4.13 (ddt, *J* = 13.3, 4.3, 2.2 Hz, 1 H, NC*H*HCH_2), 3.18–3.00 (m, 3 H, NCH*H*CHCO, CHCO, CHAr), 2.99–2.90 (m, 1 H, NCH*H*CH_2), 1.81 (dq, *J* = 12.9, 2.8 Hz, 1 H, NCH_2CHH), 1.66 (qd, *J* = 12.8, 4.6 Hz, 1 H, NCH_2CHH), 1.49 (s, 9 H, $C(CH_3)_3$);
^{13}C NMR (126 MHz, $(CD_3)_2SO$, 373 K) δ 169.8 (C=O amide), 153.4 (C=O carbamate), 148.0 (C_{Ar}), 142.4 (C_{Ar} quat), 137.7 (C_{Ar} quat), 135.7 (C_{Ar}), 133.5 (C_{Ar} quat), 130.6 (2 × C_{Ar}), 129.1 (2 × C_{Ar}), 127.2 (C_{Ar} quat), 126.1 (C_{Ar}), 121.4 (C_{Ar}), 121.3 (C_{Ar}), 118.9 (BrC_{Ar} quat), 116.3 (C_{Ar}), 78.6 ($C(CH_3)_3$), 49.2 (*C*HCO), 46.2 (NCH_2CHCO), 43.9 (*C*HAr), 43.3 (NCH_2CH_2), 32.0 (NCH_2CH_2), 27.7 ($C(CH_3)_3$);
HRMS (ESI^+) *m/z* Calculated for $C_{26}H_{29}N_3O_3{}^{79}Br$ [M+H] 510.1392; Found 510.1382.

SMILES:
O=C([C@@H]1CN(C(OC(C)(C)C)=O)CC[C@H]1C2=CC=C(Br)C=C2)NC3=C(N=CC=C4)C4=CC=C3

InChI=1S/C26H28BrN3O3/c1-26(2,3)33-25(32)30-15-13-20(17-9-11-19(27)12-10-17)21(16-30)24(31)29-22-8-4-6-18-7-5-14-28-23(18)22/h4-12,14,20-21H,13,15-16H2,1-3H3,(H,29,31)/t20-,21+/m0/s1

***tert*-Butyl (+)-(*3R,4R*)-4-(4-bromophenyl)-3-(quinolin-8-ylcarbamoyl)piperidine-1-carboxylate ((+)-6a)** and ***tert*-butyl (–)-(*3R,4S*)-4-(4-bromophenyl)-3-(quinolin-8-ylcarbamoyl)piperidine-1-carboxylate ((–)-S3a)**:

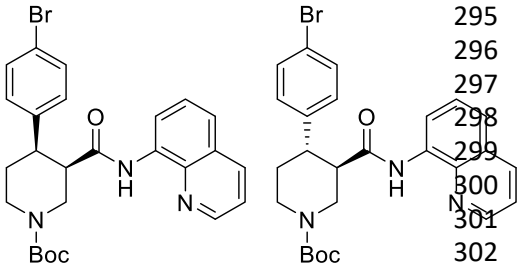

A large microwave vial (10–20 mL recommended volume) was charged with K_2CO_3 (553 mg, 4.0 mmol, 1 equiv), flame-dried, and allowed to cool under argon. *tert*-Butyl (*R*)-3-(quinolin-8-ylcarbamoyl)piperidine-1-carboxylate **(–)-5** (1.42 g, 4.0 mmol, 1 equiv), 4-bromoiodobenzene (3.40 g, 12.0 mmol, 3 equiv), $Pd(OAc)_2$ (45.1 mg, 0.2 mmol, 5 mol %) and PivOH (409 mg, 4.0 mmol, 1 equiv) were added sequentially. The reaction vessel was sealed with an aluminum cap (with molded butyl/PTFE septa) and purged with argon, then anhydrous $PhCF_3$ (2.0 mL, 2.00 M) was added by syringe. The reaction tube was then placed in a preheated oil bath and stirred at 110 ºC for 18 h. The reaction mixture was then allowed to cool to rt and EtOAc (20 mL) was added. The resulting mixture was filtered through a pad of Celite®, eluting with further EtOAc (2 × 50 mL). The solvent was removed under reduced pressure. The reaction mixture was purified by two consecutive chromatographic separations: one (0% to 5% CH_3CN/CH_2Cl_2) to isolate the minor *trans*-product *tert*-butyl (–)-(*3R,4S*)-4-(4-bromophenyl)-3-(quinolin-8-ylcarbamoyl)piperidine-1-carboxylate **(–)-S3a** followed by a second (10% to 15% acetone/pentane) to isolate the major *cis*-product *tert*-butyl (+)-(*3R,4R*)-4-(4-bromophenyl)-3-(quinolin-8-ylcarbamoyl)piperidine-1-carboxylate **(+)-6a**. The product containing fractions were combined and the solvent was removed under reduced pressure. Et_2O (20 mL) and pentane (20 mL) were added and the solvent was removed under reduced pressure to afford the minor *trans*-product **(–)-S3a** as a pale yellow solid (371 mg, 18%, 98.0% *ee*) and the major *cis*-product **(+)-6a** as a white solid (730 mg, 36%, 98.2% *ee*).

Major (**(+)-6a**):
$[\alpha]_D^{23}$ + 15.4 (*c* 1.3, $CHCl_3$).

Characterization data identical to that reported for racemic *cis*-piperidine **(±)-S2a** (see S17).

HPLC Conditions: Chiralpak IA 3-column, 85:15 *n*-hexane:*i*-PrOH, flow rate: 1 mL·min^{-1}, 35 ºC, UV detection wavelength: 210.4 nm. Retention times: 11.9 min (3*S,*4*S* enantiomer), 17.3 min (3*R,*4*R* enantiomer).

SMILES:
O=C([C@H]1CN(C(OC(C)(C)C)=O)CC[C@H]1C2=CC=C(Br)C=C2)NC3=C(N=CC=C4)C4=CC=C3

InChI=1S/C26H28BrN3O3/c1-26(2,3)33-25(32)30-15-13-20(17-9-11-19(27)12-10-17)21(16-30)24(31)29-22-8-4-6-18-7-5-14-28-23(18)22/h4-12,14,20-21H,13,15-16H2,1-3H3,(H,29,31)/t20-,21-/m0/s1

Minor (**(–)-S3a**):
$[\alpha]_D^{23}$ – 35.4 (*c* 1.3, $CHCl_3$).
Characterization data identical to that reported for racemic *trans*-piperidine **(±)-S3a** (see S17).

HPLC Conditions: Chiralpak IA 3-column, 85:15 *n*-hexane:*i*-PrOH, flow rate: 1 mL·min^{-1}, 35 ºC, UV detection wavelength: 254.1 nm. Retention times: 9.1 min (3*R,*4*S* enantiomer), 12.2 min (3*S,*4*R* enantiomer).

SMILES:
O=C([C@H]1CN(C(OC(C)(C)C)=O)CC[C@@H]1C2=CC=C(Br)C=C2)NC3=C(N=CC=C4)C4=CC=C3

InChI=1S/C26H28BrN3O3/c1-26(2,3)33-25(32)30-15-13-20(17-9-11-19(27)12-10-17)21(16-30)24(31)29-22-8-4-6-18-7-5-14-28-23(18)22/h4-12,14,20-21H,13,15-16H2,1-3H3,(H,29,31)/t20-,21+/m1/s1

***tert*-Butyl (+)-(*3S,4R*)-4-(4-bromophenyl)-3-(quinolin-8-ylcarbamoyl)piperidine-1-carboxylate ((+)-7a)**

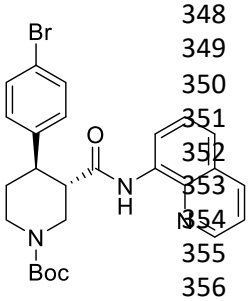

A flame-dried reaction tube was charged with *cis*-3,4-disubstituted piperidine **(+)-6a** (662 mg, 1.30 mmol, 1 equiv) and 1,8-diazabicyclo(5.4.0)undec-7-ene (DBU, 600 μL, 3.90 mmol, 3 equiv). The reaction vessel was sealed with an aluminum cap (with molded butyl/PTFE septa) and purged with argon, then anhydrous toluene (1.30 mL, 1.0 M) was added by syringe. The reaction tube was then placed in a preheated oil bath and stirred at 110 ºC for 24 h. The reaction mixture was then allowed to cool to rt and CH_2Cl_2 (5 mL) and sat. aq. NH_4Cl (5 mL) were added. The phases were separated, and the aqueous layer was extracted with CH_2Cl_2 (3 × 10 mL). The combined organic extracts were dried over Na_2SO_4 and filtered. The solvent was removed under reduced pressure. The reaction mixture was purified by flash column chromatography (15% acetone/pentane). The product containing fractions were combined and the solvent was removed under reduced pressure. Et_2O (10 mL) and pentane (10 mL) were added and the solvent was removed under reduced pressure to afford amide *tert*-butyl (+)-(*3S,4R*)-4-(4-bromophenyl)-3-(quinolin-8-ylcarbamoyl) piperidine-1-carboxylate **(+)-7a** as a white solid (621 mg, 94%, 98.4% *ee*).

$[\alpha]_D^{23}$ + 52.0 (*c* 1.0, $CHCl_3$).
Characterization data identical to that reported for racemic *trans*-piperidine **(±)-S3a** (see S17).

HPLC Conditions: Chiralpak IA 3-column, 85:15 *n*-hexane:*i*-PrOH, flow rate: 1 mL·min^{-1}, 35 ºC, UV detection wavelength: 254.1 nm. Retention times: 9.1 min (3*R,*4*S* enantiomer), 12.2 min (3*S,*4*R* enantiomer).

SMILES:
O=C([C@@H]1CN(C(OC(C)(C)C)=O)CC[C@H]1C2=CC=C(Br)C=C2)NC3=C(N=CC=C4)C4=CC=C3

InChI=1S/C26H28BrN3O3/c1-26(2,3)33-25(32)30-15-13-20(17-9-11-19(27)12-10-17)21(16-30)24(31)29-22-8-4-6-18-7-5-14-28-23(18)22/h4-12,14,20-21H,13,15-16H2,1-3H3,(H,29,31)/t20-,21+/m0/s1

tert-Butyl (+)-(*3R,4S*)-4-(4-bromophenyl)-3-(hydroxymethyl)piperidine-1-carboxylate ((+)-S4a)

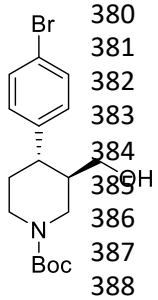

A flame-dried reaction tube was charged with amide **(–)-S3a** (102 mg, 0.20 mmol, 1 equiv), followed by di-*tert*-butyl dicarbonate (Boc_2O, 175 mg, 0.80 mmol, 4 equiv) and 4-(dimethylamino)pyridine (DMAP, 4.9 mg, 0.04 mmol, 20 mol %). The reaction vessel was sealed with an aluminum cap (with molded butyl septa) and purged with argon, then anhydrous MeCN (400 μL, 0.5 M) was added by syringe. The mixture was then stirred at 35 ºC for 22 h. The reaction mixture was then allowed to cool to rt and sat. aq. NH_4Cl (1 mL) and CH_2Cl_2 (1 mL) were added. The phases were separated, and the aqueous layer was extracted with CH_2Cl_2 (3 × 5 mL). The combined organic extracts were dried over Na_2SO_4 and filtered. The solvent was removed under reduced pressure to afford the crude *N*-Boc protected piperidine derivative.

This crude was solubilized in anhydrous THF (800 μL, 0.2 M) and the resulting solution was added dropwise to a suspension of $LiAlH_4$ (15.2 mg, 0.40 mmol, 2 equiv) in anhydrous THF (200 μL, 2.0 M) at 0 °C under argon atmosphere. The mixture was then stirred at 20 °C for 30 min. The reaction mixture was then quenched by slow addition of sat. aq. NH_4Cl (2 mL) at 0 °C and stirred at rt for 30 min. The resulting suspension was filtered through a pad of Celite®, eluting with EtOAc (3 × 5 mL). The phases were separated, and the aqueous layer was extracted with EtOAc (3 × 5 mL). The combined organic extracts were dried over Na_2SO_4 and filtered. The solvent was removed under reduced pressure. Purification by flash column chromatography (10% to 20% acetone/hexane) afforded primary alcohol **(+)-S4a** as a yellow solid (52.0 mg, 70% over 2 steps, 98.1% *ee*).

$[\alpha]_D^{23}$ + 5.0 (***c*** 0.8, $CHCl_3$).
R_f 0.21 (20% acetone/hexane);
mp = 49–54 °C;
ν_{max} (film)/cm^{-1} 3407 (OH), 2922, 1662 (C=O), 1476, 1424, 1230, 1159, 1129, 1059, 1006, 816, 769;
^{1}H NMR (400 MHz, $CDCl_3$, 298 K) δ 7.47–7.40 (m, 2 H, HC_{Ar}), 7.11–7.05 (m, 2 H, HC_{Ar}), 4.36 (br d, *J* = 13.2 Hz, 1 H, NC*H*HCHCH$_2$OH), 4.20 (br s, 1 H, NC*H*HCH$_2$), 3.43 (dd, *J* = 11.0, 3.1 Hz, 1 H, C*H*HOH), 3.26 (dd, *J* = 11.0, 6.4 Hz, 1 H, CH*H*OH), 2.87–2.62 (m, 2 H, NCH*H*CHCH$_2$OH, NCH*H*CH$_2$), 2.59–2.47 (m, 1 H, CHAr), 1.88–1.59 (m, 4 H, C*H*CH$_2$OH, NCH$_2$C*H*$_2$, OH), 1.49 (s, 9 H, C(CH$_3$)$_3$);
^{13}C NMR (101 MHz, $CDCl_3$, 298 K, observed as a mixture of rotamers) δ 154.8 (C=O), 142.8 (C_{Ar} quat), 131.8 (2 × C_{Ar}), 129.1 (2 × C_{Ar}), 120.3 (BrC_{Ar} quat), 79.7 (*C*(CH$_3$)$_3$), 62.9 (*C*H$_2$OH), 46.5 (br m, NCH$_2$CHCH$_2$OH), 44.2 and 43.6 (NCH$_2$CH$_2$, *C*HAr, *C*HCH$_2$OH), 33.8 (NCH$_2$*C*H$_2$), 28.5 (C(*C*H$_3$)$_3$);
HRMS (ESI$^+$) ***m/z*** Calculated for $C_{19}H_{27}N_2O_3Na^{79}Br$ [M+CH_3CN+Na Adduct] 433.1103; Found 433.1110.

HPLC Conditions: Chiralpak ID 3-column, 90:10 *n*-hexane:*i*-PrOH, flow rate: 1 mL·min^{-1}, 35 ºC, UV detection wavelength: 210.4 nm. Retention times: 8.0 min (3*R,*4*S* enantiomer), 8.6 min (3*S,*4*R* enantiomer).

SMILES: BrC1=CC=C([C@@H]2[C@@H](CO)CN(C(OC(C)(C)C)=O)CC2)C=C1

InChI=1S/C17H24BrNO3/c1-17(2,3)22-16(21)19-9-8-15(13(10-19)11-20)12-4-6-14(18)7-5-12/h4-7,13,15,20H,8-11H2,1-3H3/t13-,15-/m1/s1

***tert*-Butyl (–)-(3*S*,4*R*)-4-(4-bromophenyl)-3-(hydroxymethyl)piperidine-1-carboxylate ((–)-8a)**

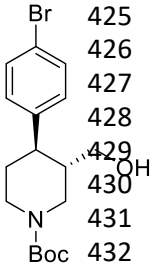

A flame-dried round-bottom flask was charged with amide **(+)-7a** (565 mg, 1.11 mmol, 1 equiv), followed by di-*tert*-butyl dicarbonate (Boc_2O, 969 mg, 4.44 mmol, 4 equiv) and 4-(dimethylamino)pyridine (DMAP, 26.9 mg, 0.22 mmol, 20 mol %). The reaction vessel was sealed with an aluminum cap (with molded butyl septa) and purged with argon, then anhydrous MeCN (3.7 mL) and anhydrous CH_2Cl_2 (0.5 mL) were added by syringe. The mixture (0.3 M) was then stirred at 35 ºC for 22 h. The reaction mixture was then allowed to cool to rt and sat. aq. NH_4Cl (5 mL) and CH_2Cl_2 (5 mL) were added. The phases were separated, and the aqueous layer was extracted with CH_2Cl_2 (3 × 10 mL). The combined organic extracts were dried over Na_2SO_4 and filtered. The solvent was removed under reduced pressure to afford the crude *N*-Boc protected piperidine derivative.

This crude was solubilized in anhydrous THF (3.5 mL, 0.3 M) and the resulting solution was added dropwise to a suspension of $LiAlH_4$ (84.2 mg, 2.22 mmol, 2 equiv) in anhydrous THF (2.0 mL, 1.0 M) at 0 °C under argon atmosphere. The mixture was then stirred at 20 °C for 30 min. The reaction mixture was then quenched by slow addition of sat. aq. NH_4Cl (5 mL) at 0 °C and stirred at rt for 30 min. The resulting suspension was filtered through a pad of Celite®, eluting with EtOAc (3 × 10 mL). The phases were separated, and the aqueous layer was extracted with EtOAc (3 × 10 mL). The combined organic extracts were dried over Na_2SO_4 and filtered. The solvent was removed under reduced pressure. Purification by flash column chromatography (10% to 20% acetone/hexane) afforded primary alcohol **(–)-8a** as a white solid (316 mg, 77% over 2 steps, 98.1% *ee*).

$[\alpha]_D^{23}$ – 8.0 (*c* 1.0, $CHCl_3$).

Characterization data identical to that reported for enantiomeric alcohol **(+)-S4a** (see S20).

HPLC Conditions: Chiralpak ID 3-column, 90:10 *n*-hexane:*i*-PrOH, flow rate: 1 mL·min^{-1}, 35 ºC, UV detection wavelength: 210.4 nm. Retention times: 8.0 min (3*R*,4*S* enantiomer), 8.6 min (3*S*,4*R* enantiomer).

SMILES: BrC1=CC=C([C@H]2[C@H](CO)CN(C(OC(C)(C)C)=O)CC2)C=C1

InChI=1S/C17H24BrNO3/c1-17(2,3)22-16(21)19-9-8-15(13(10-19)11-20)12-4-6-14(18)7-5-12/h4-7,13,15,20H,8-11H2,1-3H3/t13-,15-/m0/s1

***tert*-Butyl (3*S*,4*R*)-3-((benzo[*d*][1,3]dioxol-5-yloxy)methyl)-4-(4-bromophenyl)piperidine-1-carboxylate ((–)-9a)**

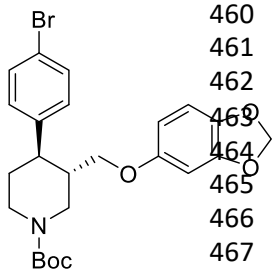

Alcohol **(–)-8a** (280 mg, 0.76 mmol, 1 equiv) and triethylamine (147 μL, 1.10 mmol, 1.4 equiv) were added to a flame-dried round-bottom flask, dissolved in anhydrous CH_2Cl_2 (4.0 mL, 0.2 M) and cooled down to 0 °C. Methanesulfonyl chloride (75 μL, 0.97 mmol, 1.3 equiv) was then added by Gilson pipette. After stirring 5 min at 0 °C, the reaction mixture was stirred at 25 °C for 2 h, then diluted with CH_2Cl_2 (5 mL) and sat. aq. $NaHCO_3$ (5 mL). The phases were separated, and the aqueous layer was extracted with CH_2Cl_2 (3 × 10 mL). The combined organic extracts were dried over Na_2SO_4 and filtered. The solvent was removed under reduced pressure to afford the crude mesylated alcohol derivative.

NaH (60% dispersion in mineral oil, 51.8 mg, 1.30 mmol, 1.7 equiv) was added to a solution of sesamol (168 mg, 1.20 mmol, 1.6 equiv) in anhydrous THF (4.0 mL, 0.3 M) at 0 °C. The mixture was then stirred at 25 °C for 1 h. A solution of the crude mesylated alcohol in anhydrous THF (5.0 mL, 0.1 M) was then added dropwise to this suspension. The resulting mixture was stirred at 70 °C for 18 h. The reaction mixture was then quenched by addition of H_2O (5 mL) and diluted with EtOAc (5 mL).

The phases were separated, and the aqueous layer was extracted with EtOAc (4 × 10 mL). The combined organic extracts were dried over Na_2SO_4 and filtered. The solvent was removed under reduced pressure. Purification by flash column chromatography (5% acetone/pentane) afforded piperidine **(–)-9a** as a white solid (225 mg, 60% over 2 steps).

$[\alpha]_D^{23}$ – 36.0 (*c* 1.0, $CHCl_3$).
R_f 0.20 (5% acetone/pentane);
mp = 53–58 °C;
ν_{max} (film)/cm^{-1} 2915, 1685 (C=O), 1483, 1424, 1230, 1163, 1129, 1036, 928, 816, 769;
^{1}H NMR (400 MHz, $CDCl_3$, 298 K) δ 7.45–7.38 (m, 2 H, HC_{Ar}), 7.10–7.03 (m, 2 H, HC_{Ar}), 6.64 (d, *J* = 8.5 Hz, 1 H, HC_{Ar}), 6.36 (d, *J* = 2.5 Hz, 1 H, HC_{Ar}), 6.14 (dd, *J* = 8.5, 2.5 Hz, 1 H, HC_{Ar}), 5.89 (s, 2 H, OCH_2O), 4.44 (br s, 1 H, NC*H*HCHCH$_2$OAr), 4.25 (br s, 1 H, NC*H*HCH$_2$), 3.61 (dd, *J* = 9.4, 2.8 Hz, 1 H, C*H*HOAr), 3.45 (dd, *J* = 9.4, 6.4 Hz, 1 H, CH*H*OAr), 2.92–2.73 (br m, 2 H, NCH*H*CHCH$_2$OAr, NCH*H*CH$_2$), 2.67 (td, *J* = 11.7, 3.9 Hz, 1 H, CHAr), 2.08–1.97 (br m, 1 H, C*H*CH$_2$OAr), 1.85–1.77 (br m, 1 H, NCH$_2$C*H*H), 1.72 (td, *J* = 12.6, 4.3 Hz, 1 H, NCH$_2$CH*H*), 1.50 (s, 9 H, C(CH$_3$)$_3$);
^{13}C NMR (101 MHz, $CDCl_3$, 298 K) δ 154.7 (C=O), 154.2 (OC_{Ar} quat), 148.1 (OC_{Ar} quat), 142.4 (C_{Ar} quat), 141.7 (OC_{Ar} quat), 131.8 (2 × C_{Ar}), 129.1 (2 × C_{Ar}), 120.4 (BrC_{Ar} quat), 107.8 (C_{Ar}), 105.5 (C_{Ar}), 101.1 (OCH_2O), 98.0 (C_{Ar}), 79.7 (*C*(CH$_3$)$_3$), 68.7 (*C*H$_2$OAr), 47.3 (br m, N*C*H$_2$CHCH$_2$OAr), 44.2 (N*C*H$_2$CH$_2$, *C*HAr), 41.7 (*C*HCH$_2$OAr), 33.7 (NCH$_2$*C*H$_2$), 28.4 (C(*C*H$_3$)$_3$);
HRMS (ESI$^+$) *m/z* Calculated for $C_{24}H_{29}NO_5{}^{79}Br$ [M+H] 490.1229; Found 490.1240.

SMILES: BrC1=CC=C([C@H]2[C@H](COC3=CC(OCO4)=C4C=C3)CN(C(OC(C)(C)C)=O)CC2)C=C1

InChI=1S/C24H28BrNO5/c1-24(2,3)31-23(27)26-11-10-20(16-4-6-18(25)7-5-16)17(13-26)14-28-19-8-9-21-22(12-19)30-15-29-21/h4-9,12,17,20H,10-11,13-15H2,1-3H3/t17-,20-/m0/s1

(3*S*,4*R*)-3-((Benzo[d][1,3]dioxol-5-yloxy)methyl)-4-(4-bromophenyl)piperidine-1-ium chloride (2 · HCl)

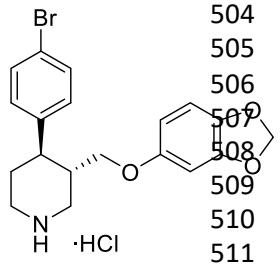

4 N HCl in 1,4-dioxane (500 μL, 2.00 mmol, 10 equiv) was added to a solution of *N*-Boc protected piperidine **(–)-9a** (98.1 mg, 0.20 mmol, 1 equiv) in 1,4-dioxane (500 μL, 0.4 M) at 0 °C under air. The solution was stirred at 25 ºC for 18 h, then an ice-cold 1:1 mixture of Et_2O/pentane (1 mL) was added and formation of a solid precipitate was observed. This was filtered and washed with further ice-cold Et_2O/pentane mixture (2 × 5 mL). The solid precipitate was dried under reduced pressure to afford (3*S*,4*R*)-3-((benzo[d][1,3]dioxol-5-yloxy)methyl)-4-(4-bromophenyl) piperidine-1-ium chloride **2** · HCl as an off-white solid (73.5 mg, 86%).

$[\alpha]_D^{23}$ – 82.0 (*c* 1.0, MeOH);
mp = 206–209 ºC;
ν_{max} (film)/cm^{-1} 3317 (NH), 2926, 2687, 1484, 1182, 1103, 1033, 932, 846, 813, 787;
^{1}H NMR (400 MHz, CD_3OD, 298 K) δ 7.50–7.44 (m, 2 H, HC_{Ar}), 7.24–7.18 (m, 2 H, HC_{Ar}), 6.63 (d, *J* = 8.4 Hz, 1 H, HC_{Ar}), 6.39 (d, *J* = 2.5 Hz, 1 H, HC_{Ar}), 6.18 (dd, *J* = 8.5, 2.5 Hz, 1 H, HC_{Ar}), 5.87–5.84 (m, 2 H, OCH_2O), 3.71–3.62 (m, 2 H, C*H*HOAr, NC*H*HCHCH$_2$OAr), 3.59–3.49 (m, 2 H, CH*H*OAr, NC*H*HCH$_2$), 2.21–2.11 (m, 2 H, NCH*H*CHCH$_2$OAr, NCH*H*CH$_2$), 3.03–2.91 (m, 1 H, CHAr), 2.49–2.37 (m, 1 H, C*H*CH$_2$OAr), 2.10–2.01 (m, 2 H, NCH$_2$C*H*$_2$);
^{13}C NMR (101 MHz, CD_3OD, 298 K) δ 155.3 (OC_{Ar} quat), 149.7 (OC_{Ar} quat), 143.5 (C_{Ar} quat), 142.4 (OC_{Ar} quat), 133.0 (2 × C_{Ar}), 130.5 (2 × C_{Ar}), 122.0 (BrC_{Ar} quat), 108.8 (C_{Ar}), 106.7 (C_{Ar}), 102.5 (OCH_2O), 98.9 (C_{Ar}), 69.0 (*C*H$_2$OAr), 47.7 (N*C*H$_2$CHCH$_2$OAr), 45.5 (N*C*H$_2$CH$_2$), 42.9 (*C*HAr), 40.6 (*C*HCH$_2$OAr), 31.4 (NCH$_2$*C*H$_2$);

526 HRMS (ESI$^+$) *m/z* Calculated for $C_{19}H_{21}NO_3{}^{79}Br$ [M–Cl] 390.0705; Found 390.0698.
527
528 SMILES: BrC1=CC=C([C@H]2[C@H](COC3=CC(OCO4)=C4C=C3)CNCC2)C=C1.Cl
529
530 InChI=1S/C19H20BrNO3.ClH/c20-15-3-1-13(2-4-15)17-7-8-21-10-14(17)11-22-16-5-6-18-19(9-16)24-
531 12-23-18;/h1-6,9,14,17,21H,7-8,10-12H2;1H/t14-,17-;/m0./s1
532
533

Synthesis of I-analogue of (–)-paroxetine (compounds **(±)-S2b**, **(±)-S3b**, **(+)-6b**, **(+)-7b**, **(–)-S3b**, **(–)-8b**, **(+)-S4b**, **(–)-9b** and **3** · HCl)

***tert*-Butyl *cis*-(±)-4-(4-iodophenyl)-3-(quinolin-8-ylcarbamoyl)piperidine-1-carboxylate ((±)-S2b)** and ***tert*-butyl *trans*-(±)-4-(4-iodophenyl)-3-(quinolin-8-ylcarbamoyl)piperidine-1-carboxylate ((±)-S3b):**

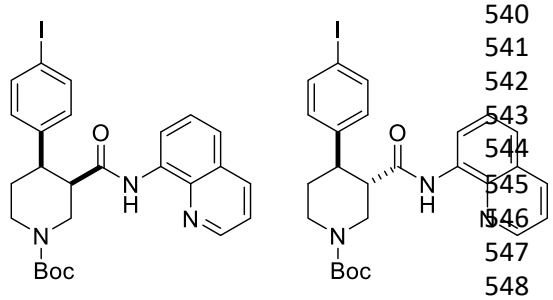

A reaction tube was charged with K_2CO_3 (69.1 mg, 0.50 mmol, 1 equiv), flame-dried, and allowed to cool under argon. *tert*-Butyl (±)-3-(quinoline-8-ylcarbamoyl)piperidine-1-carboxylate (**(±)-S1**) (178 mg, 0.50 mmol, 1 equiv), 1,4-diiodobenzene (660 mg, 2.00 mmol, 4 equiv), $Pd(OAc)_2$ (5.60 mg, 25.0 μmol, 5 mol %) and PivOH (51.2 mg, 0.50 mmol, 1 equiv) were added sequentially. The reaction vessel was sealed with an aluminum cap (with molded butyl/PTFE septa) and purged with argon, then anhydrous $PhCF_3$ (500 μL, 1.0 M) was added by syringe. The reaction tube was then placed in a preheated oil bath and stirred at 110 ºC for 18 h. The reaction mixture was allowed to cool to rt and EtOAc (10 mL) was added. The resulting mixture was filtered through a pad of Celite®, eluting with further EtOAc (2 × 10 mL). The solvent was removed under reduced pressure, and the crude material was purified by flash column chromatography (0% to 5% CH_3CN/CH_2Cl_2). The product containing fractions were combined and the solvent was removed under reduced pressure. Et_2O (5 mL) and pentane (5 mL) were added and the solvent was removed under reduced pressure to afford the minor product *tert*–butyl *trans*-(±)-4-(4-iodophenyl)-3-(quinolin-8-ylcarbamoyl) piperidine-1-carboxylate **(±)-S3b** as a pale yellow solid (52.2 mg, 19%) followed by the major product *tert*-butyl *cis*-(±)-4-(4-iodophenyl)-3-(quinolin-8-ylcarbamoyl)piperidine-1-carboxylate **(±)-S2b** as a pale yellow solid (97.9 mg, 35%).

Major (**(±)-S2b**):
R_f 0.30 (5% CH_3CN/CH_2Cl_2);
mp = 91–95 °C (from Et_2O/pentane);
ν_{max} (film)/cm^{-1} 3343 (NH), 2926, 1685 (C=O), 1521, 1483, 1424, 1364, 1323, 1245, 1159, 1118, 1003, 824, 790, 757;
^{1}H NMR (500 MHz, $(CD_3)_2SO$, 373 K) δ 9.75 (br s, 1 H, NH), 8.83 (dd, *J* = 4.2, 1.7 Hz, 1 H, HC_{Ar}), 8.45 (dd, *J* = 7.6, 1.4 Hz, 1 H, HC_{Ar}), 8.31 (dd, *J* = 8.3, 1.7 Hz, 1 H, HC_{Ar}), 7.60–7.53 (m, 4 H, HC_{Ar}), 7.48 (t, *J* = 8.0 Hz, 1 H, HC_{Ar}), 7.19–7.12 (m, 2 H, HC_{Ar}), 4.42 (ddd, *J* = 14.9, 3.7, 1.8 Hz, 1 H, NC*H*HCHCO), 4.25 (ddt, *J* = 13.2, 4.7, 2.4 Hz, 1 H, NC*H*HCH_2), 3.35–3.28 (m, 2 H, NCH*H*CHCO, CHCO), 3.14 (dt, *J* = 12.4, 4.2 Hz, 1 H, CHAr), 3.01–2.92 (m, 1 H, NCH*H*CH_2), 2.67 (qd, *J* = 12.4, 4.6 Hz, 1 H, NCH_2C*H*H), 1.71 (dq, *J* = 13.0, 3.4 Hz, 1 H, NCH_2CH*H*), 1.25 (s, 9 H, $C(CH_3)_3$);
^{13}C NMR (126 MHz, $(CD_3)_2SO$, 373 K) δ 169.8 (C=O amide), 153.4 (C=O carbamate), 147.9 (C_{Ar}), 142.5 (C_{Ar} quat), 137.6 (C_{Ar} quat), 136.3 (2 × C_{Ar}), 135.7 (C_{Ar}), 133.9 (C_{Ar} quat), 129.3 (2 × C_{Ar}), 127.2 (C_{Ar} quat), 126.1 (C_{Ar}), 121.2 (C_{Ar}), 120.8 (C_{Ar}), 115.7 (C_{Ar}), 90.9 (IC_{Ar} quat), 77.9 (*C*$(CH_3)_3$), 46.2 (NCH_2CHCO), 45.6 (*C*HCO), 42.9 (NCH_2CH_2), 41.8 (*C*HAr), 27.4 (C(*C*$H_3)_3$), 25.0 (NCH_2CH_2);
HRMS (ESI$^+$) *m/z* Calculated for $C_{26}H_{29}N_3O_3{}^{127}I$ [M+H] 558.1254; Found 558.1260.

SMILES:
O=C([C@H]1CN(C(OC(C)(C)C)=O)CC[C@H]1C2=CC=C(I)C=C2)NC3=C(N=CC=C4)C4=CC=C3

InChI=1S/C26H28IN3O3/c1-26(2,3)33-25(32)30-15-13-20(17-9-11-19(27)12-10-17)21(16-30)24(31)29-22-8-4-6-18-7-5-14-28-23(18)22/h4-12,14,20-21H,13,15-16H2,1-3H3,(H,29,31)/t20-,21-/m0/s1

Minor (**(±)-S3b**):
R_f 0.41 (5% CH_3CN/CH_2Cl_2);
mp = 93–96 °C (from Et_2O/pentane); ν_{max} (film)/cm^{-1} 3336 (NH), 2922, 1677 (C=O), 1521, 1483, 1424, 1323, 1230, 1156, 1062, 1003, 824, 757;
^1H NMR (500 MHz, $(CD_3)_2SO$, 373 K) δ 9.73 (br s, 1 H, NH), 8.85 (dd, *J* = 4.2, 1.7 Hz, 1 H, HC_{Ar}), 8.39 (dd, *J* = 7.7, 1.3 Hz, 1 H, HC_{Ar}), 8.31 (dd, *J* = 8.3, 1.7 Hz, 1 H, HC_{Ar}), 7.62–7.55 (m, 2 H, HC_{Ar}), 7.55–7.51 (m, 2 H, HC_{Ar}), 7.47 (t, *J* = 8.0 Hz, 1 H, HC_{Ar}), 7.19–7.14 (m, 2 H, HC_{Ar}), 4.35 (ddd, *J* = 12.8, 3.8, 1.8 Hz, 1 H, NC*H*HCHCO), 4.12 (ddt, *J* = 13.3, 4.4, 2.1 Hz, 1 H, NC*H*HCH_2), 3.17–2.99 (m, 3 H, NCH*H*CHCO, CHCO, CHAr), 2.98–2.90 (m, 1 H, NCH*H*CH_2), 1.80 (dq, *J* = 13.3, 3.0 Hz, 1 H, NCH_2CHH), 1.65 (qd, *J* = 12.7, 4.6 Hz, 1 H, NCH_2CH*H*), 1.48 (s, 9 H, $C(CH_3)_3$);
^{13}C NMR (126 MHz, $(CD_3)_2SO$, 373 K) δ 169.8 (C=O amide), 153.4 (C=O carbamate), 148.1 (C_{Ar}), 142.8 (C_{Ar} quat), 137.7 (C_{Ar} quat), 136.6 (2 × C_{Ar}), 135.7 (C_{Ar}), 133.5 (C_{Ar} quat), 129.3 (2 × C_{Ar}), 127.2 (C_{Ar} quat), 126.1 (C_{Ar}), 121.4 (C_{Ar}), 121.3 (C_{Ar}), 116.3 (C_{Ar}), 91.1 (IC_{Ar} quat), 78.6 (*C*$(CH_3)_3$), 49.1 (*C*HCO), 46.2 (NCH_2CHCO), 44.0 (*C*HAr), 43.3 (NCH_2CH_2), 32.0 (NCH_2CH_2), 27.7 ($C(CH_3)_3$);
HRMS (ESI$^+$) *m/z* Calculated for $C_{26}H_{29}N_3O_3{}^{127}I$ [M+H] 558.1254; Found 558.1247.

SMILES:
O=C([C@@H]1CN(C(OC(C)(C)C)=O)CC[C@H]1C2=CC=C(I)C=C2)NC3=C(N=CC=C4)C4=CC=C3

InChI=1S/C26H28IN3O3/c1-26(2,3)33-25(32)30-15-13-20(17-9-11-19(27)12-10-17)21(16-30)24(31)29-22-8-4-6-18-7-5-14-28-23(18)22/h4-12,14,20-21H,13,15-16H2,1-3H3,(H,29,31)/t20-,21+/m0/s1

***tert*-Butyl (+)-(*3R,4R*)-4-(4-iodophenyl)-3-(quinolin-8-ylcarbamoyl)piperidine-1-carboxylate ((+)-6b)** and ***tert*-butyl (–)-(*3R,4S*)-4-(4-iodophenyl)-3-(quinolin-8-ylcarbamoyl)piperidine-1-carboxylate ((–)-S3b)**:

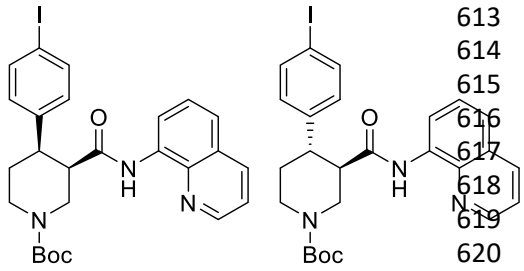

A large microwave vial (10–20 mL recommended volume) was charged with K_2CO_3 (553 mg, 4.0 mmol, 1 equiv), flame-dried, and allowed to cool under argon. *tert*-Butyl (*R*)-3-(quinolin-8-ylcarbamoyl)piperidine-1-carboxylate **(–)-5** (1.42 g, 4.0 mmol 1 equiv), 1,4-diiodobenzene (5.28 g, 16.0 mmol, 4 equiv), $Pd(OAc)_2$ (45.1 mg, 0.2 mmol, 5 mol %) and PivOH (409 mg, 4.0 mmol, 1 equiv) were added sequentially. The reaction vessel was sealed with an aluminum cap (with molded butyl/PTFE septa) and purged with argon, then anhydrous $PhCF_3$ (2.0 mL, 2.00 M) was added by syringe. The reaction tube was then placed in a preheated oil bath and stirred at 110 ºC for 18 h. The reaction mixture was then allowed to cool to rt and EtOAc (20 mL) was added. The resulting mixture was filtered through a pad of Celite®, eluting with further EtOAc (2 × 50 mL). The solvent was removed under reduced pressure. The reaction mixture was purified by two consecutive chromatographic separations: one (0% to 5% CH_3CN/CH_2Cl_2) to isolate the minor *trans*-product *tert*-butyl (–)-(*3R,4S*)-4-(4-iodophenyl)-3-(quinolin-8-ylcarbamoyl)piperidine-1-carboxylate **(–)-S3b** followed by a second (10% to 15% acetone/pentane) to isolate the major *cis*-product *tert*-butyl (+)-(*3R,4R*)-4-(4-iodophenyl)-3-(quinolin-8-ylcarbamoyl)piperidine-1-carboxylate **(+)-6b**. The product containing fractions were combined and the solvent was removed under reduced pressure. Et_2O (20 mL) and pentane (20 mL) were added and the solvent was removed under reduced pressure to afford the minor *trans*-product **(–)-S3b** as a pale orange solid (441 mg, 20%, 98.1% *ee*) and the major *cis*-product **(+)-6b** (775 mg, 35%, 98.2% *ee*).

Major (**(+)-6b**):
$[\alpha]_D^{23}$ + 9.1 (*c* 1.1, $CHCl_3$).
Characterization data identical to that reported for racemic *cis*-piperidine **(±)-S2b** (see S24).

HPLC Conditions: Chiralpak IA 3-column, 85:15 *n*-hexane:*i*-PrOH, flow rate: 1 mL·min^{-1}, 35 ºC, UV detection wavelength: 210.4 nm. Retention times: 12.2 min (3*S,*4*S* enantiomer), 17.7 min (3*R,*4*R* enantiomer).

SMILES:
O=C([C@H]1CN(C(OC(C)(C)C)=O)CC[C@H]1C2=CC=C(I)C=C2)NC3=C(N=CC=C4)C4=CC=C3

InChI=1S/C26H28IN3O3/c1-26(2,3)33-25(32)30-15-13-20(17-9-11-19(27)12-10-17)21(16-30)24(31)29-22-8-4-6-18-7-5-14-28-23(18)22/h4-12,14,20-21H,13,15-16H2,1-3H3,(H,29,31)/t20-,21-/m0/s1

Minor (**(–)-S3b**):
$[\alpha]_D^{23}$ – 45.5 (*c* 1.1, $CHCl_3$).
Characterization data identical to that reported for racemic *trans*-piperidine **(±)-S3b** (see S24).

HPLC Conditions: Chiralpak IA 3-column, 85:15 *n*-hexane:*i*-PrOH, flow rate: 1 mL·min^{-1}, 35 ºC, UV detection wavelength: 254.1 nm. Retention times: 9.4 min (3*R,*4*S* enantiomer), 13.3 min (3*S,*4*R* enantiomer).

SMILES:
O=C([C@H]1CN(C(OC(C)(C)C)=O)CC[C@@H]1C2=CC=C(I)C=C2)NC3=C(N=CC=C4)C4=CC=C3

InChI=1S/C26H28IN3O3/c1-26(2,3)33-25(32)30-15-13-20(17-9-11-19(27)12-10-17)21(16-30)24(31)29-22-8-4-6-18-7-5-14-28-23(18)22/h4-12,14,20-21H,13,15-16H2,1-3H3,(H,29,31)/t20-,21+/m1/s1

***tert*-Butyl (+)-(*3S,4R*)-4-(4-iodophenyl)-3-(quinolin-8-ylcarbamoyl)piperidine-1-carboxylate ((+)-7b)**

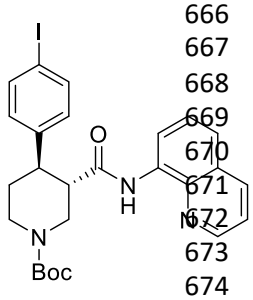

A flame-dried reaction tube was charged with *cis*-3,4-disubstituted piperidine **(+)-6b** (687 mg, 1.23 mmol, 1 equiv) and 1,8-diazabicyclo(5.4.0)undec-7-ene (DBU, 550 μL, 3.70 mmol, 3 equiv). The reaction vessel was sealed with an aluminum cap (with molded butyl/PTFE septa) and purged with argon, then anhydrous toluene (1.20 mL, 1.0 M) was added by syringe. The reaction tube was then placed in a preheated oil bath and stirred at 110 ºC for 24 h. The reaction mixture was then allowed to cool to rt and CH_2Cl_2 (5 mL) and sat. aq. NH_4Cl (5 mL) were added. The phases were separated, and the aqueous layer was extracted with CH_2Cl_2 (3 × 10 mL). The combined organic extracts were dried over Na_2SO_4 and filtered. The solvent was removed under reduced pressure. The reaction mixture was purified by flash column chromatography (10% acetone/pentane). The product containing fractions were combined and the solvent was removed under reduced pressure. Et_2O (10 mL) and pentane (10 mL) were added and the solvent was removed under reduced pressure to afford amide *tert*-butyl (+)-(*3S,4R*)-4-(4-iodophenyl)-3-(quinolin-8-ylcarbamoyl) piperidine-1-carboxylate **(+)-7b** as a white solid (626 mg, 91%, 98.0% *ee*).

$[\alpha]_D^{23}$ + 48.0 (*c* 1.0, $CHCl_3$).
Characterization data identical to that reported for racemic *trans*-piperidine **(±)-S3b** (see S24).

HPLC Conditions: Chiralpak IA 3-column, 85:15 *n*-hexane:*i*-PrOH, flow rate: 1 mL·min^{-1}, 35 ºC, UV detection wavelength: 254.1 nm. Retention times: 9.4 min (3*R,*4*S* enantiomer), 13.3 min (3*S,*4*R* enantiomer).

SMILES:
O=C([C@@H]1CN(C(OC(C)(C)C)=O)CC[C@H]1C2=CC=C(I)C=C2)NC3=C(N=CC=C4)C4=CC=C3
InChI=1S/C26H28IN3O3/c1-26(2,3)33-25(32)30-15-13-20(17-9-11-19(27)12-10-17)21(16-30)24(31)29-22-8-4-6-18-7-5-14-28-23(18)22/h4-12,14,20-21H,13,15-16H2,1-3H3,(H,29,31)/t20-,21+/m0/s1

tert-Butyl (+)-(*3R,4S*)-4-(4-iodophenyl)-3-(hydroxymethyl)piperidine-1-carboxylate ((+)-S4b)

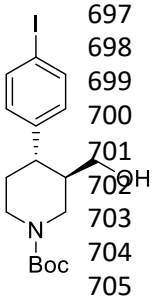

A flame-dried reaction tube was charged with amide **(–)-S3b** (111 mg, 0.20 mmol, 1 equiv), followed by di-*tert*-butyl dicarbonate (Boc_2O, 175 mg, 0.80 mmol, 4 equiv) and 4-(dimethylamino)pyridine (DMAP, 4.9 mg, 0.04 mmol, 20 mol %). The reaction vessel was sealed with an aluminum cap (with molded butyl septa) and purged with argon, then anhydrous MeCN (400 μL, 0.5 M) was added by syringe. The mixture was then stirred at 40 ºC for 22 h. The reaction mixture was then allowed to cool to rt and sat. aq. NH_4Cl (1 mL) and CH_2Cl_2 (1 mL) were added. The phases were separated, and the aqueous layer was extracted with CH_2Cl_2 (3 × 5 mL). The combined organic extracts were dried over Na_2SO_4 and filtered. The solvent was removed under reduced pressure to afford the crude *N*-Boc protected piperidine derivative.

This crude was solubilized in anhydrous THF (800 μL, 0.2 M) and the resulting solution was added dropwise to a suspension of $LiAlH_4$ (15.2 mg, 0.40 mmol, 2 equiv) in anhydrous THF (200 μL, 2.0 M) at 0 °C under argon atmosphere. The mixture was then stirred at 20 °C for 30 min. The reaction mixture was then quenched by slow addition of sat. aq. NH_4Cl (2 mL) at 0 °C and stirred at rt for 30 min. The resulting suspension was filtered through a pad of Celite®, eluting with EtOAc (3 × 5 mL). The phases were separated, and the aqueous layer was extracted with EtOAc (3 × 5 mL). The combined organic extracts were dried over Na_2SO_4 and filtered. The solvent was removed under reduced pressure. Purification by flash column chromatography (10% to 15% acetone/pentane) afforded primary alcohol **(+)-S4b** as a white solid (52.3 mg, 63% over 2 steps, 98.1% *ee*, containing approx. 10% deiodinated derivative).

$[\alpha]_D^{23}$ + 2.0 (*c* 1.0, $CHCl_3$).
R_f 0.24 (15% acetone/pentane);
mp = 53–59 °C;
ν_{max} (film)/cm^{-1} 3422 (OH), 2922, 1662 (C=O), 1479, 1424, 1364, 1234, 1163, 1129, 1059, 1006, 816, 764; ^{1}H NMR (400 MHz, $CDCl_3$, 298 K) δ 7.66–7.61 (m, 2 H, HC_{Ar}), 6.99–6.93 (m, 2 H, HC_{Ar}), 4.36 (br d, *J* = 13.2 Hz, 1 H, NC*H*HCHCH$_2$OH), 4.20 (br s, 1 H, NC*H*HCH$_2$), 3.44 (dt, *J* = 11.0, 3.5 Hz, 1 H, C*H*HOH), 3.26 (dt, *J* = 11.3, 5.8 Hz, 1 H, CH*H*OH), 2.87–2.63 (m, 2 H, NCH*H*CHCH$_2$OH, NCH*H*CH$_2$), 2.51 (td, *J* = 10.2, 5.2 Hz, 1 H, CHAr), 1.87–1.72 (m, 2 H, C*H*CH$_2$OH, NCH$_2$C*H*H), 1.71–1.58 (m, 2 H, NCH$_2$CH*H*, OH), 1.49 (s, 9 H, C(CH$_3$)$_3$);
^{13}C NMR (101 MHz, $CDCl_3$, 298 K, observed as a mixture of rotamers) δ 154.8 (C=O), 143.5 (C_{Ar} quat), 137.7 (2 × C_{Ar}), 129.5 (2 × C_{Ar}), 91.7 (IC_{Ar} quat), 79.7 (*C*(CH$_3$)$_3$), 63.0 (*C*H$_2$OH), 46.4 (br m, NCH$_2$CHCH$_2$OH), 44.4 and 43.5 (NCH$_2$CH$_2$, *C*HAr, *C*HCH$_2$OH), 33.8 (NCH$_2$*C*H$_2$), 28.5 (C(*C*H$_3$)$_3$);
HRMS (ESI$^+$) ***m/z*** Calculated for $C_{17}H_{25}NO_3{}^{127}I$ [M+H] 418.0879; Found 418.0886.

HPLC Conditions: Chiralpak ID 3-column, 90:10 *n*-hexane:*i*-PrOH, flow rate: 1 mL·min^{-1}, 35 ºC, UV detection wavelength: 230.1 nm. Retention times: 6.7 min (3*R,*4*S* enantiomer), 7.4 min (3*S,*4*R* enantiomer).

SMILES: IC1=CC=C([C@@H]2[C@@H](CO)CN(C(OC(C)(C)C)=O)CC2)C=C1

InChI=1S/C17H24INO3/c1-17(2,3)22-16(21)19-9-8-15(13(10-19)11-20)12-4-6-14(18)7-5-12/h4-7,13,15,20H,8-11H2,1-3H3/t13-,15-/m1/s1

***tert*-Butyl (–)-(*3S,4R*)-4-(4-iodophenyl)-3-(hydroxymethyl)piperidine-1-carboxylate ((–)-8b)**

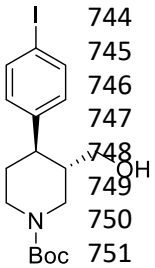

A flame-dried round-bottom flask was charged with amide **(+)-7b** (558 mg, 1.00 mmol, 1 equiv), followed by di-*tert*-butyl dicarbonate (Boc_2O, 873 mg, 4.00 mmol, 4 equiv) and 4-(dimethylamino)pyridine (DMAP, 24.4 mg, 0.20 mmol, 20 mol %). The reaction vessel was sealed with an aluminum cap (with molded butyl septa) and purged with argon, then anhydrous MeCN (3.3 mL) and anhydrous CH_2Cl_2 (0.5 mL) were added by syringe. The mixture (0.3 M) was then stirred at 40 ºC for 22 h. The reaction mixture was then allowed to cool to rt and sat. aq. NH_4Cl (5 mL) and CH_2Cl_2 (5 mL) were added. The phases were separated, and the aqueous layer was extracted with CH_2Cl_2 (3 × 10 mL). The combined organic extracts were dried over Na_2SO_4 and filtered. The solvent was removed under reduced pressure to afford the crude *N*-Boc protected piperidine derivative.

This crude solubilized in anhydrous THF (3.5 mL, 0.3 M) and the resulting solution was added dropwise to a suspension of $LiAlH_4$ (75.9 mg, 2.00 mmol, 2 equiv) in anhydrous THF (1.5 mL, 1.0 M) at 0 °C under argon atmosphere. The mixture was then stirred at 20 °C for 30 min. The reaction mixture was then quenched by slow addition of sat. aq. NH_4Cl (5 mL) at 0 °C and stirred at rt for 30 min. The resulting suspension was filtered through a pad of Celite®, eluting with EtOAc (3 × 10 mL). The phases were separated, and the aqueous layer was extracted with EtOAc (3 × 10 mL). The combined organic extracts were dried over Na_2SO_4 and filtered. The solvent was removed under reduced pressure. Purification by flash column chromatography (10% to 15% acetone/pentane) afforded primary alcohol **(–)-8b** as a white solid (315 mg, 68% over 2 steps, 98.0% *ee*, containing approx. 15% deiodinated derivative).

$[\alpha]_D^{23}$ – 8.0 (*c* 1.0, $CHCl_3$).

Characterization data identical to that reported for enantiomeric alcohol **(+)-S4b** (see S27).

HPLC Conditions: Chiralpak ID 3-column, 90:10 *n*-hexane:*i*-PrOH, flow rate: 1 mL·min^{-1}, 35 ºC, UV detection wavelength: 230.1 nm. Retention times: 6.7 min (3*R,4S* enantiomer), 7.4 min (3*S,4R* enantiomer).

SMILES: IC1=CC=C([C@H]2[C@H](CO)CN(C(OC(C)(C)C)=O)CC2)C=C1

InChI=1S/C17H24INO3/c1-17(2,3)22-16(21)19-9-8-15(13(10-19)11-20)12-4-6-14(18)7-5-12/h4-7,13,15,20H,8-11H2,1-3H3/t13-,15-/m0/s1

***tert*-Butyl (3*S*,4*R*)-3-((benzo[d][1,3]dioxol-5-yloxy)methyl)-4-(4-iodophenyl)piperidine-1-carboxylate ((–)-9b)**

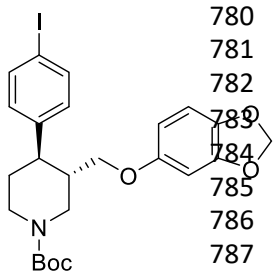

Alcohol **(–)-8b** (203 mg, 0.49 mmol, 1 equiv) and triethylamine (96 μL, 0.69 mmol, 1.4 equiv) were added to a flame-dried round-bottom flask, dissolved in anhydrous CH_2Cl_2 (2.5 mL, 0.2 M) and cooled down to 0 °C. Methanesulfonyl chloride (49 μL, 0.64 mmol, 1.3 equiv) was then added by Gilson pipette. After stirring 5 min at 0 °C, the reaction mixture was stirred at 25 °C for 2 h, then diluted with CH_2Cl_2 (5 mL) and sat. aq. $NaHCO_3$ (5 mL). The phases were separated, and the aqueous layer was extracted with CH_2Cl_2 (3 × 10 mL). The combined organic extracts were dried over Na_2SO_4 and filtered. The solvent was removed under reduced pressure to afford the crude mesylated alcohol derivative.

NaH (60% dispersion in mineral oil, 45.2 mg, 1.10 mmol, 2.2 equiv) was added to a solution of sesamol (135 mg, 0.98 mmol, 2 equiv) in anhydrous DMF (3.0 mL, 0.3 M) at 0 °C. The mixture was

then stirred at 25 °C for 1 h. A solution of the crude mesylated alcohol in dry DMF (2.0 mL, 0.2 M) was then added dropwise to this suspension. The resulting mixture was stirred at 90 °C for 20 h. The reaction mixture was quenched by addition of H_2O (5 mL) and aq NaOH 1 N (5 mL) and EtOAc (10 mL) were then added. The phases were separated, and the aqueous layer was extracted with EtOAc (4 × 20 mL). The combined organic extracts were washed with brine (2 × 50 mL), dried over Na_2SO_4 and filtered. The solvent was removed under reduced pressure. Purification by flash column chromatography (5% acetone/pentane) afforded piperidine **(–)-9b** as a white solid (188 mg, 71% over 2 steps).

$[\alpha]_D^{23}$ – 43.3 (*c* 1.2, $CHCl_3$).
R_f 0.15 (5% acetone/pentane);
mp = 51–54 °C; ν_{max} (film)/cm^{-1} 2919, 1685 (C=O), 1483, 1424, 1230, 1163, 1129, 1036, 1106, 928, 813, 764; ^{1}H NMR (400 MHz, $CDCl_3$, 298 K) δ 7.65–7.59 (m, 2 H, HC_{Ar}), 6.67–6.91 (m, 2 H, HC_{Ar}), 6.64 (d, *J* = 8.4 Hz, 1 H, HC_{Ar}), 6.36 (d, *J* = 2.5 Hz, 1 H, HC_{Ar}), 6.14 (dd, *J* = 8.5, 2.5 Hz, 1 H, HC_{Ar}), 5.89 (s, 2 H, OCH_2O), 4.43 (br s, 1 H, NC*H*HCHCH$_2$OAr), 4.25 (br s, 1 H, NC*H*HCH$_2$), 3.61 (dd, *J* = 9.4, 2.9 Hz, 1 H, C*H*HOAr), 3.45 (dd, *J* = 9.4, 6.4 Hz, 1 H, CH*H*OAr), 2.91–2.71 (br m, 2 H, NCH*H*CHCH$_2$OAr, NCH*H*CH$_2$), 2.65 (td, *J* = 11.8, 3.8 Hz, 1 H, CHAr), 2.08–1.96 (br m, 1 H, C*H*CH$_2$OAr), 1.86–1.76 (br m, 1 H, NCH$_2$C*H*H), 1.76–1.63 (m, 1 H, NCH$_2$CH*H*), 1.50 (s, 9 H, C(CH$_3$)$_3$);
^{13}C NMR (101 MHz, $CDCl_3$, 298 K) δ 154.7 (C=O), 154.2 (OC_{Ar} quat), 148.1 (OC_{Ar} quat), 143.1 (C_{Ar} quat), 141.7 (OC_{Ar} quat), 137.7 (2 × C_{Ar}), 129.4 (2 × C_{Ar}), 107.8 (C_{Ar}), 105.5 (C_{Ar}), 101.1 (OCH_2O), 98.0 (C_{Ar}), 91.8 (IC_{Ar} quat), 79.7 (*C*(CH$_3$)$_3$), 68.7 (*C*H$_2$OAr), 47.0 (br m, N*C*H$_2$CHCH$_2$OAr), 44.3 (N*C*H$_2$CH$_2$, *C*HAr), 41.6 (*C*HCH$_2$OAr), 33.6 (NCH$_2$*C*H$_2$), 28.4 (C(*C*H$_3$)$_3$);
HRMS (ESI$^+$) *m/z* Calculated for $C_{24}H_{29}NO_5{}^{127}I$ [M+H] 538.1090; Found 538.1104.

SMILES: IC1=CC=C([C@H]2[C@H](COC3=CC(OCO4)=C4C=C3)CN(C(OC(C)(C)C)=O)CC2)C=C1

InChI=1S/C24H28INO5/c1-24(2,3)31-23(27)26-11-10-20(16-4-6-18(25)7-5-16)17(13-26)14-28-19-8-9-21-22(12-19)30-15-29-21/h4-9,12,17,20H,10-11,13-15H2,1-3H3/t17-,20-/m0/s1

(3*S*,4*R*)-3-((Benzo[d][1,3]dioxol-5-yloxy)methyl)-4-(4-iodophenyl)piperidine-1-ium chloride (3 · HCl)

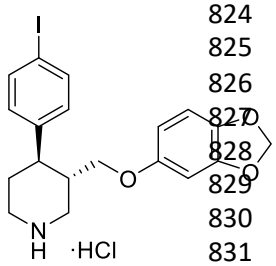

4 N HCl in 1,4-dioxane (250 μL, 1.00 mmol, 10 equiv) was added to a solution of *N*-Boc protected piperidine **(–)-9b** (56.9 mg, 0.10 mmol) in 1,4-dioxane (250 μL, 0.4 M). at 0 °C under air. The solution was stirred at 25 ºC for 18 h, then an ice-cold 1:1 mixture of Et_2O/pentane (1 mL) was added and formation of a solid precipitate was observed. This was filtered and washed with further ice-cold Et_2O/pentane mixture (2 × 5 mL). The solid precipitate was dried under reduced pressure to afford (3*S*,4*R*)-3-((benzo[d][1,3]dioxol-5-yloxy)methyl)-4-(4-iodophenyl)piperidine-1-ium chloride **3** · HCl (38.5 mg, 81%) as an off-white solid.

$[\alpha]_D^{23}$ – 86.0 (*c* 0.9, MeOH).
mp = 203–205 ºC;
ν_{max} (film)/cm^{-1} 3321 (NH), 2926, 2807, 1618, 1484, 1185, 1103, 1033, 1003, 932, 846, 813, 787;
^{1}H NMR (400 MHz, CD_3OD, 298 K) δ 7.71–7.64 (m, 2 H, HC_{Ar}), 7.11–7.04 (m, 2 H, HC_{Ar}), 6.63 (d, *J* = 8.5 Hz, 1 H, HC_{Ar}), 6.39 (d, *J* = 2.5 Hz, 1 H, HC_{Ar}), 6.18 (dd, *J* = 8.5, 2.5 Hz, 1 H, HC_{Ar}), 5.89–5.82 (m, 2 H, OCH_2O), 3.71–3.62 (m, 2 H, C*H*HOAr, NC*H*HCHCH$_2$OAr), 3.60–3.48 (m, 2 H, CH*H*OAr, NC*H*HCH$_2$), 2.21–2.11 (m, 2 H, NCH*H*CHCH$_2$OAr, NCH*H*CH$_2$), 3.00–2.90 (m, 1 H, CHAr), 2.49–2.37 (m, 1 H, C*H*CH$_2$OAr), 2.09–2.00 (m, 2 H, NCH$_2$C*H*$_2$);

^{13}C NMR (101 MHz, CD_3OD, 298 K) δ 155.2 (OC_{Ar} quat), 149.7 (OC_{Ar} quat), 143.5 (C_{Ar} quat), 143.0 (OC_{Ar} quat), 139.1 (2 × C_{Ar}), 130.7 (2 × C_{Ar}), 108.8 (C_{Ar}), 106.6 (C_{Ar}), 102.5 (OCH_2O), 98.9 (C_{Ar}), 93.1 (IC_{Ar} quat), 68.9 (*C*H_2OAr), 47.7 (N*C*H_2CHCH_2OAr), 45.4 (N*C*H_2CH_2), 43.0 (*C*HAr), 40.5 (*C*HCH_2OAr), 31.3 (NCH_2*C*H_2);
HRMS (ESI$^+$) *m/z* Calculated for $C_{19}H_{21}NO_3{}^{127}I$ [M–Cl] 438.0566; Found 438.0571.

SMILES: IC1=CC=C([C@H]2[C@H](COC3=CC(OCO4)=C4C=C3)CNCC2)C=C1.Cl

InChI=1S/C19H20INO3.ClH/c20-15-3-1-13(2-4-15)17-7-8-21-10-14(17)11-22-16-5-6-18-19(9-16)24-12-23-18;/h1-6,9,14,17,21H,7-8,10-12H2;1H/t14-,17-;/m0./s1

NMR Spectra for Novel Compounds

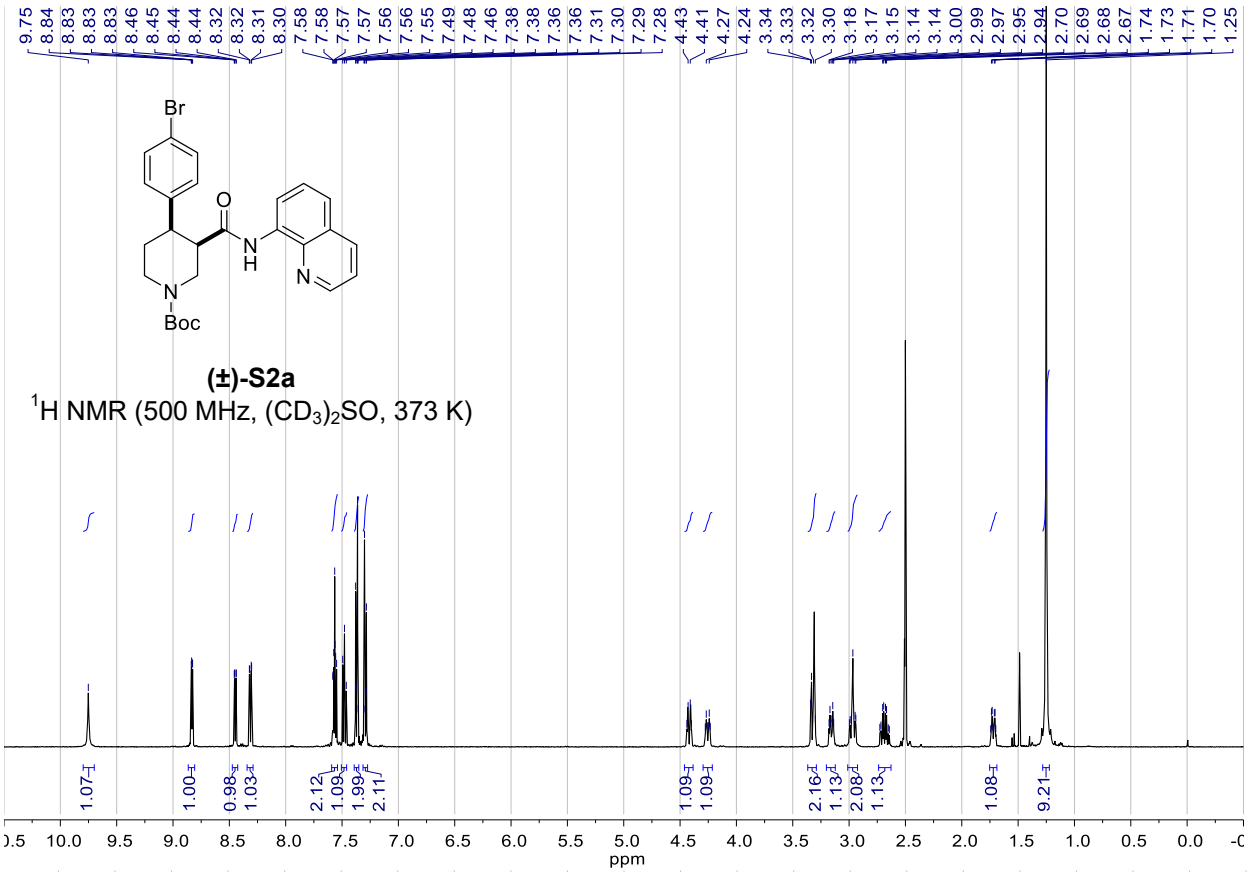
Br
O
N
H
N
N
Boc
(±)-S2a
1H NMR (500 MHz, (CD3)2SO, 373 K)
ppm

879

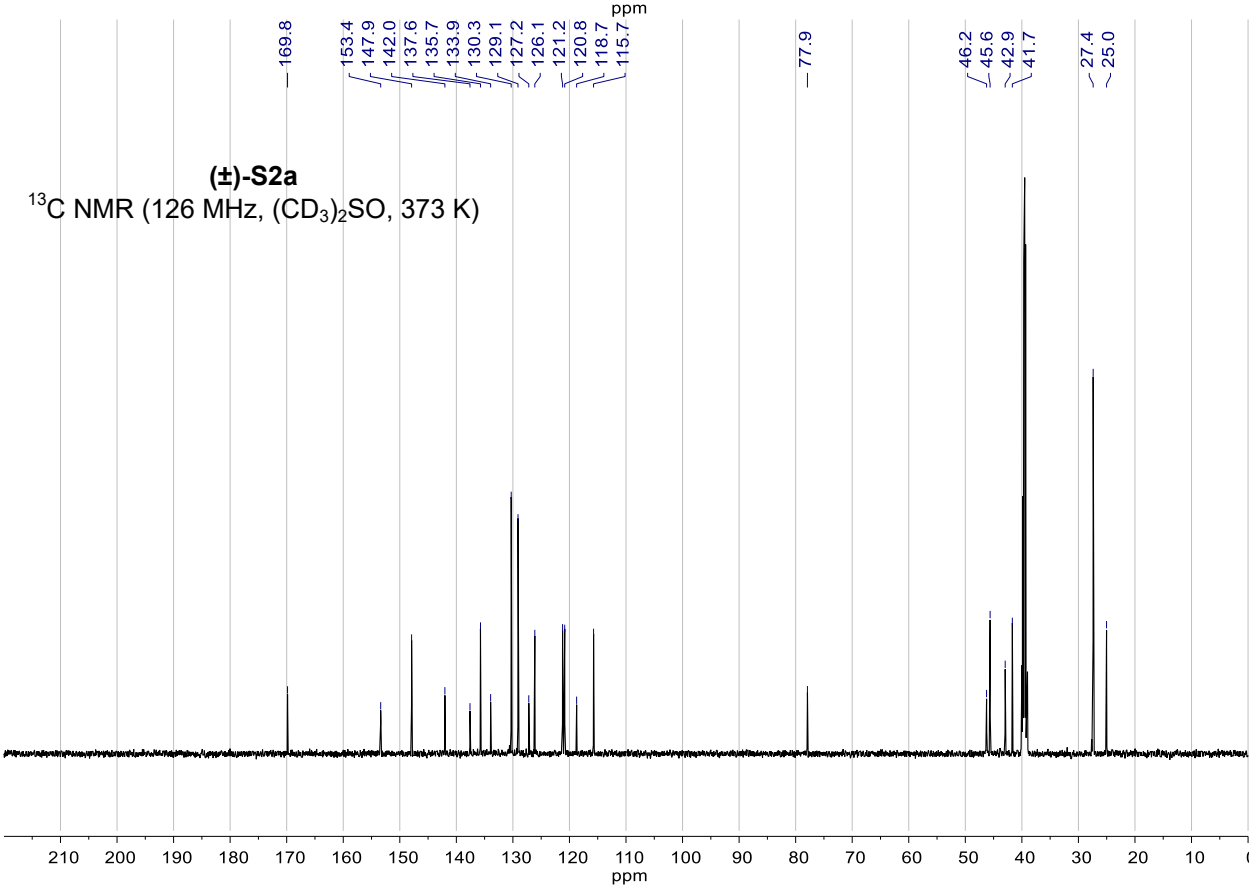
(±)-S2a
13C NMR (126 MHz, (CD3)2SO, 373 K)
ppm

880

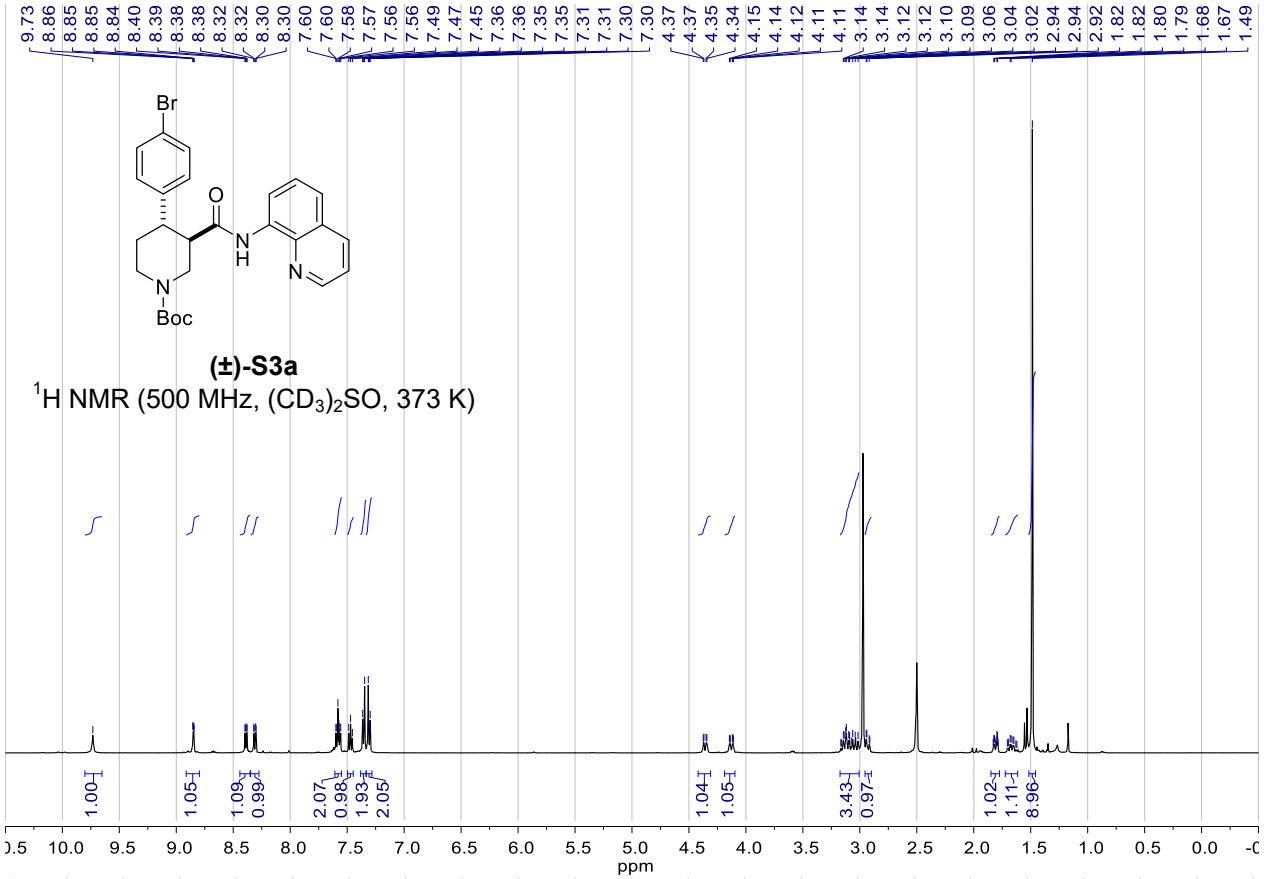
Br
O
N
H
N
N
Boc
(±)-S3a
1H NMR (500 MHz, (CD3)2SO, 373 K)
ppm

881

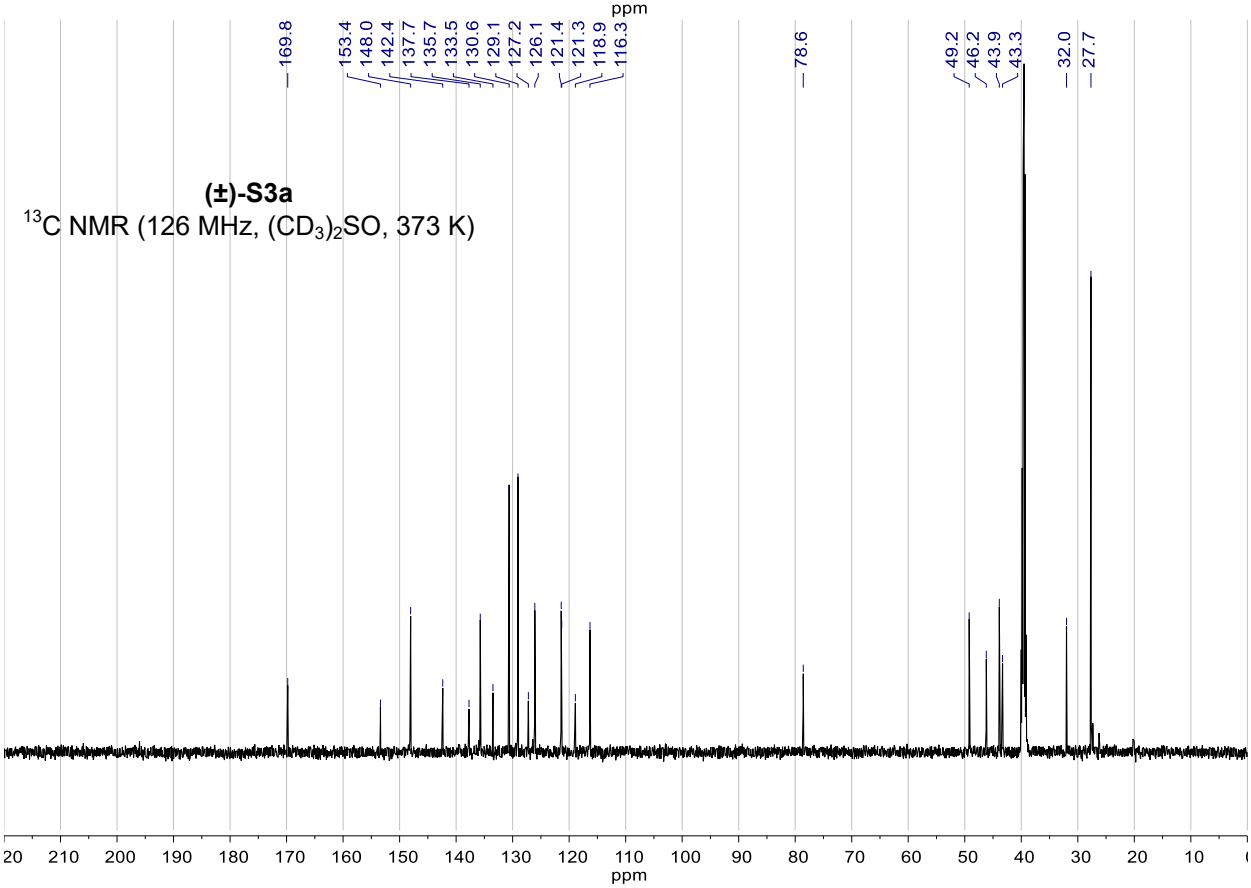
(±)-S3a
13C NMR (126 MHz, (CD3)2SO, 373 K)
ppm

882

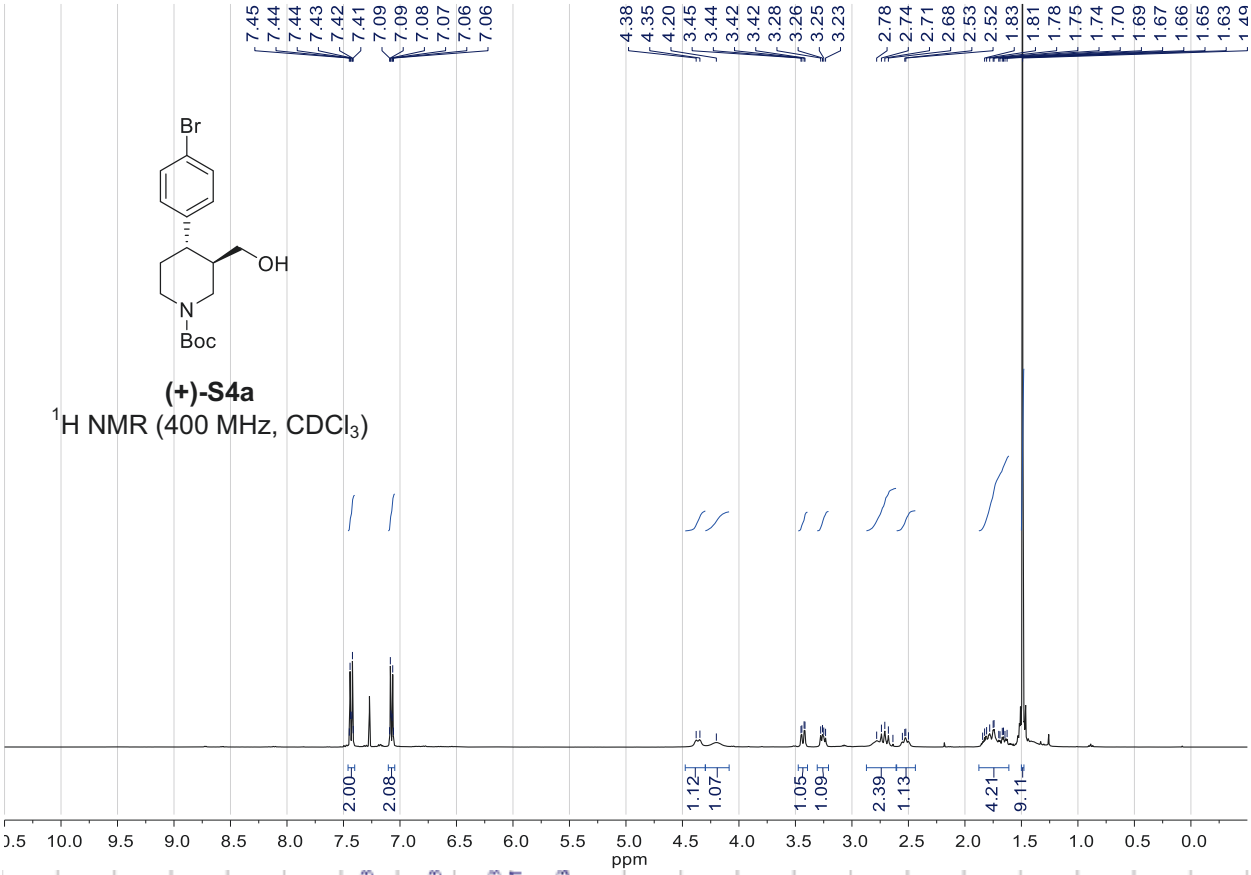
Br
OH
N
Boc
(+)-S4a
1H NMR (400 MHz, CDCl3)
ppm

883

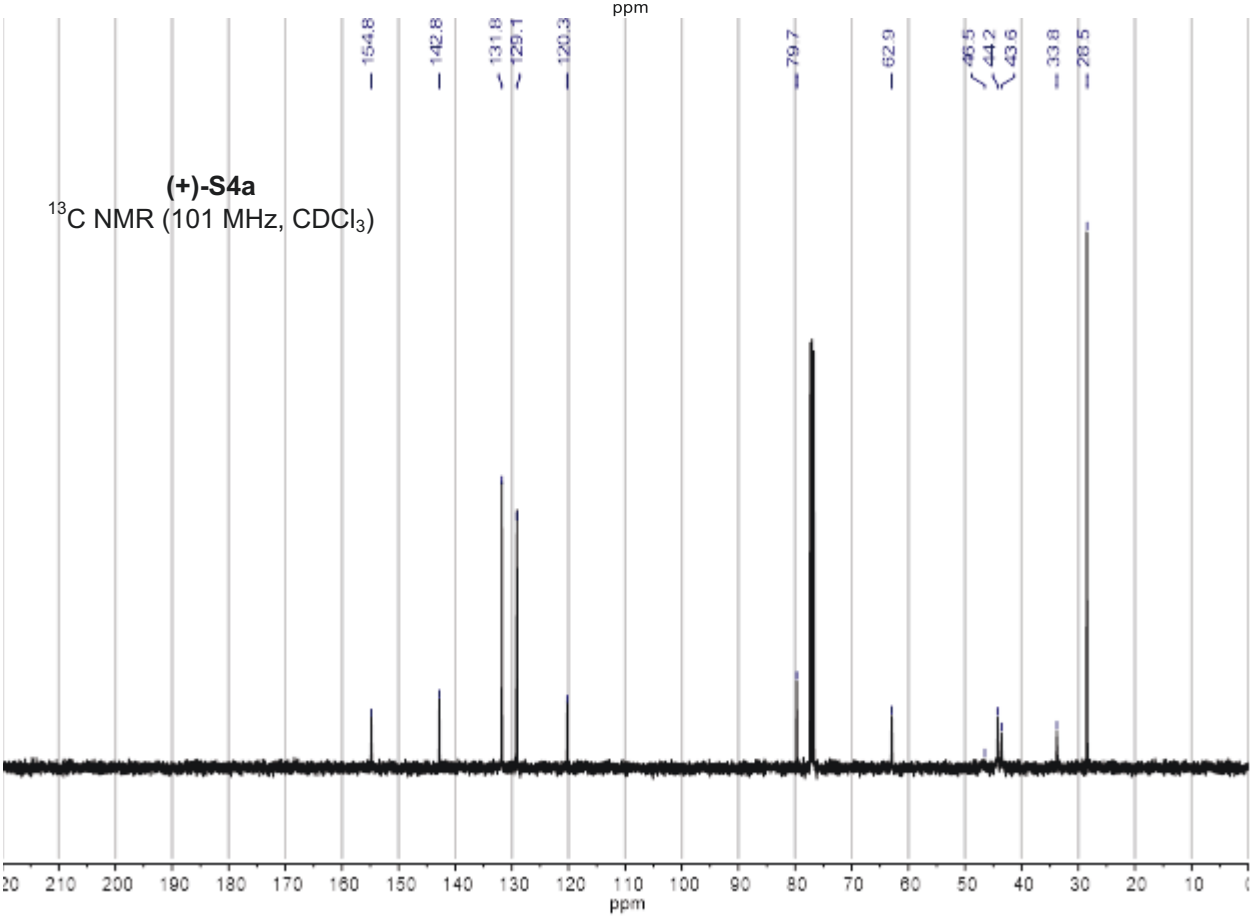
(+)-S4a
13C NMR (101 MHz, CDCl3)
ppm

884

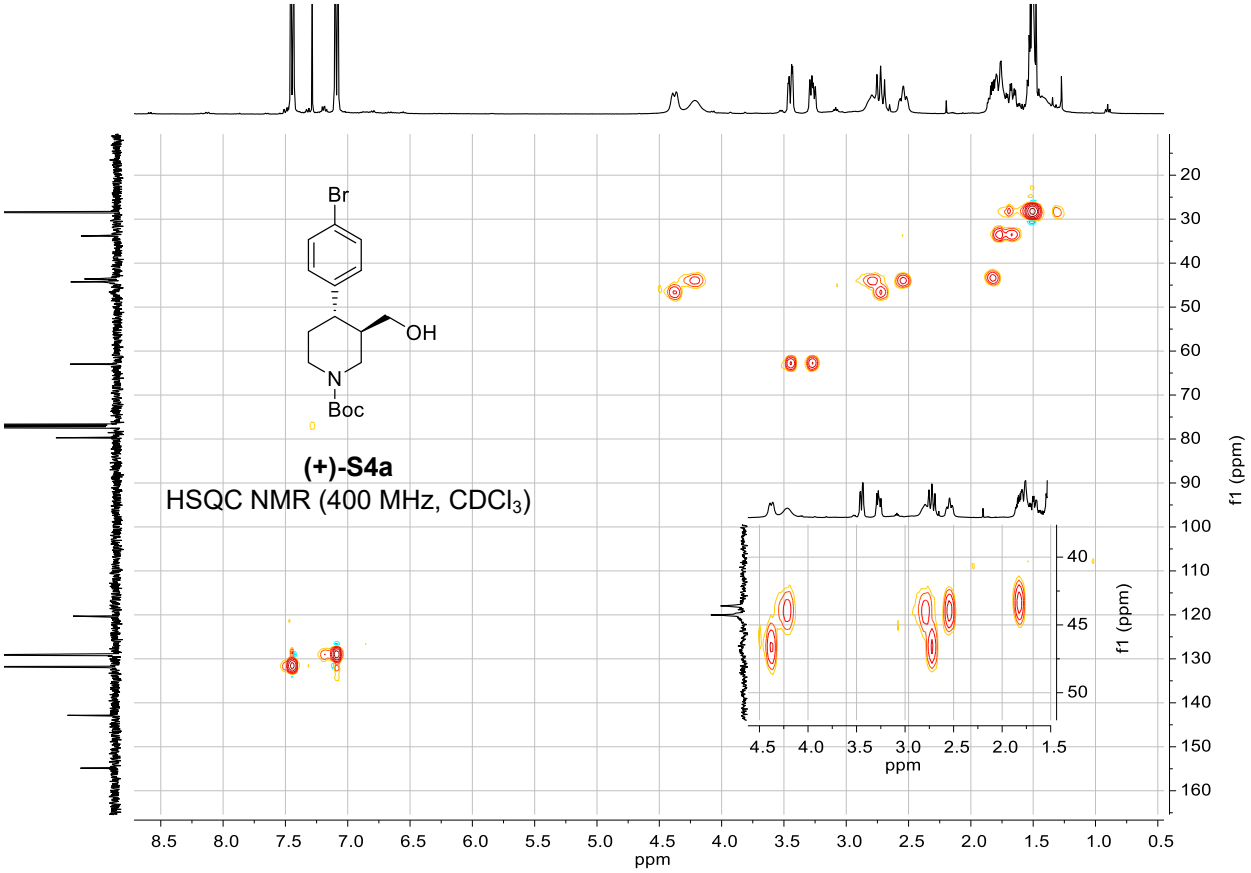

885

886

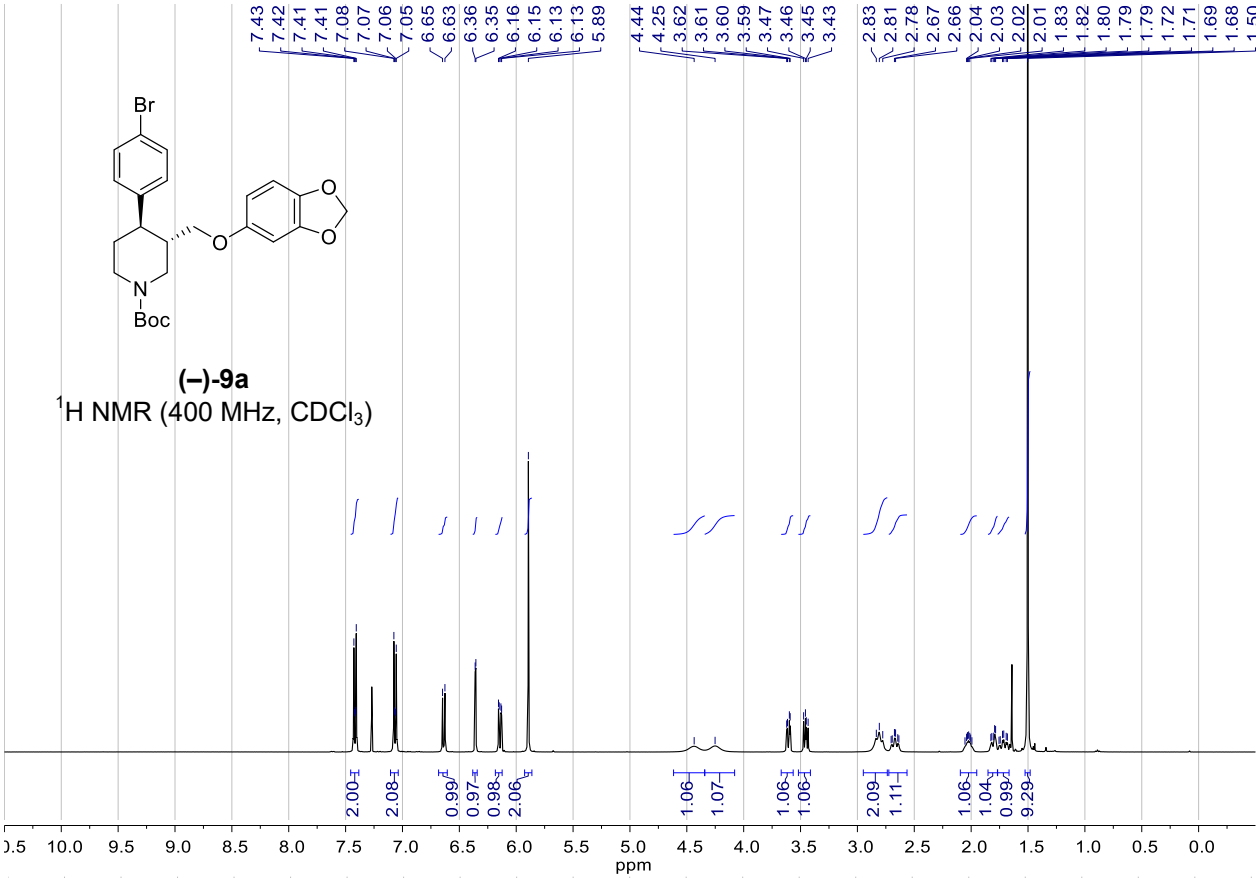
Br
O
O
O
N
Boc
(–)-9a
1H NMR (400 MHz, CDCl3)
ppm

887

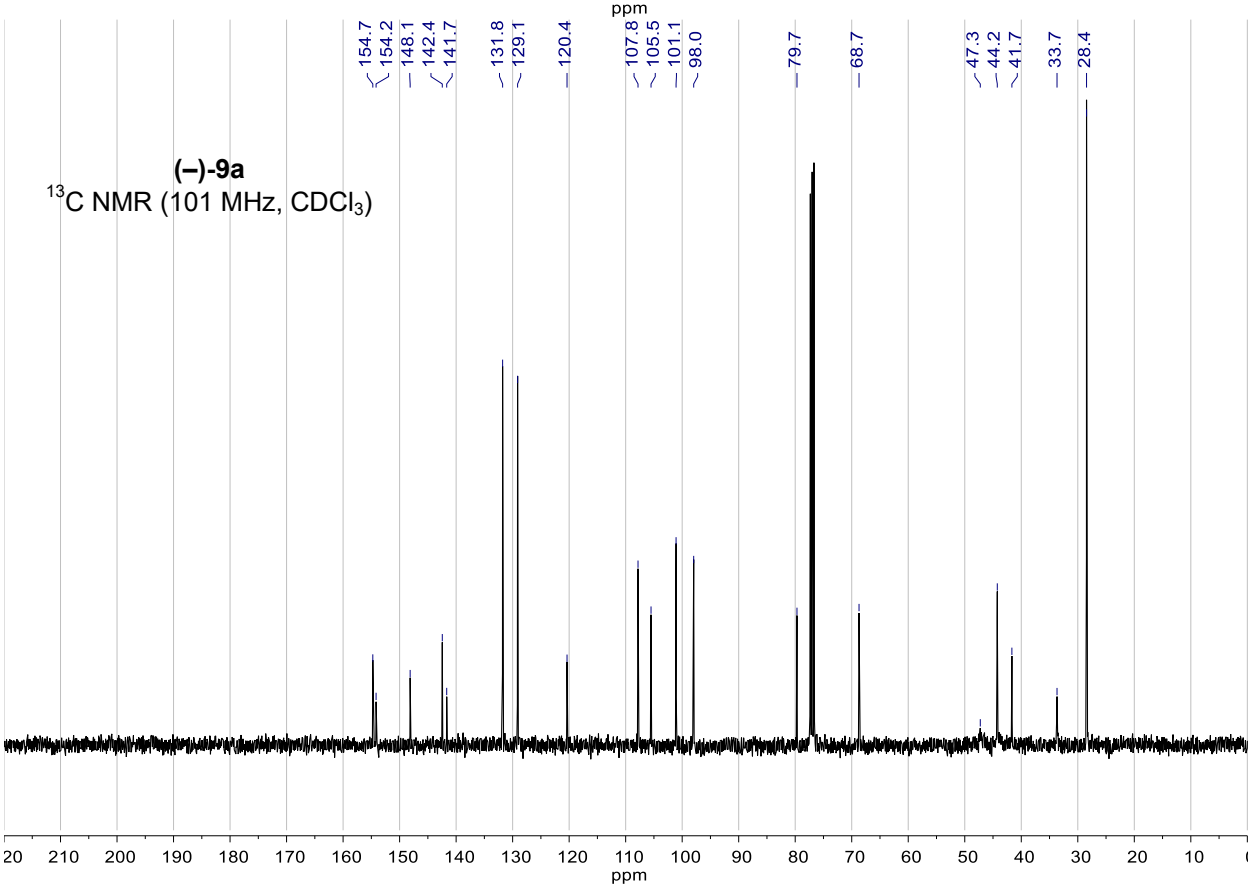
(–)-9a
13C NMR (101 MHz, CDCl3)
ppm

888

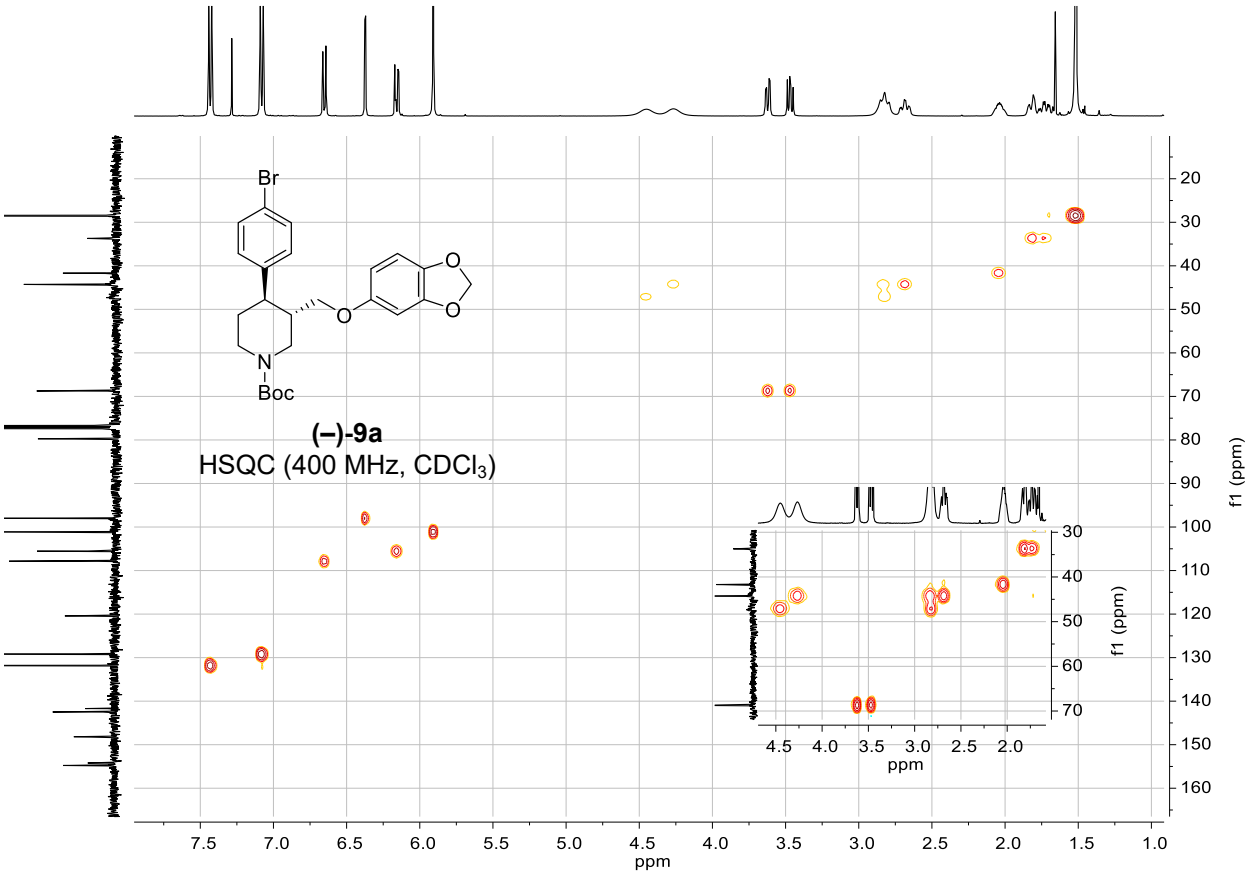

889

890

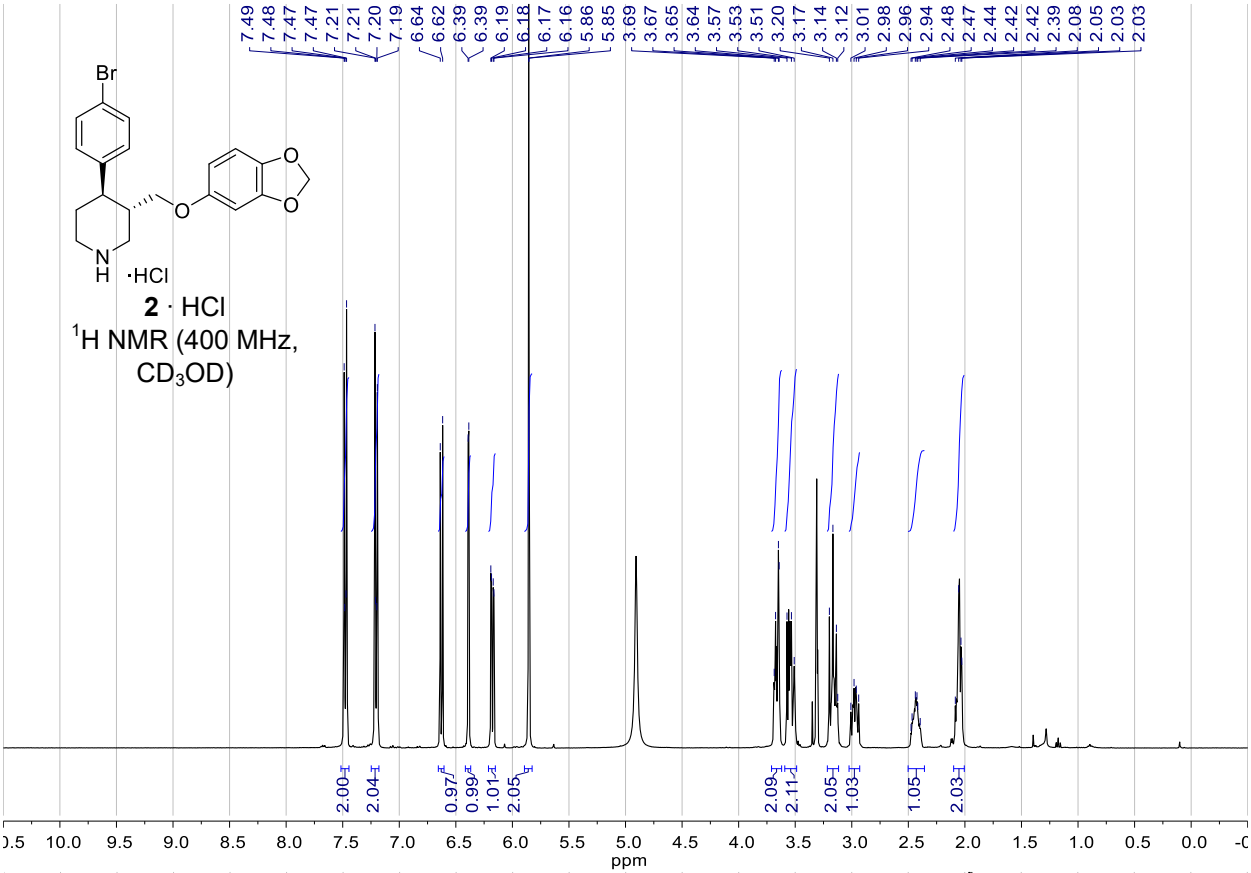
Br
O
O
O
N
H ·HCl
2 · HCl
1H NMR (400 MHz, CD3OD)
ppm

891

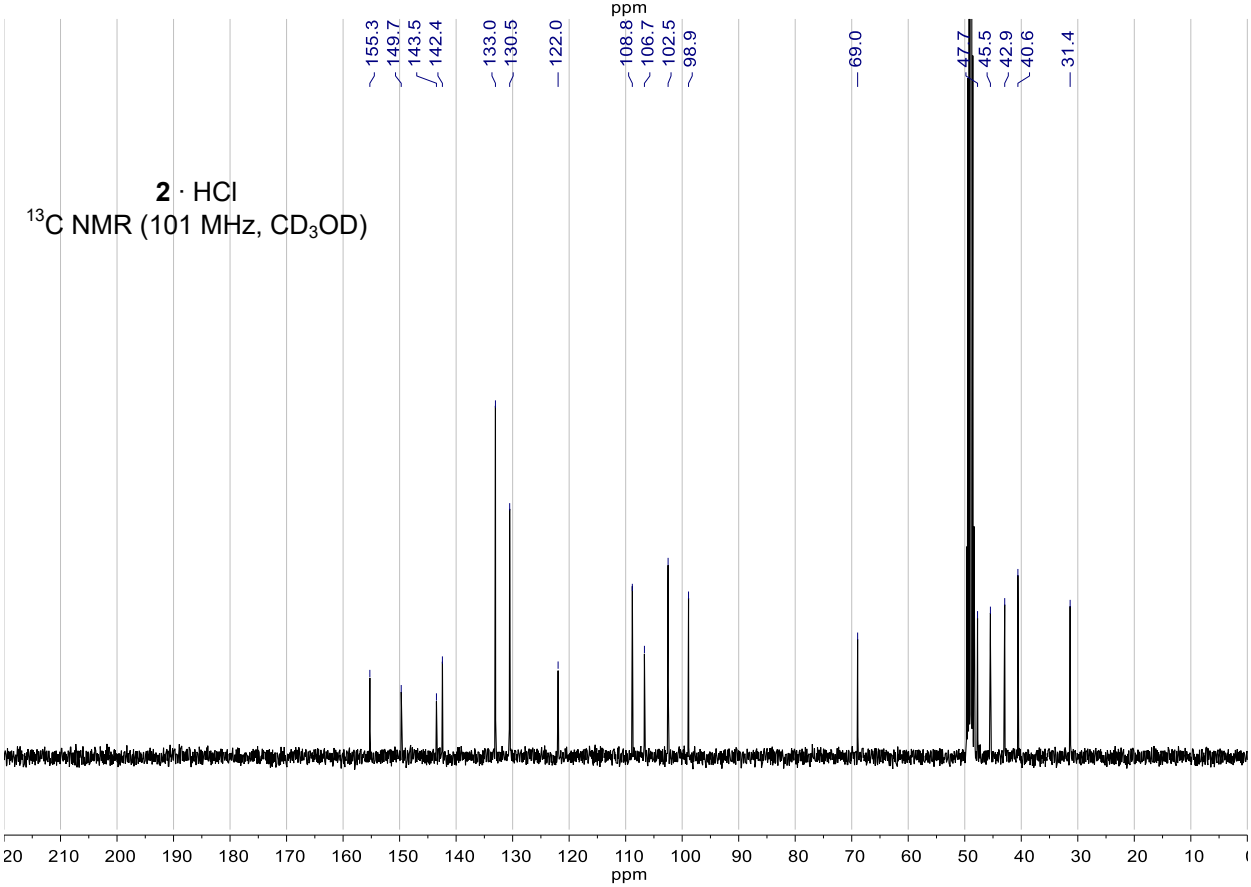
2 · HCl
13C NMR (101 MHz, CD3OD)
ppm

892

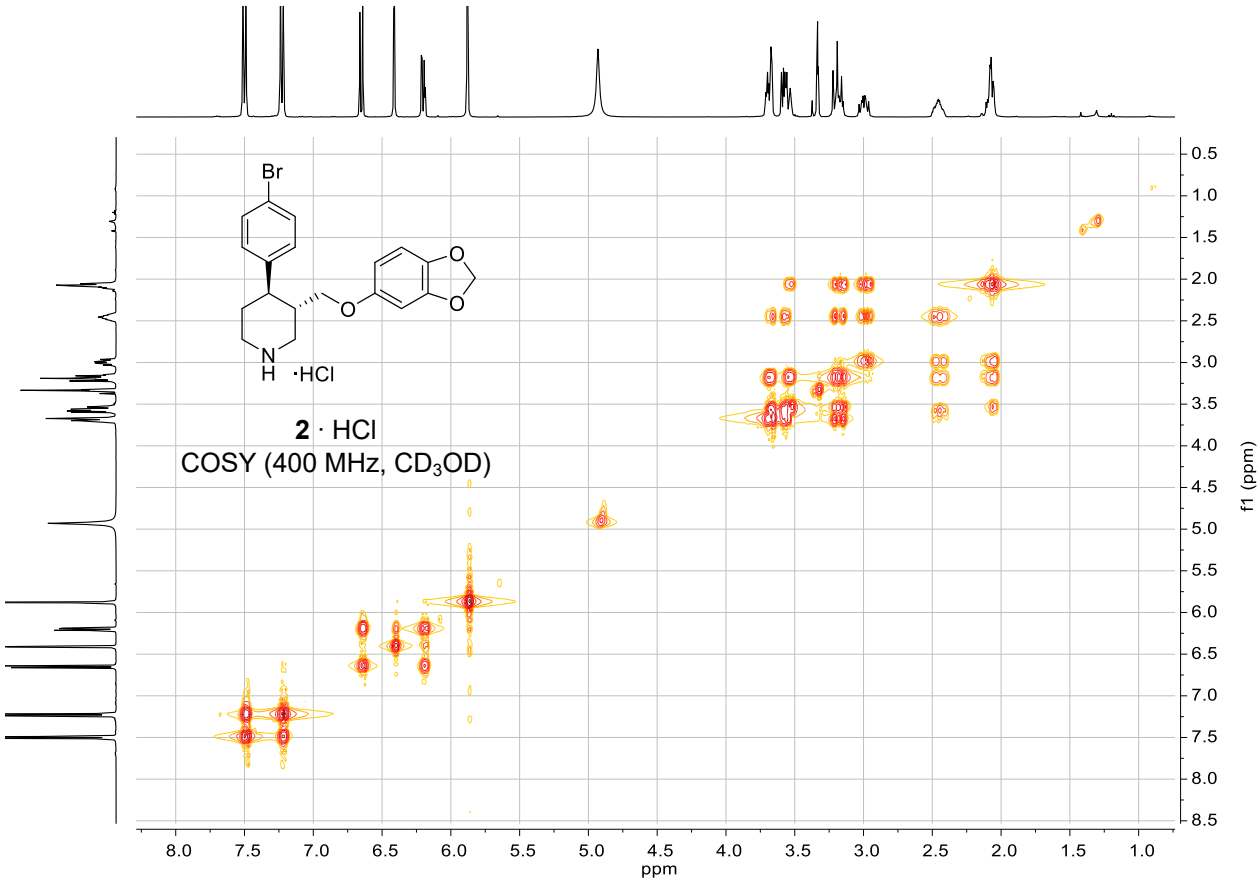
Br
O
O
O
N
H ·HCl
2 · HCl
COSY (400 MHz, CD3OD)
ppm
f1 (ppm)

893

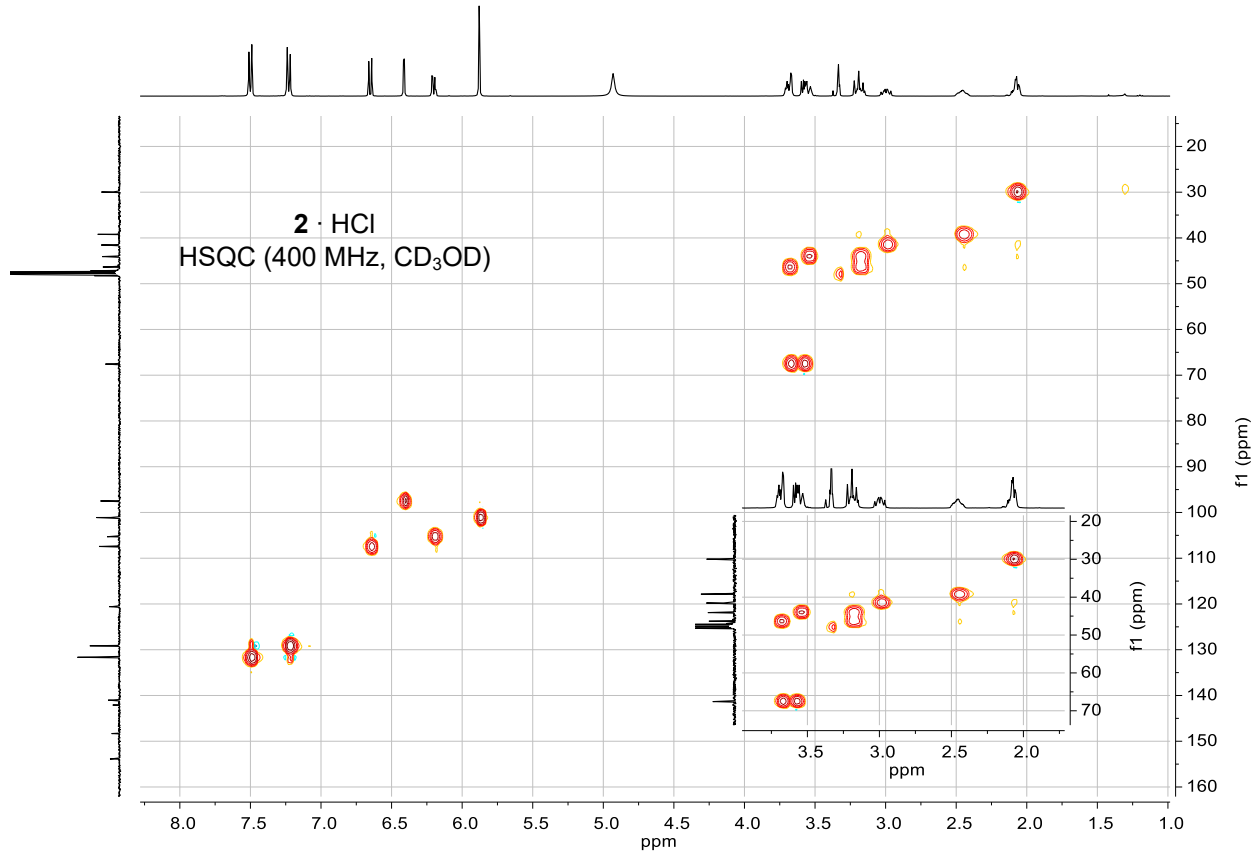
2 · HCl
HSQC (400 MHz, CD3OD)
ppm
f1 (ppm)

894

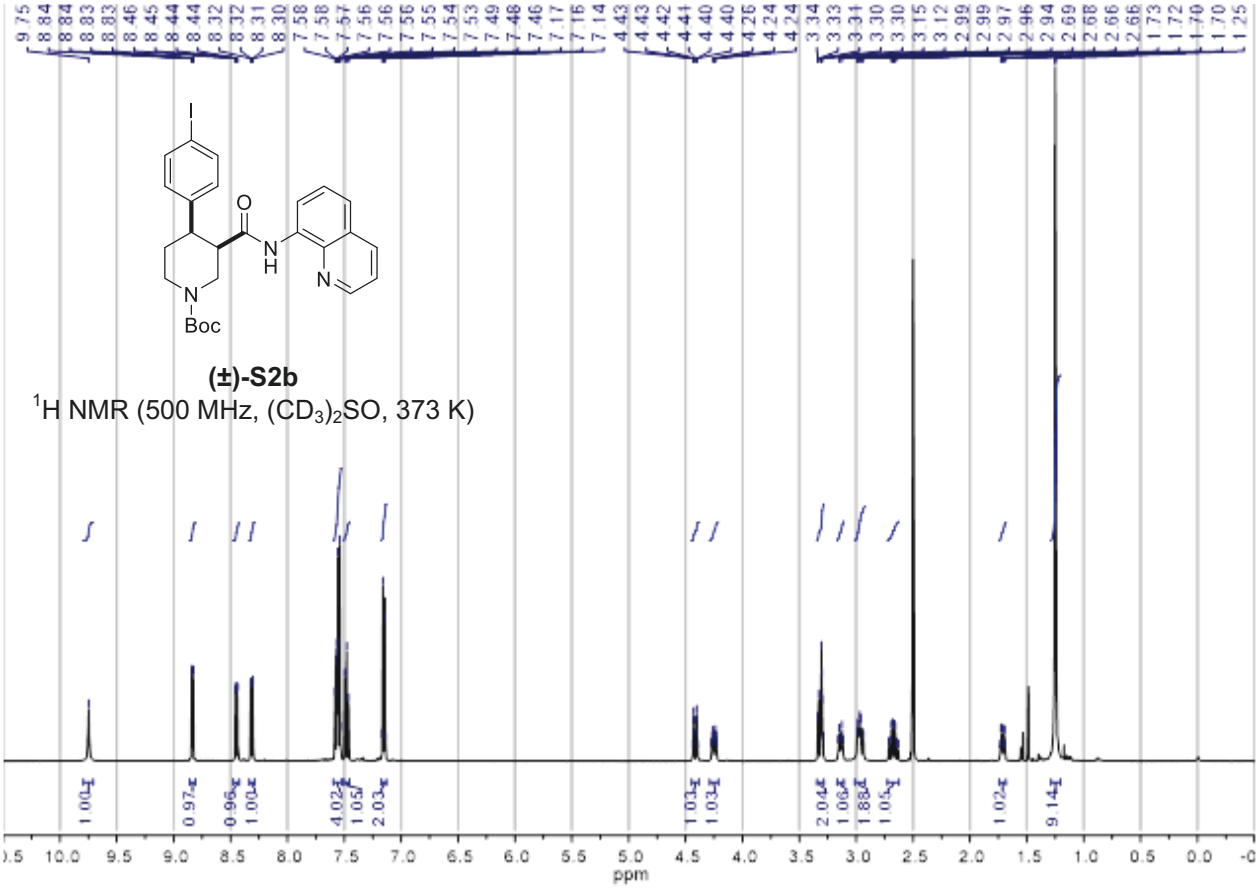

(±)-S2b

^{1}H NMR (500 MHz, $(CD_3)_2SO$, 373 K)

895

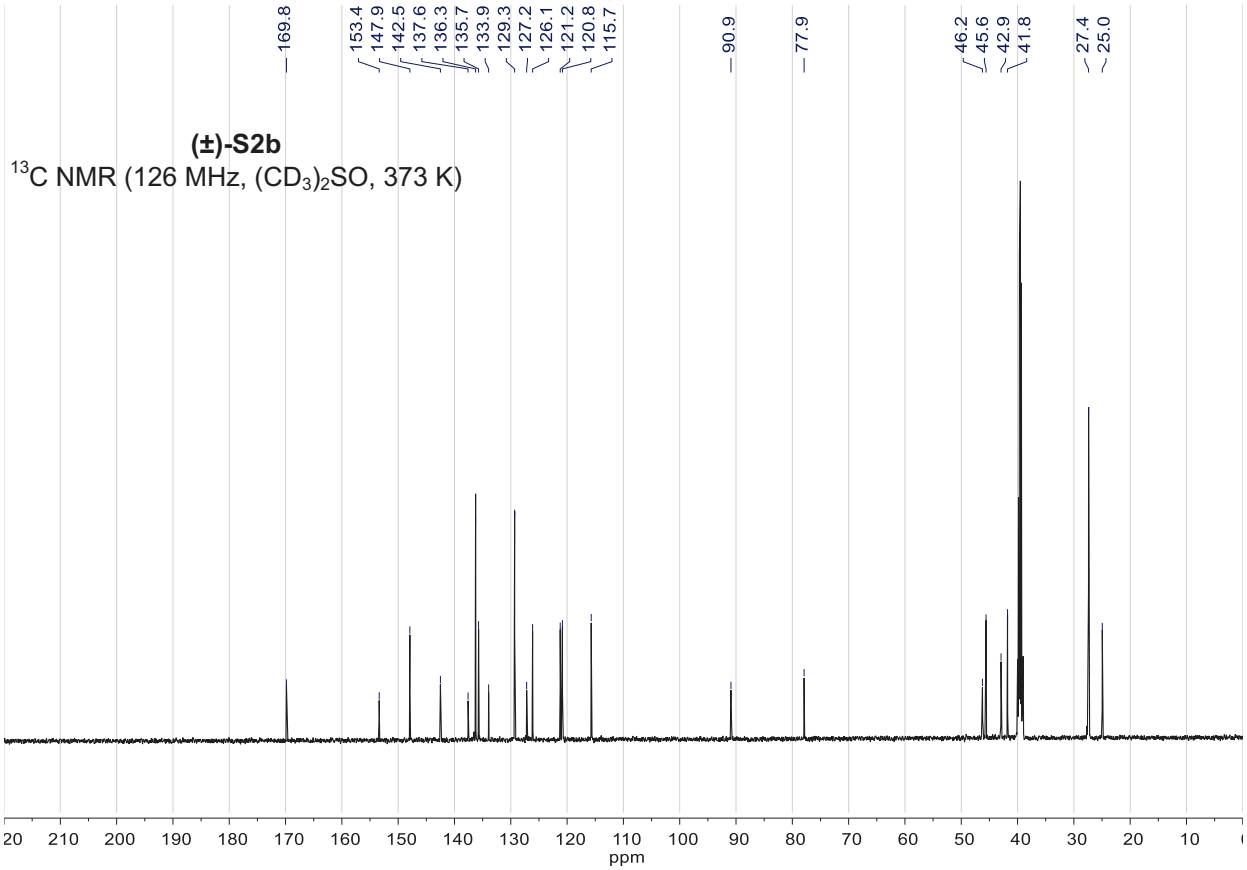

(±)-S2b

^{13}C NMR (126 MHz, $(CD_3)_2SO$, 373 K)

896

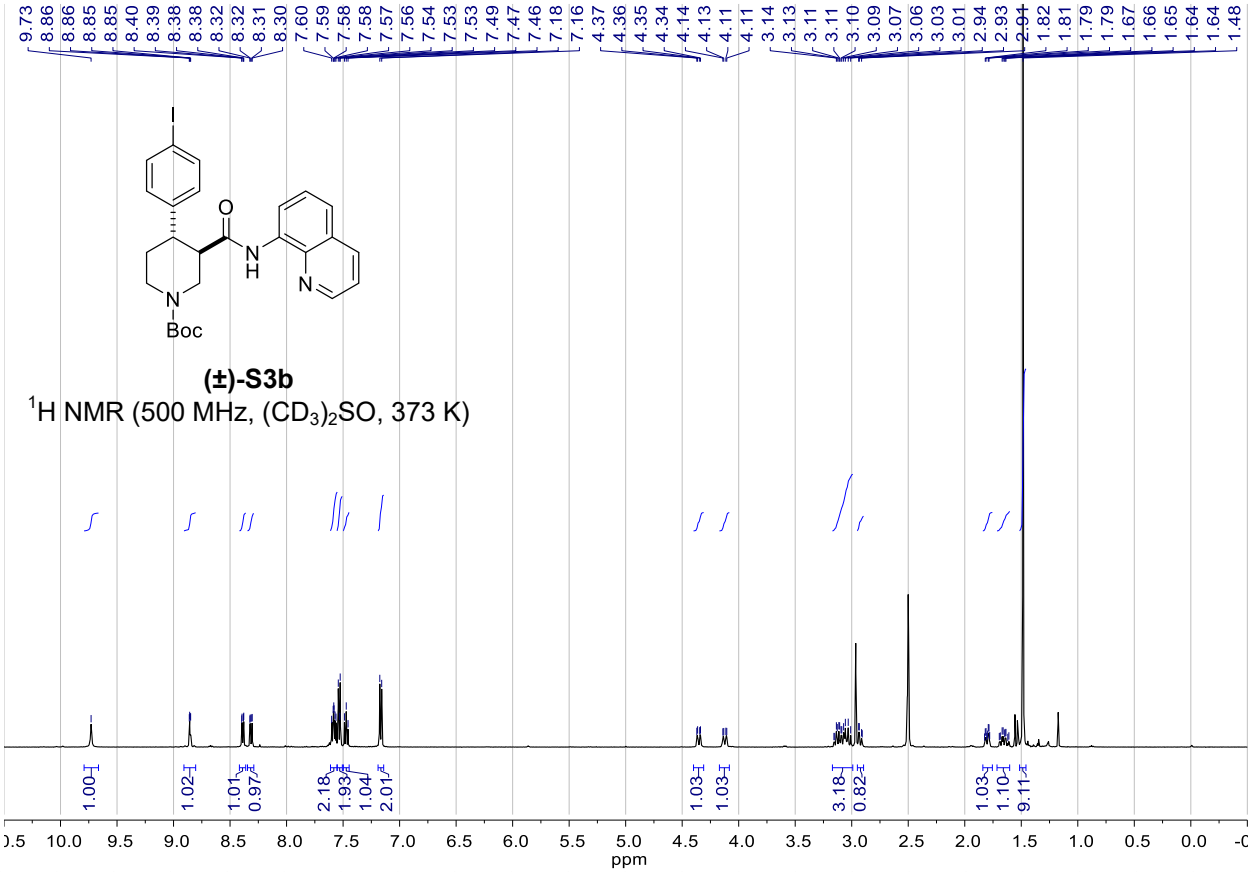
9.73 8.86 8.86 8.85 8.85 8.40 8.39 8.38 8.38 8.32 8.32 8.31 8.30 7.60 7.59 7.58 7.58 7.57 7.56 7.54 7.53 7.53 7.49 7.47 7.46 7.18 7.16 4.37 4.36 4.35 4.34 4.14 4.13 4.11 4.11 3.14 3.13 3.11 3.11 3.10 3.09 3.07 3.06 3.03 3.01 2.94 2.93 2.91 1.82 1.81 1.79 1.79 1.67 1.66 1.65 1.64 1.64 1.48
I
O
N
H
N
N
Boc
(±)-S3b
1H NMR (500 MHz, (CD3)2SO, 373 K)
1.00 1.02 1.01 0.97 2.18 1.93 1.04 2.01 1.03 1.03 3.18 0.82 1.03 1.10 9.11
ppm

897

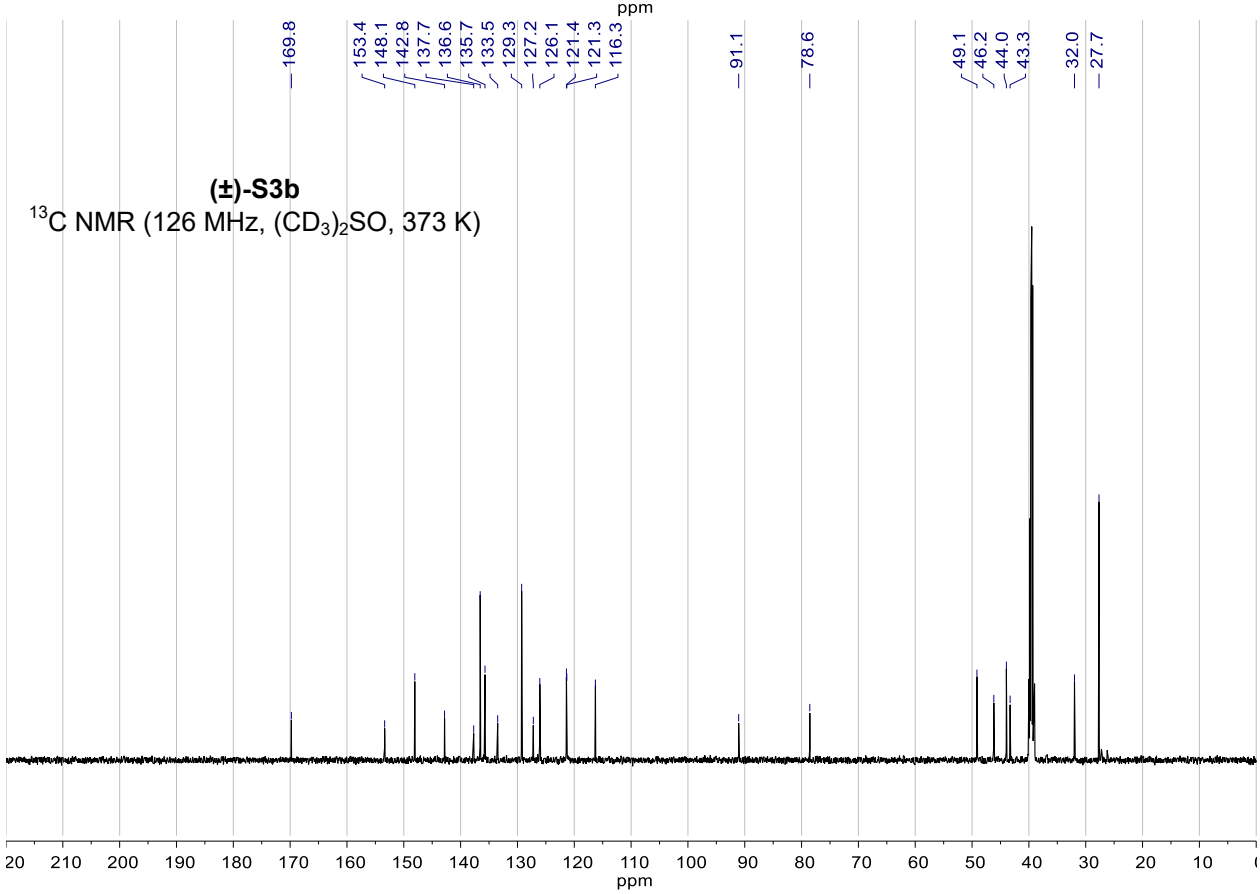
169.8 153.4 148.1 142.8 137.7 136.6 135.7 133.5 129.3 127.2 126.1 121.4 121.3 116.3 91.1 78.6 49.1 46.2 44.0 43.3 32.0 27.7
(±)-S3b
13C NMR (126 MHz, (CD3)2SO, 373 K)
ppm

898

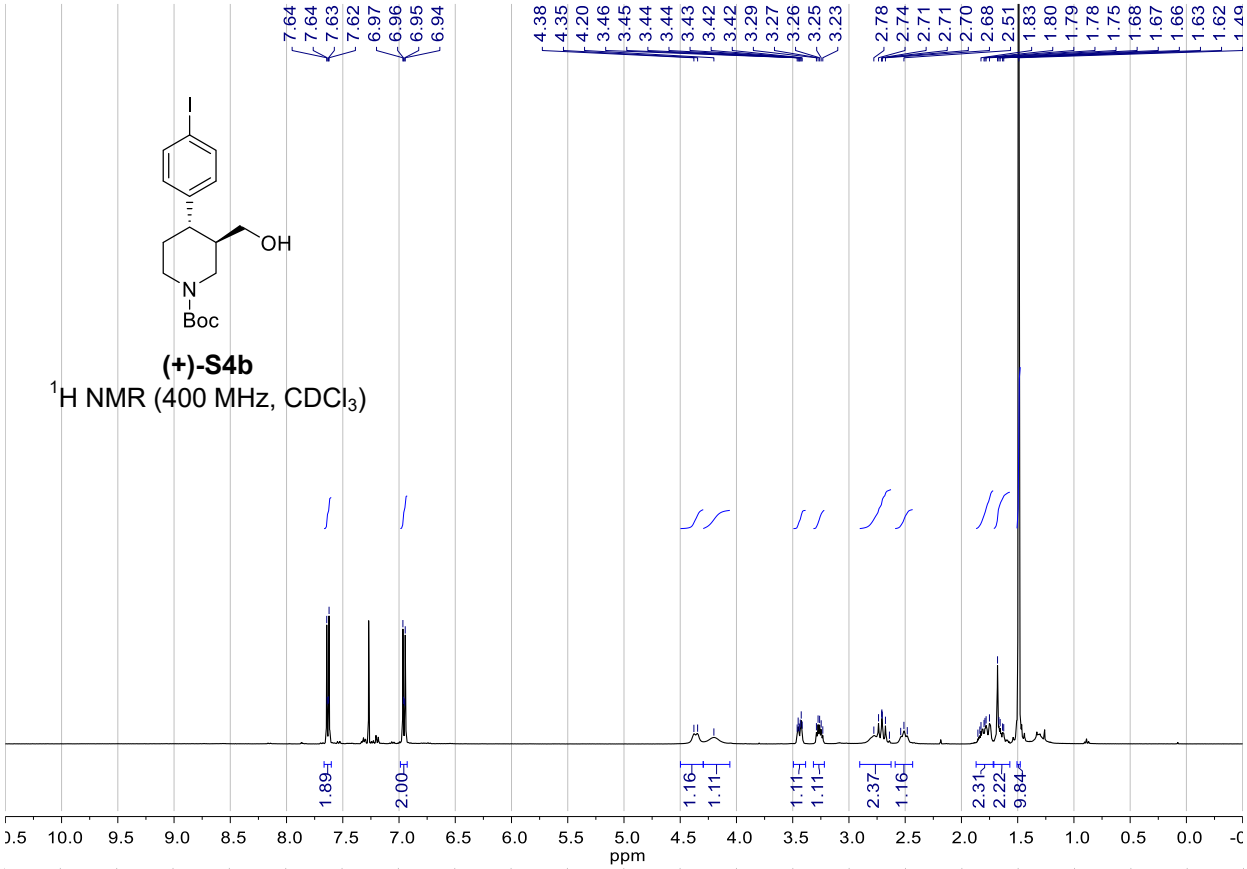
7.64
7.64
7.63
7.62
6.97
6.96
6.95
6.94
4.38
4.35
4.20
3.46
3.45
3.44
3.44
3.43
3.42
3.42
3.29
3.27
3.26
3.25
3.23
2.78
2.74
2.71
2.71
2.70
2.68
2.51
1.83
1.80
1.79
1.78
1.75
1.68
1.67
1.66
1.63
1.62
I
OH
N
Boc
(+)-S4b
1H NMR (400 MHz, CDCl3)
1.89
2.00
1.16
1.11
1.11
1.11
2.37
1.16
2.31
2.22
9.84
ppm

899

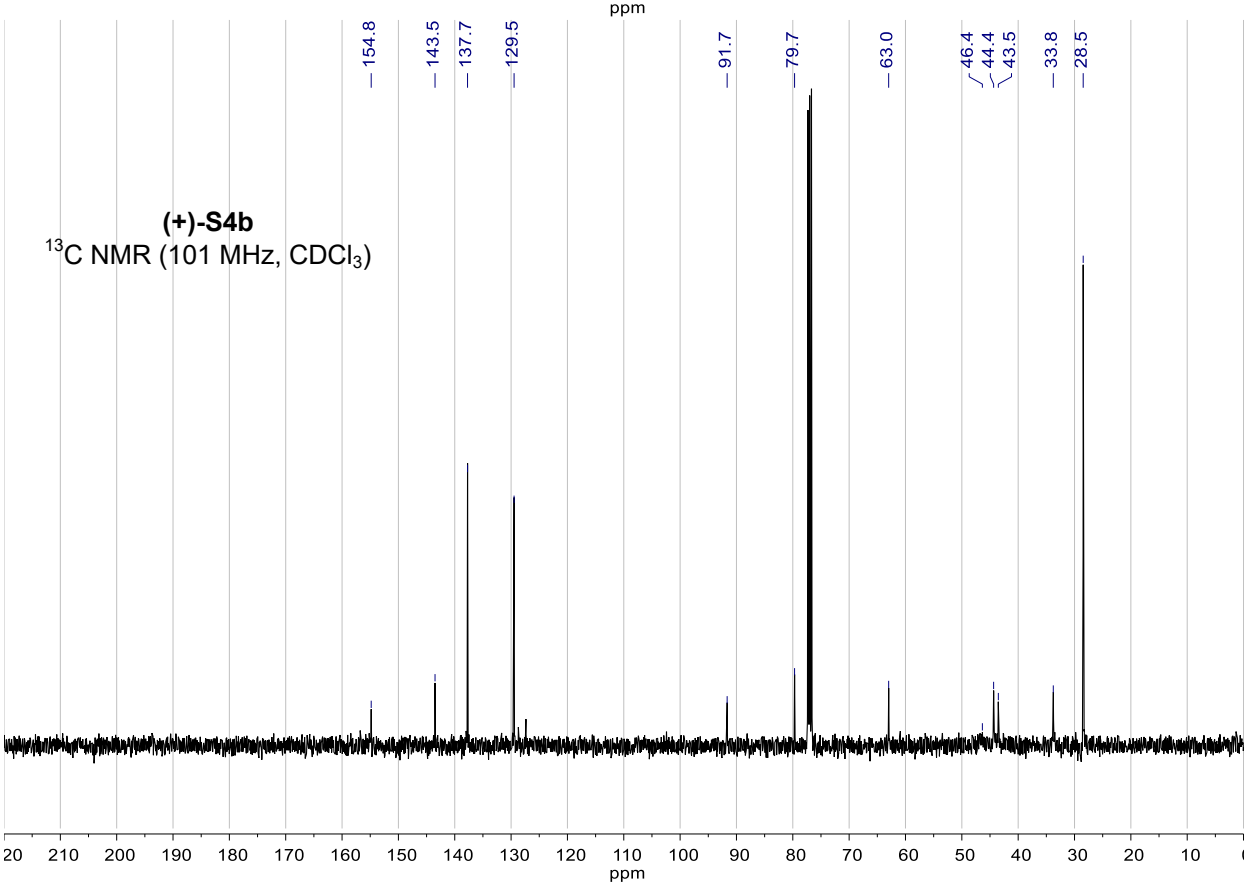
154.8
143.5
137.7
129.5
91.7
79.7
63.0
46.4
44.4
43.5
33.8
28.5
(+)-S4b
13C NMR (101 MHz, CDCl3)
ppm

900

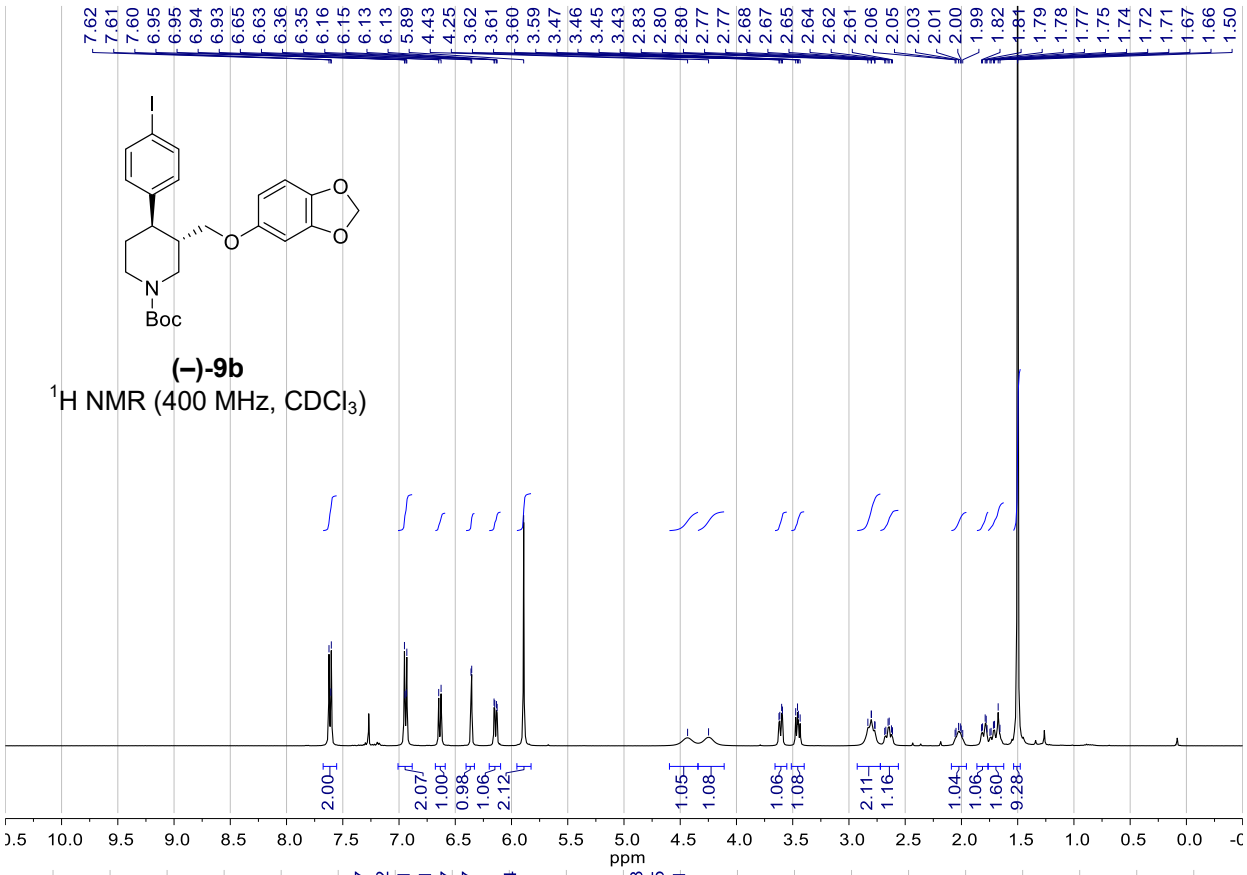

901

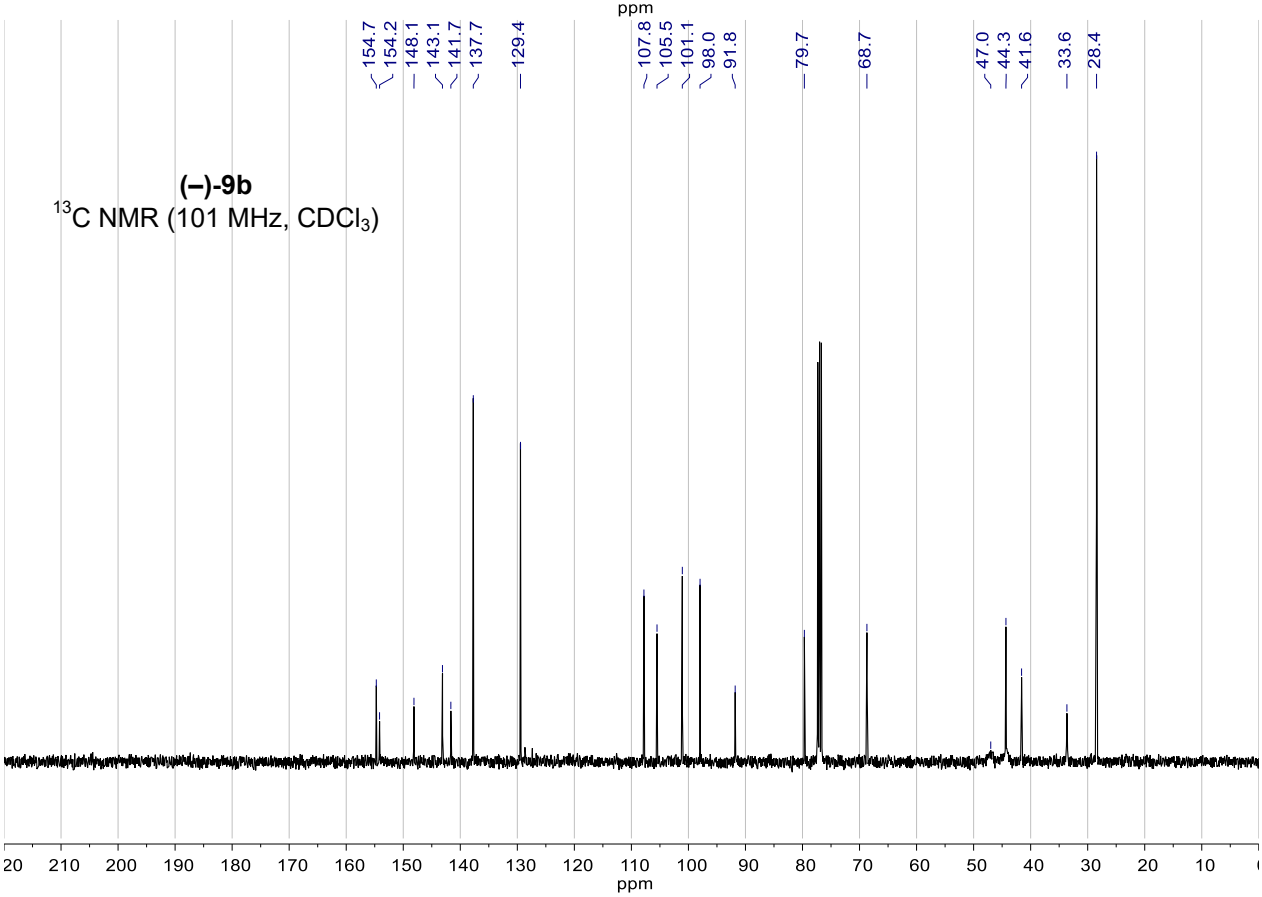

902

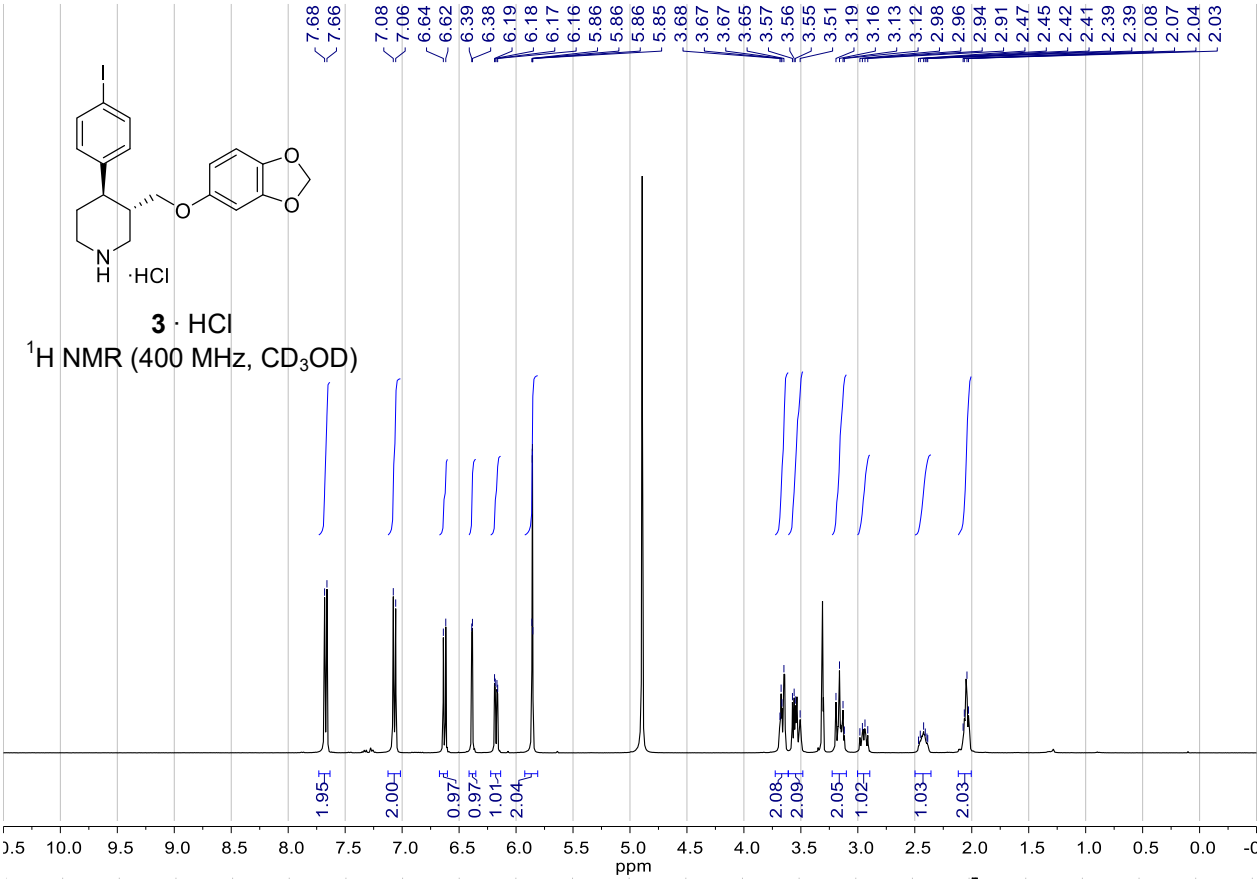
7.68
7.66
7.08
7.06
6.64
6.62
6.39
6.38
6.19
6.18
6.17
6.16
5.86
5.86
5.86
5.85
3.68
3.67
3.67
3.65
3.57
3.56
3.55
3.51
3.19
3.16
3.13
3.12
2.98
2.96
2.94
2.91
2.47
2.45
2.42
2.41
2.39
2.39
2.08
2.07
2.04
2.03
I
O
O
O
N
H
·HCl
3 · HCl
1H NMR (400 MHz, CD3OD)
1.95
2.00
0.97
0.97
1.01
2.04
2.08
2.09
2.05
1.02
1.03
2.03
ppm

903

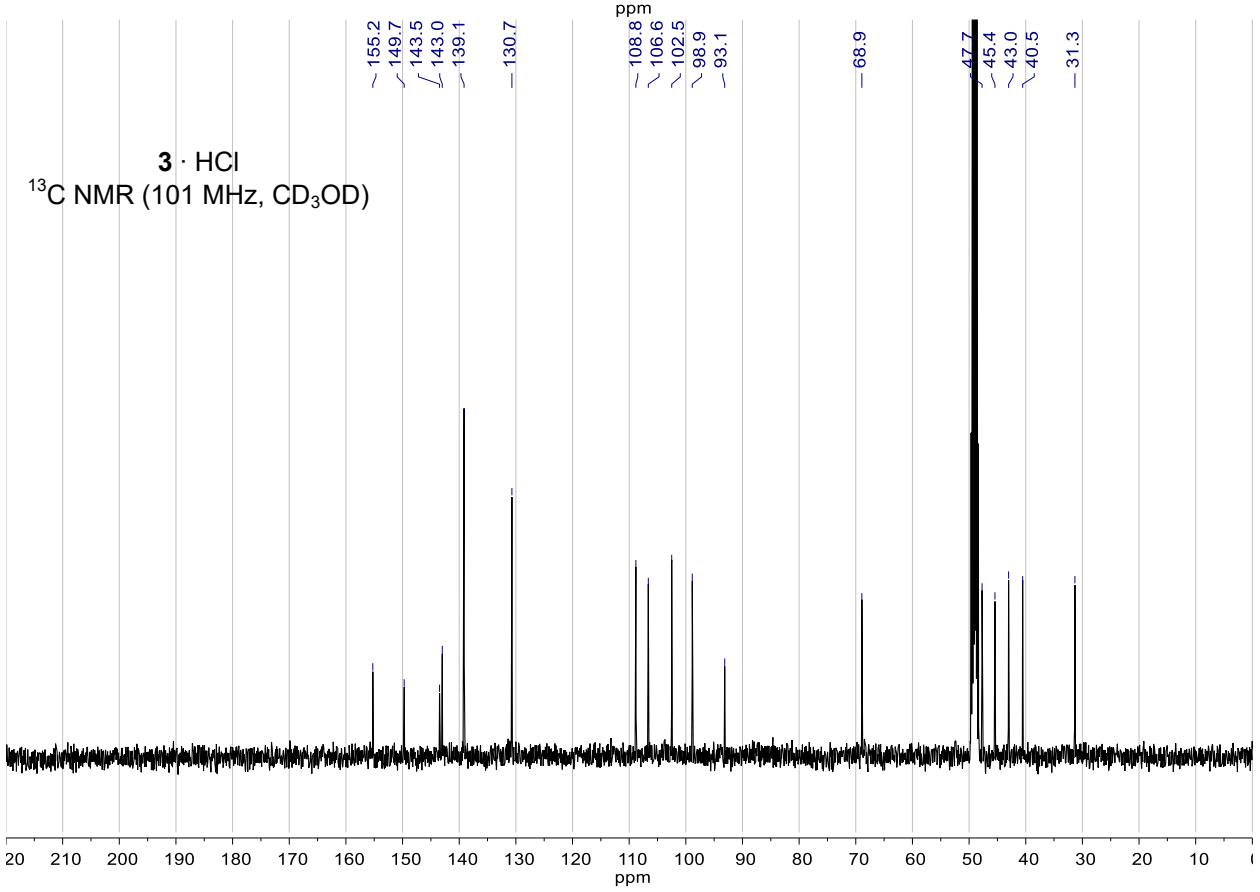
155.2
149.7
143.5
143.0
139.1
130.7
108.8
106.6
102.5
98.9
93.1
68.9
47.7
45.4
43.0
40.5
31.3
3 · HCl
13C NMR (101 MHz, CD3OD)
ppm

904